

VANE SHEAR DETERMINATION OF THE VISCOELASTIC
SHEAR MODULUS OF SUBMARINE SEDIMENTS

Herbert Scott Stevenson

VANE SHEAR DETERMINATION OF THE VISCOELASTIC
SHEAR MODULUS OF SUBMARINE SEDIMENTS

A Thesis

by

Herbert Scott Stevenson

Submitted to the Graduate College of
Texas A&M University in
partial fulfillment of the requirement for the degree of
MASTER OF SCIENCE

December 1973

Major Subject: Civil Engineering

T158018

Library
School of Public Health to School
Berkeley, California 94710

VANE SHEAR DETERMINATION OF THE VISCOELASTIC
SHEAR MODULUS OF SUBMARINE SEDIMENTS

A Thesis

by

Herbert Scott Stevenson
//

Submitted to the Graduate College of
Texas A&M University in
partial fulfillment of the requirement for the degree of
MASTER OF SCIENCE

December 1973

Major Subject: Civil Engineering

ABSTRACT

VANE SHEAR DETERMINATION OF THE VISCOELASTIC SHEAR MODULUS OF SUBMARINE SEDIMENTS (DECEMBER 1973)

Herbert Scott Stevenson, B.S.,
University of California, Los Angeles

Directed by: Dr. Wayne A. Dunlap

Submarine clay sediments exhibit time dependent stress-deformation characteristics and can be described by a viscoelastic relaxation modulus. A method is developed for determination of the relaxation modulus in shear which utilizes viscoelastic theory and torque versus rotation data from vane shear tests. The modulus, $G(t)$, is described by the power law:

$$G(t) = G_1 t^{-n}$$

where t is time, and G_1 and n are constants. G_1 and n are determined from vane tests on deep sediment core samples. G_1 is rotation angle dependent. The validity of the procedure is supported by predictions of in situ vane test torque versus rotation curves which agree favorably with data obtained using an in situ vane device. G_1 correlates with maximum vane shear strength and n correlates with liquidity index. Additional work is indicated.

ACKNOWLEDGMENTS

The author gratefully acknowledges those who contributed to this study. A special note of gratitude is extended to Professors Wayne A. Dunlap and Richard A. Schapery for their hours of enlightening discussion and guidance during all phases of the study. Professor Dunlap provided needed guidance concerning equipment design and other aspects of the experimental program. Professor Schapery first proposed the method for using the vane shear device to measure a viscoelastic shear modulus and provided guidance in the use of the viscoelastic theory and in interpretation of data.

Messrs. Lionel Milberger, Tom Bennett and Ron Boggess provided able and willing assistance in electronics design, transducer construction and instrumentation. Mr. Milberger's help with finding and eliminating instrumentation problems was indispensable. Messrs. Peter Trabant, Bill Hottman and Lamar Roemer X-rayed the samples and ran the Atterberg limits on each sample. Their help is greatly appreciated.

Special notes of thanks are extended to Mrs. Mary Ann Beeson and Mrs. Nancy Steele for their expert typing, to Mr. Robert Franseen, whose superb drafting is evident throughout the paper, and to the author's wife, Connie, whose help and endurance during report preparation was indispensable.

ACKNOWLEDGMENTS

The author gratefully acknowledges those who contributed to this study. A special note of gratitude is extended to Professors Wayne A. Dunlap and Richard A. Schapery for their hours of enlightening discussion and guidance during all phases of the study. Professor Dunlap provided needed guidance concerning equipment design and other aspects of the experimental program. Professor Schapery first proposed the method for using the vane shear device to measure a viscoelastic shear modulus and provided guidance in the use of the viscoelastic theory and in interpretation of data.

Messrs. Lionel Milberger, Tom Bennett and Ron Boggess provided able and willing assistance in electronics design, transducer construction and instrumentation. Mr. Milberger's help with finding and eliminating instrumentation problems was indispensable. Messrs. Peter Trabant, Bill Hottman and Lamar Roemer X-rayed the samples and ran the Atterberg limits on each sample. Their help is greatly appreciated.

Special notes of thanks are extended to Mrs. Mary Ann Beeson and Mrs. Nancy Steele for their expert typing, to Mr. Robert Franseen, whose superb drafting is evident throughout the paper, and to the author's wife, Connie, whose help and endurance during report preparation was indispensable.

Great appreciation is expressed to Chevron Oil Field Research Company which provided funds for this project.

TABLE OF CONTENTS

	Page
INTRODUCTION	1
BACKGROUND	7
Characterization of Viscoelastic Materials	7
Viscoelasticity in Sea Floor Sediments-Physical Basis	11
Experience with the Vane Shear Test	16
THEORETICAL BASIS FOR EXPERIMENT	24
Calculation of Shear Modulus from Vane Test Data - Elastic Assumption	25
Obtaining the Linear Viscoelasticity Solution from the Elastic Equation	26
Computational Procedure and Characterization of Nonlinearity	30
Determination of the Vane Geometry Factor, B	32
EXPERIMENTAL PROGRAM	40
Description and Operation of Apparatus	41
Sample Selection	45
Experimental Determination of Vane Geometry Factor - B	49
Sample Test Procedure	49
Data Reduction	52
RESULTS AND DISCUSSION	57
Experimental Results	57
Comparison of Laboratory and In Situ Results	64
Comment	74
CONCLUSIONS	76
APPENDIX I. - REFERENCES	78
APPENDIX II. - NOTATION	82

TABLE OF CONTENTS (CONTINUED)

	Page
APPENDIX III. - DESCRIPTION OF EQUIPMENT	84
APPENDIX IV. - EQUIPMENT CALIBRATION AND CHECK OUT	94
APPENDIX V. - X-RAYS OF SAMPLES TESTED	97
APPENDIX VI. - TORQUE VERSUS ROTATION AND LOG-LOG PLOTS OF \bar{G} VERSUS TIME	103
VITA	124

LIST OF TABLES

Table		Page
1	Samples Tested	47
2	Experimental Values of G_1 and n	58
3	Miniature Laboratory Vane Shear Strengths, Natural Water Contents and Atterberg Limits and Indices for Test Samples	66

LIST OF FIGURES

Figure		Page
1	Simple Rheological Models	9
2	Nonlinear Rheological Model for Sea Floor Clays Proposed by Sherif et al. [from Sherif et al. (36)] . .	12
3	Depiction of Flocculent and Disperse Clay Structures [from Wu (43)]	13
4	Basic Vane Shear Test	16
5	Down Hole Submarine Vane Test and Borer of Fenske [From Fenske (11)]	20
6	Comparison of In Situ and Laboratory Ultimate Shear Strengths [after Fenske (11)]	21
7	Down Hole Wire Line Submarine Vane Shear Device of McClelland Engineers [from Doyle et al. (9)]	22
8	Normalized Torque Versus Rotation Angle at Various Rotation Rates	31
9	Modulus Versus Time for Various Angles of Rotation .	31
10	Shearing Stresses Acting on Element of Clay Due to Rotating Cylinder	35
11	Deformation of Clay Surrounding Rotating Cylinder . .	35
12	Test Apparatus for Laboratory Vane Shear Rate Tests .	42
13	Details of Vane Shear Device	43
14	The Test Vane	44
15	Torque Transducer Calibration Arrangement	46
16	X-Ray Photograph of Acceptable Sample	48
17	X-Ray Photograph of Unacceptable Sample Showing Fissures Due to Gas Expansion	48

LIST OF FIGURES (CONTINUED)

Figure		Page
18	Wykeham Farrance Motorized Miniature Laboratory Vane Shear Device	51
19	Example of Torque-Rotation-Time data (axes added) . .	53
20	Example of Torque Versus Rotation Angle Plot (B-1, 46 Feet)	55
21	Example of Log-Log Plot of Time Averaged Modulus Versus Time (B-1, 46 Feet)	56
22	G_1 Versus θ , Borehole B-1, 19 Feet	59
23	G_1 Versus θ , Borehole B-1, 46 Feet	59
24	G_1 Versus θ , Borehole B-1, 61 Feet	60
25	G_1 Versus θ , Borehole B-1, 85.5 Feet	60
26	G_1 Versus θ , Borehole B-1, 100 Feet	61
27	G_1 Versus θ , Borehole B-2, 22.5 Feet	61
28	G_1 Versus θ , Borehole B-2, 40.5 Feet	62
29	G_1 Versus θ , Borehole B-2, 72.5 Feet	62
30	G_1 Versus θ , Borehole B-2, 104.5 Feet	63
31	G_1 Versus θ , Borehole B-3, 55 Feet	63
32	Variation in n and G_1 with depth	65
33	G_1 Versus Liquidity Index	67
34	G_1 Versus Ultimate Vane Shear Strength	67

LIST OF FIGURES (CONTINUED)

Figure		Page
35	n Versus Liquidity Index	68
36	n Versus Ultimate Vane Shear Strength	68
37	Comparison of Predicted and Measured in Situ Normalized Torque Versus Rotation Angle-B-1, 46 Feet	71
38	Comparison of Predicted and Measured in Situ Normalized Torque Versus Rotation Angle-B-1, 61 Feet	72
39	Comparison of Predicted and Measured in Situ Normalized Torque Versus Rotation Angle-B-1, 100 Feet	73
40	Motor Control and Transducer Circuitry Unit	90
41	Schematic of Motor Control and Transducer Circuitry Unit	91
42	X-Ray Photograph, Sample B-1, 19 Feet	98
43	X-Ray Photograph, Sample B-1, 46 Feet	98
44	X-Ray Photograph, Sample B-1, 61 Feet	99
45	X-Ray Photograph, Sample B-1, 85.5 Feet	99
46	X-Ray Photograph, Sample B-1, 100 Feet	100
47	X-Ray Photograph, Sample B-2, 22.5 Feet	100
48	X-Ray Photograph, Sample B-2, 40.5 Feet	101
49	X-Ray Photograph, Sample B-2, 72.5 Feet	101
50	X-Ray Photograph, Sample B-2, 104.5 Feet	102
51	X-Ray Photograph, Sample B-3, 55 Feet	102
52	Torque Versus Rotation, Sample B-1, 19 Feet	104

LIST OF FIGURES (CONTINUED)

Figure		Page
53	Log-Log Plot of \bar{G} Versus Time, Sample B-1, 19 Feet	105
54	Torque Versus Rotation, Sample B-1, 46 Feet	106
55	Log-Log Plot of \bar{G} Versus Time, Sample B-1, 46 Feet	107
56	Torque Versus Rotation, Sample B-1, 61 Feet	108
57	Log-Log Plot of \bar{G} Versus Time, Sample B-1, 61 Feet	109
58	Torque Versus Rotation, Sample B-1, 85.5 Feet	110
59	Log-Log Plot of \bar{G} Versus Time, Sample B-1, 85.5 Feet	111
60	Torque Versus Rotation, Sample B-1, 100 Feet	112
61	Log-Log Plot of \bar{G} Versus Time, Sample B-1, 100 Feet	113
62	Torque Versus Rotation, Sample B-2, 22.5 Feet	114
63	Log-Log Plot of \bar{G} Versus Time, Sample B-2, 22.5 Feet	115
64	Torque Versus Rotation, Sample B-2, 40.5 Feet	116
65	Log-Log Plot of \bar{G} Versus Time, Sample B-2, 40.5 Feet	117
66	Torque Versus Rotation, Sample B-2, 72.5 Feet	118
67	Log-Log Plot of \bar{G} Versus Time, Sample B-2, 72.5 Feet	119
68	Torque Versus Rotation, Sample B-2, 104.5 Feet	120
69	Log-Log Plot of \bar{G} Versus Time, Sample B-2, 104.5 Feet	121

LIST OF FIGURES (CONTINUED)

Figure		Page
70	Torque Versus Rotation, Sample B-3, 55 Feet	122
71	Log-Log Plot of \bar{G} Versus Time, Sample B-3, 55 Feet	123

INTRODUCTION

In recent years foundation engineers have realized the importance of developing a reliable and accurate means of characterizing the stress-deformation behavior of submarine sediments. The only parameters available for design use have been the so-called engineering properties of the sediment, as determined from laboratory tests. These properties include ultimate shear strength (cohesion), Atterberg limits and other measures upon which much of the practice of soil mechanics is based. These parameters yield no quantitative information as to the stress-deformation behavior of the sediments prior to failure. In particular, they provide no means of characterizing time (and frequency) dependence of the sediment shearing resistance. Time dependence of the stress-strain relationship is particularly important in a large class of problems where dynamic, cyclic or vibration loadings exist, or in long term (creep) deformation analysis.

Sea floor instability has been recognized as a serious engineering problem (38)*. Review of previous efforts at prediction and analysis of instability of deltaic sediments will illustrate the need for characterizing the time dependency of the sediment.

*Numbers in parenthesis refer to references in Appendix I. (The citations follow the style of the Journal of Soil Mechanics and Foundations Division, American Society of Civil Engineers.)

Slides are known to have occurred in areas off the Mississippi River Delta of very slight slope, where conventional statical equilibrium analysis (using ultimate strength) yields factors of safety well above 1.0. It has thus been concluded that these slides are not entirely gravity controlled but are triggered by some mechanism causing the sediment to become unstable. Henkel (20) first produced a simplified model to indicate that bottom instability could be induced by cyclic hydrostatic bottom pressure variations caused by storm waves. Subsequent theoretical and experimental investigations have tended to verify that storm waves can induce instability and more complex methods of analysis have been proposed (42, 26). Wright and Dunham (42) developed a finite element model for the state of stress and deformation in the sediment when subjected to wave induced cyclic shear stresses. They treated the problem as one of static elasticity and assumed a hyperbolic stress-deformation relation. This, together with measured values of ultimate shear strength and an assumed value of Poisson's ratio, allowed estimation of an elastic shear modulus (non time-dependent). Gravity is neglected in the model and no information regarding the actual failure mechanism is obtainable. Mitchell, Tsui and Sangrey (26) set forth a method of analysis based on a gravity controlled failure which occurs because of wave induced reduction in soil shear strength. As with the finite element analysis, the strength reduction

approach is dependent on a measure of the ultimate shear strength of the sediment. No stress-strain characteristics are used and no information concerning the actual mechanism of failure is obtained. Additional experimental and theoretical treatments of submarine slides were recently reported (8, 1). These serve to further confirm that storm waves are the likely trigger mechanism but have added nothing toward an understanding of the mechanism of failure.

To fully understand the phenomenon a broad approach must be taken. The following elements are deemed essential to a realistic analysis:

1. Prediction of the state of the sea surface and the resulting particle motions and the dynamic pressures in the water column.
2. Determination of the dynamic stress-deformation characteristics of the bottom and sub-bottom sediments.
3. Analytical determination of the dynamic response of the bottom and sub-bottom material prior to failure and the interaction of this response with the water motion.
4. Determination of the sea state (wave conditions) that will produce complete bottom instability, and prediction of the subsequent characteristics of the failed mass.

Available analytical and statistical methods (21) can provide a reasonably accurate solution to element 1 above. Element 3 has



been partially treated by Gade (14) although this work dealt more with the effect of the bottom on the waves rather than the waves on the bottom. The works previously mentioned (1, 8, 26, 42) have attempted to provide answers relative to element 4; however, without sediment stress-deformation characteristics under dynamic loading and a realistic model of the combined motion of the water-sediment system (elements 2 and 3 above), these analyses have not provided a general slope instability theory. Schapery (34) has proposed a theoretical wave analysis of the combined motion of the water-sediment system which may provide this realistic model and lead to characterization of the onset and occurrence of instability. This work is currently in progress. Determination of the dynamic stress-deformation characteristics of the *in situ* sediments (element 2 above) remains.

With the foregoing in mind the general objective of this study was to investigate the *in situ* dynamic stress-deformation characteristics of sea floor clay sediments and to determine a means of quantifying these characteristics. The word *in situ* is a key word here. It is well known that sediment samples recovered from the sea floor undergo considerable and unpredictable disturbance due to mechanical sampling disturbance, expansion of gases in the sample, and other factors (28). Even with the most careful sampling procedures, the material properties obtained from laboratory tests of these samples cannot be called true measures of



these properties for the in situ material. The implication is, then, that determination of in situ material relationships should be based upon an in situ test conducted, insofar as possible, in the natural sediment environment.

The only known in situ soil strength measuring device capable of obtaining in situ sediment shearing resistance data at deep penetrations in bottom sediments is the wire line down hole vane shear device in use by McClelland Engineers, Inc. (9). This device has been used extensively for ultimate shear strength measurements. In addition, the vane in this device can be rotated at different rates and a continuous readout of torque (measure of sediment resistance to shear) versus rotation angle (measure of deformation) is available.

At the outset then, it was decided to pursue development of a procedure to utilize a down hole vane shear device to quantify a dynamic stress-deformation relation for sea floor clays. Schapery (34) proposed a method of obtaining such a relation from torque versus rotation vane shear data which treats the sediment as a nonlinear viscoelastic material. Specifically the proposed procedure results in the computation of a time dependent (viscoelastic) relaxation modulus in shear which can be generalized into a complex shear modulus.

This research, then, was undertaken with the following specific objectives:



1. To investigate (by literature review) the factors affecting the stress-deformation characteristics of sea floor clays and to review previous studies of the use of vane shear apparatus.
2. Determine the feasibility of characterizing sea floor clays by a viscoelastic shear modulus and of computing the modulus from vane shear data.
3. To investigate the use of the down hole vane shear device to obtain the required data for shear modulus determination.

BACKGROUND

No published information relating vane shear test data to viscoelastic sediment properties has been found in the literature. Several recent studies have characterized sea floor sediments as viscoelastic materials but few have quantified a relationship; although viscoelastic theory and experimental procedures are highly developed. The vane shear test has been widely studied as a means to determine the ultimate shear strength of clays and recently has been extended to in situ use for sea floor clays and more sophisticated laboratory studies.

In this section the basic nature and mathematical treatment of viscoelastic materials will be briefly reviewed; the literature characterizing clays as viscoelastic materials will be reviewed; and the proposed physical basis for the viscoelastic stress-deformation characteristics of sea floor sediments will be summarized. In addition, a review of the use of the vane shear test will be made.

Characterization of Viscoelastic Materials. - A material is said to be viscoelastic if stress in it is a function of current and/or past values of strain and strain rate. In more general terms, stress is a function of strain history. Ferry (12), Fung (13), Pipkin (30), among others, have presented detailed treatments of the fundamentals of viscoelasticity theory. In the

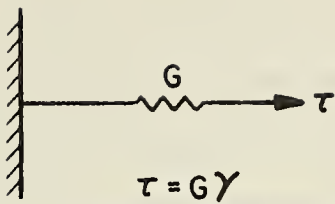
theory of linear viscoelasticity the material is often viewed as possessing properties of both linearly elastic (Hookean) solids and Newtonian fluids, and they are represented by combinations of the familiar spring and dashpot models (30, 44). Mathematically each Hookean element deforms in simple shear stress conditions according to:

$$\tau(t) = G \gamma(t) \dots \dots \dots (1)$$

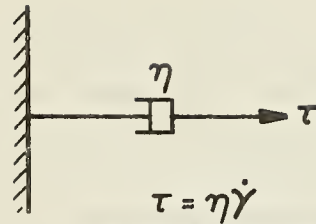
where $\gamma(t)$ is the shear strain, $\tau(t)$ is the corresponding stress and G is the elastic modulus in shear. Each Newtonian element deforms according to:

$$\tau(t) = \eta \dot{\gamma}(t) \dots \dots \dots (2)$$

where η is the fluid viscosity and $\dot{\gamma}(t)$ is the strain rate. In addition to the two fundamental model elements for representing viscoelastic materials, some investigators have employed the non-linear yield stress element, which is represented by a block, resting on a surface, which requires some minimum (yield) stress, τ_y , to set it in motion. Fig. 1 depicts the elementary model elements along with several common rheological models which have been employed for describing soil behavior. The differential equations of the associated stress-strain relations in shear are also shown. Yong and Warkentin (44) present additional models and develop the associated stress-strain equations. Suklje (39) presents an extensive treatment of the rheological nature of soils, including development of viscoelastic theories.



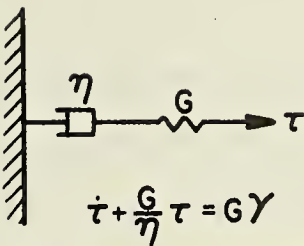
a. HOOKEAN SPRING



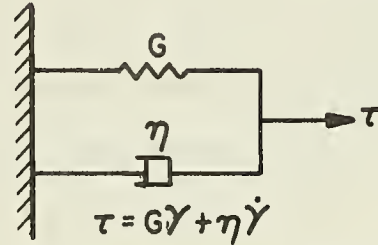
b. NEWTONIAN DASHPOT



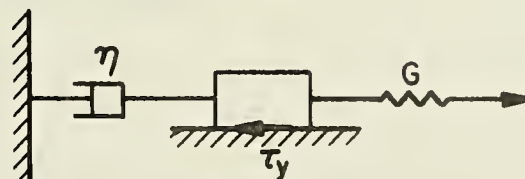
c. YIELD STRESS ELEMENT



d. MAXWELL MODEL



e. KELVIN-VOIGHT MODEL



$$\begin{aligned} \tau &= G\gamma \text{ at } \tau_y > \tau \\ \tau &= G\gamma + \eta \dot{\gamma} \text{ at } \tau_y < \tau \end{aligned}$$

f. BINGHAM MODEL

FIG. 1. - SIMPLE RHEOLOGICAL MODELS

These simple models are useful in visualizing material behavior, but, for most real materials, are too simple to provide accurate predictions of material behavior unless a large number of elements are used. Therefore, a more general mathematical statement for viscoelastic stress-strain behavior is desired. Linear viscoelastic materials, by definition, obey the law of superposition which says the response due to two simultaneous inputs is equal to the response due to one input alone, plus the response due to the other. These materials also obey the proportionality relation, that, at any t , the response due to an input times a constant equals the constant times the response due to input alone. For these materials the stress (or strain) response due to any continuous time dependent strain (or stress) input can be obtained by summing the responses due to an arbitrarily large number of input "steps" from the time of the beginning of load application (for nonaging materials) to any time of interest (30). For the case of a series of shear strain input steps we thus may obtain:

$$\tau(t) = \sum_{\alpha=1}^n G(t - t_{\alpha}) \Delta\gamma_{\alpha} \dots \dots \dots (3)$$

where: $G(t)$ is the shear modulus, a functional of time, n is the number of strain steps, $\Delta\gamma_{\alpha}$ is the strain change at step α and $t - t_{\alpha}$ is the time elapsed since application of strain step α . By passing this sum to the limit we obtain the so called heredity

or convolution integral for a linear, nonaging viscoelastic material undergoing any (time dependent) simple shearing strain input beginning at the time $t = 0$ (30).

$$\tau(t) = \int_0^t G(t - t') \frac{d\gamma(t')}{dt'} dt' \dots \dots \dots (4)$$

where $G(t)$ is the time dependent modulus and t' (taking the place of t_α Eq. 3) is a dummy variable of integration. The convolution equation, (Eq. 4), based on the linearity assumption, forms the basis for much of the mathematical treatment of viscoelasticity, and can be applied to the solution for stress or strain responses, given the function $G(t)$, or as a means of finding the response function, $G(t)$, from experimental stress-strain data. Eq. 4 will be utilized in later developments in this study.

Viscoelasticity in Sea Floor Sediments - Physical Basis. -

Investigations by Singh and Mitchell (37) and Mitchell et al. (25), among others, have provided experimental evidence that creep deformation in clay soils can be treated by viscoelastic stress-strain-time functions. On the basis of these results Schapery (32, 33) has included clays among such diverse materials as polymers, metals and biological tissue in characterizing nonlinear viscoelastic materials. There are many additional examples in the literature of the treatment of clays, in various modes of deformation, using viscoelastic rheological models or analyses (29, 35, 39, 43). In addition, several recent investigations have

specifically characterized sea floor clays as viscoelastic materials (36, 27, 6). Sherif et al. (36) and Monney (27) proposed the nonlinear model shown in Fig. 2 and showed creep test data on submarine sediments which were in close agreement with those predicted by the model. Monney (27) has pointed out that this

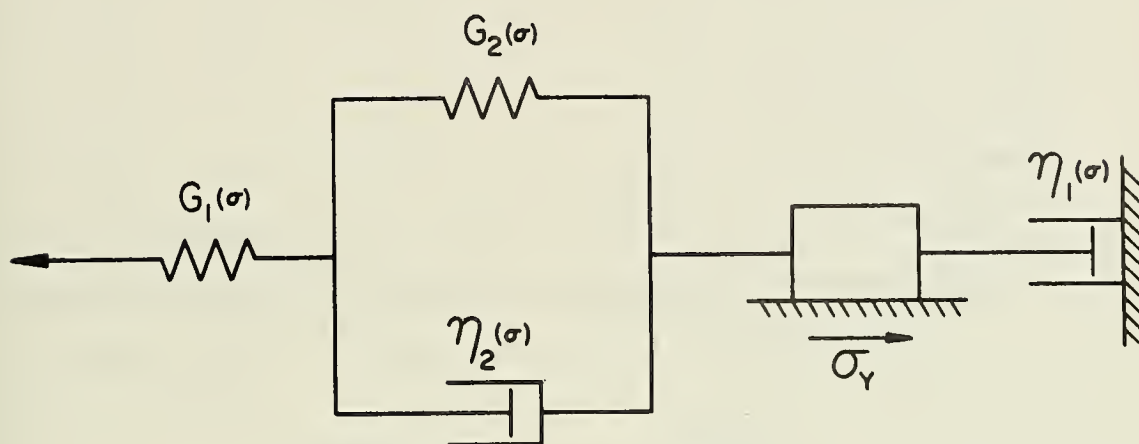


FIG. 2. - NONLINEAR RHEOLOGICAL MODEL FOR SEA FLOOR CLAYS PROPOSED BY SHERIF ET AL. [FROM SHERIF ET AL. (36)]

model is consistent with the work of Cohen (6) which indicated that nondispersed clay sediments behaved as nonlinear viscoelastic materials. Other experimental evidence supporting the treatment of submarine clays as viscoelastic materials is presented by Carpenter et al. (5) who used shear viscometer data on undisturbed samples of Mississippi Delta clays to obtain a constitutive equation for stress which involved strain and strain rates.

The physical mechanism of the stress-deformation response of clays is not well understood. However, a review of the probable causes of rate dependent behavior in submarine sediments is appropriate. Scott (35) and Wu (43) present general reviews of the factors affecting clay structure and stiffness. According to Sherif et al. (36) viscoelasticity in submarine sediments is largely a result of very high water contents and the type of clay structure. Salt water deposited clays can be thought of as composed of mineral platelets arranged in the so called flocculent or card house structure, such as depicted in Fig. 3, although several different proposals have been advanced for the exact structure (24). It is believed that, during the marine

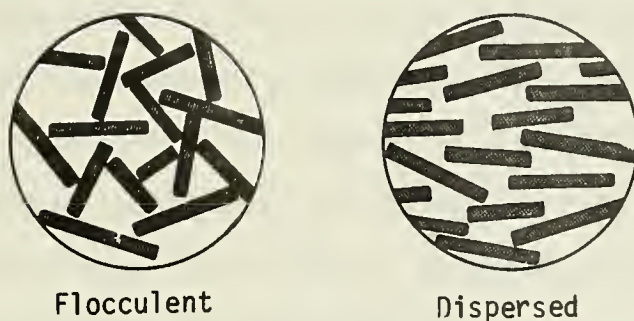


FIG. 3. - DEPICTION OF FLOCCULENT AND DISPERSED CLAY STRUCTURES
[FROM WU (43)]

depositional process, the individual clay particles acquire strong positive charges along their edges due to high hydrogen ion concentrations in these regions (43). In addition, due to isomorphous substitution (43) the flat sides of the platelets take on negative

surface charges. The result is that, as these particles settle, there are strong edge to face attractive forces which overcome weaker repulsive forces and cause the particles to come into contact or bond together in the edge to face or card house or flocculent structure (43). Lambe (22) has characterized the attractive forces as largely van der Waal's forces.

The water in the interstitial spaces exists in two states, pore water and absorbed water. The pore water is "free" in the interstitial spaces while the adsorbed water is a layer or film of water molecules held tightly to each clay particle by hydrogen bonding and other forces. According to Grim (16) the adsorbed water is actually more dense, and much more viscous than the pore water. It must be noted that the above description of clay structure and formation is highly simplified. Complex ionic interactions are involved in the depositional process which depend on the type of clay mineral involved and the ionic content of the water (16); however, treatment of these in detail is beyond the intent of this discussion.

From this simplified model of clay structure the process of deformation under shear can be considered and some of the factors affecting the viscoelastic nature of submarine clays can be identified. When the flocculent clay structure is subjected to shear the bonds between the particles are first strained. As the bonding forces are progressively overcome along a shear

surface, and shearing continues, the viscous shear resistance of the pore water becomes important as the clay particles along the shear surface tend to orient themselves into a more dispersed or oriented structure (see Fig. 3, page 13) (35).

Interparticle contacts along the shear surface are broken as the particles move to the dispersed structure. This may have several effects. Part of the normal stress across the failure surface will be shifted to the pore water causing an increase in pore water pressure. The increased pore water pressure tends to force water out of the strained area. If sheared rapidly the water cannot escape (undrained condition) and the result is decreased shear resistance. If sheared very slowly (drained condition), so that the pore water can escape the effect of the shifting of the particles to a dispersed structure will be less. The shear resistance will then tend to be greater. The rate of migration (drainage) of the pore water in the clay is, of course, a function of its viscosity.

Leonards and Girault (23) have presented evidence that the adsorbed water may also play a role in the viscoelastic behavior of clays.

Summarizing, viscoelastic behavior in sea floor clays may be attributed to a combination of clay structural changes, shearing and migration of the pore water, and effects of the adsorbed water. These phenomena are controlled by the type of clay

mineral, the ionic constituents of the water at the time the clay was deposited, the void ratio (i.e. relative amount of water in the pores for saturated sediments), the viscosity of the pore water, and the rate of shearing.

Experience With the Vane Shear Test. - Since the classic work of Cadling and Odenstad (4) the vane shear test for shear strength of clays has become a widely used test both in situ and in the laboratory. The conventional vane test consists of turning a four bladed (usually rectangular blades) vane in the soil and measuring the torque required to shear the soil around the cylinder of revolution of the vane. The basic test is depicted in Fig. 4. Until recently almost all vane shear

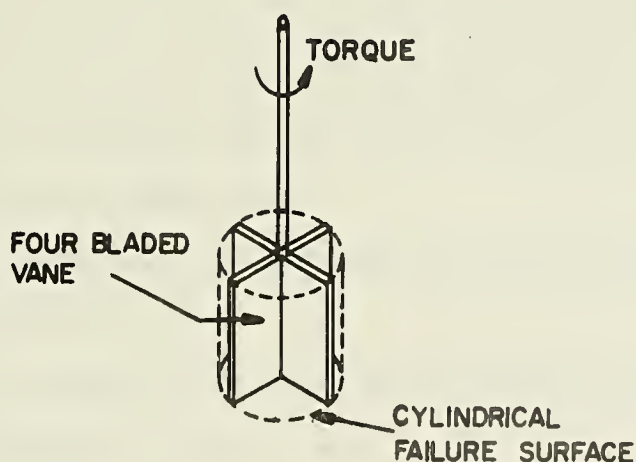


FIG. 4. - BASIC VANE SHEAR TEST

instruments were hand operated and the torque was measured by noting the deflection of a calibrated spring integral to the vane shaft. This discussion is intended to briefly summarize the theory and use of the vane shear test and to describe recent investigations of its use on submarine sediments, both in situ and in the laboratory.

Cadling and Odenstad (4) presented the most complete mathematical treatment of the vane test to date and provided the first substantial experimental evidence of its applicability in clays. Their experiments provided evidence that:

1. The failure surface caused by rotating a four bladed vane in clay is closely approximated by a right circular cylinder.
2. The effect of progressive failure (failure starting in front of the edge of the blades and propagating along the cylindrical surface) was negligible in ultimate strength tests.
3. The strength of the clay was affected by the vane rotation rate.
4. A vane length to diameter ratio of about two was most suitable for in situ tests.

Gibbs (15) offered further evidence that the failure surface is cylindrical. Eden and Hamilton (10) and Gibbs (15) showed that vane insertion causes minimal disturbance effects.

The calculation of the shear strength from vane tests using rectangular blades is normally accomplished using the equation:

$$T_{\max} = C_u \left(\frac{\pi d^2 L}{2} + \frac{\pi d^3}{6} \right) \dots \dots \dots (5)$$

where

T_{\max} = maximum vane shaft torque measured to failure

C_u = ultimate soil shear strength (also called cohesion)

d = vane diameter

L = vane length

Eq. 5 is obtained by summing the torque due to the shear resistance of the clay over the cylindrical failure surface, and the top and bottom.

The vane test is particularly applicable to very soft clays for which it is difficult to obtain and test undisturbed samples by other soil strength tests (4, 41). L. Casagrande first reported use of the in situ vane shear test in underwater sediments (4). He used the test in river sediments at water contents above the liquid limit. These and later tests (4) indicated the vane shear determined strengths were 1-2 times the strengths determined on laboratory samples using other tests. Gray (17) compared strengths from field vane tests to those obtained from laboratory tests of samples obtained in thin walled core tubes. The clay was sensitive and low strength. The laboratory vane shear strengths were less than the in situ

values but were greater than the strengths as determined from other laboratory tests. The lower laboratory values were attributed to sampling disturbance (17).

Fenske (11) conducted the first comprehensive study of the use of the vane test on submarine sediments. His tests were conducted in Mississippi River delta sediments off the coast of Louisiana. In situ vane shear strengths were measured to depths of 241 feet where the water depth was 66 feet. The device used was a combination vane shear device and borehole drilling head as shown in Fig. 5. Fenske conducted extensive comparisons of in situ vane, miniature laboratory vane from undisturbed cores and unconfined compression strengths. Fig. 6 summarizes the comparison and indicates that the act of sampling and raising submarine sediments to the surface changes the strength properties. Hall (18) demonstrated the use of the more refined Swedish Foil Sampler to reduce sample disturbance, but this device is complex and is not easily applicable to ocean work. The occurrence of disturbance due to submarine sampling and recovery is largely a result of mechanical sampling disturbance and the expansion of dissolved gases as the hydrostatic pressure is reduced (28).

With the increasing requirement to design foundations for sea floor structures several additional recent investigations of in situ vane testing have been conducted (31, 7, 9). Richards et al. (31) and Demars and Taylor (7) were concerned with

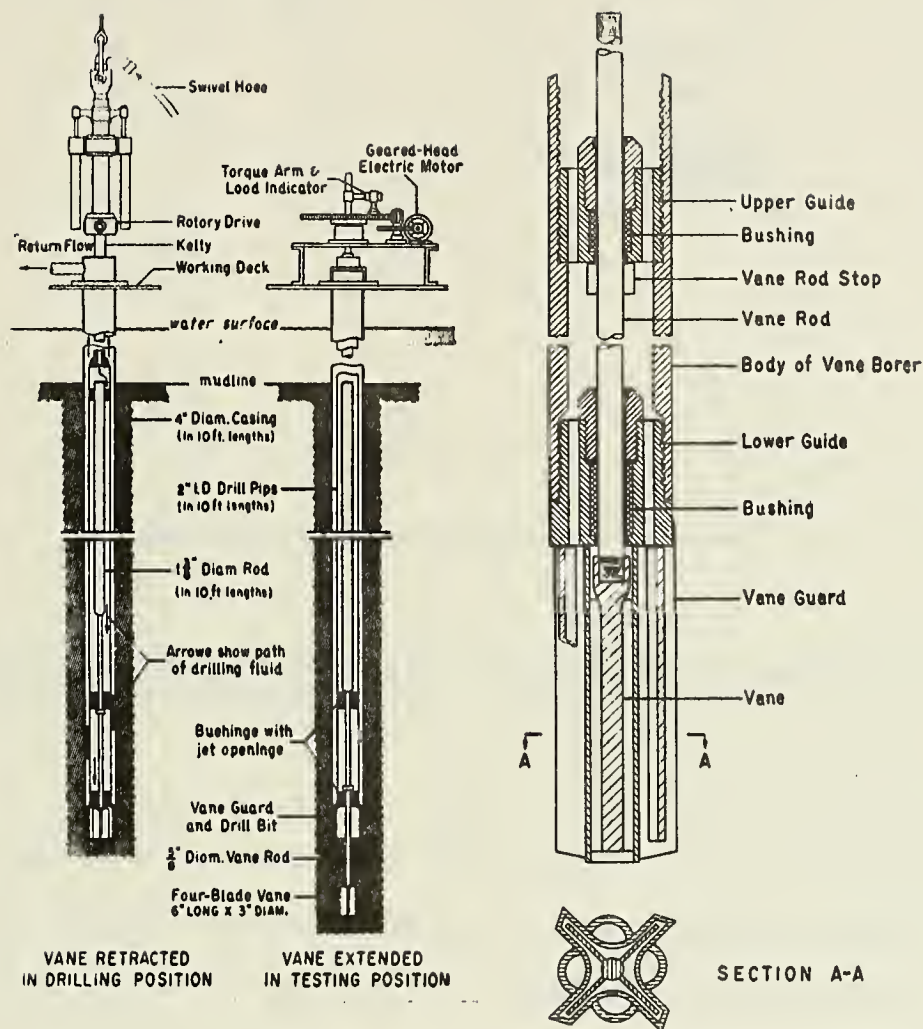


FIG. 5. - DOWN HOLE SUBMARINE VANE TEST AND BORER OF FENSKE
[FROM FENSKE (11)]

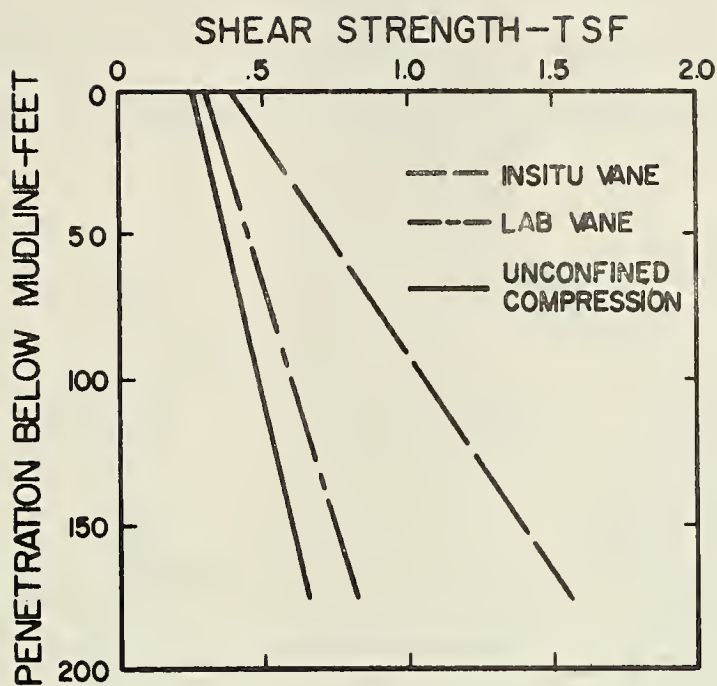


FIG. 6. - COMPARISON OF IN SITU AND LABORATORY ULTIMATE SHEAR STRENGTHS [AFTER FENSKE (11)]

evaluation of bottom resting devices capable of obtaining vane shear strengths to sediment depths of only a few feet. These studies are further evidence of the applicability of the vane test and tend to confirm the comparisons obtained by Fenske. Doyle et al. (9) have demonstrated a remotely controlled wire line vane test device, developed by McClelland Engineers, Inc., for down hole vane measurements in undersea clays. The device is lowered inside the borehole casing and can be used alternately with the 2.25 inch wire line core sampler used extensively



offshore. This allows practically continuous in situ vane testing and "undisturbed" sampling for the full length of a bore hole. The device and sequence of operation is depicted in Fig. 7. It

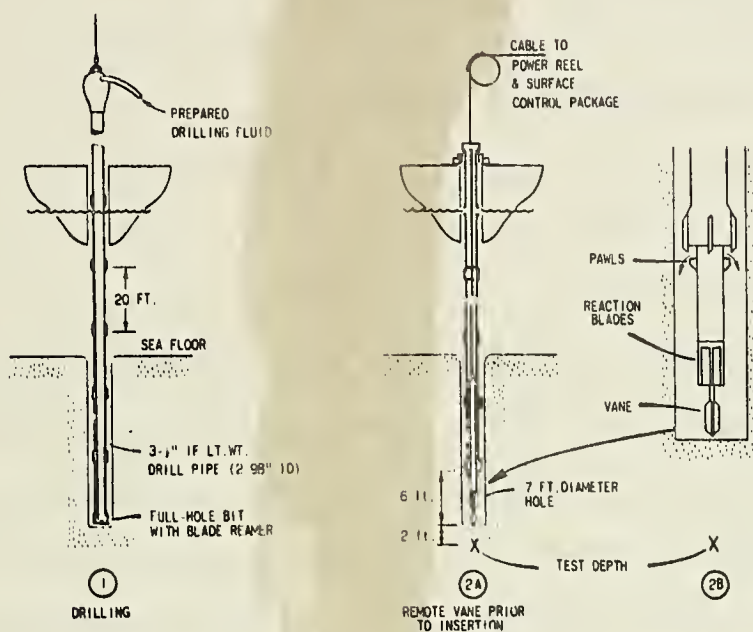


FIG. 7. - DOWN HOLE WIRE LINE SUBMARINE VANE SHEAR DEVICE OF McCLELLAND ENGINEERS [FROM DOYLE ET AL. (9)]

can be operated from a floating platform and is considered by the author to be the only practicable deep penetration sea floor test device presently available. The wire line vane device is capable of several different vane rotation rates and of measuring torque versus rotation angle data. (This fact will be useful later in this study.)



Coincidental with the development of in situ vane tests there has been a recent trend toward sophistication of the laboratory vane instruments for sea floor sediment sample tests. Precision and sensitivity beyond the capabilities of hand cranked, spring loaded torque measurement devices is required in the study of sea floor sediments. In addition, the recognition of the importance of the rheologic nature of sea floor clays has prompted the development of vane shear instruments which provide a constant readout of torque versus rotation (27). The most recent instruments employ controlled speed motorized vanes and measure torque using strain gauged torque transducers (27, 19). These devices avoid the problems of inaccurate determination of actual vane rotation angle and speed, and the build up of strain energy in the load measuring spring of the conventional devices is eliminated. Furthermore, a continuous record of torque versus vane rotation is obtainable. It shall be later demonstrated that these features are essential to the vane shear determination of the viscoelastic properties of submarine clays.



THEORETICAL BASIS FOR EXPERIMENT

One objective of this research was to develop a procedure to determine a viscoelastic shear modulus for sea floor sediments. Such a procedure can be only as good as the samples tested. As noted in the previous section the mere act of sampling and recovering samples seriously disturbs them. Thus a determination based upon in situ measurements would be most desirable. As a matter of practical importance, it has been noted that in situ sediment shearing resistance versus rotation data at different rotation rates can be obtained using the wire line vane shear device of McClelland Engineers. It was thus deemed desirable to develop a laboratory vane shear test and analysis procedure which could be evaluated and, if valid, extended for use with in situ data. This section derives the equations and outlines the computational method used. The theory presented here is an exposition of the proposed procedure of Schapery (34) for computation of the viscoelastic shear modulus from vane test data. The procedure involves initial solution under the assumption of linearly elastic sediment, from which the linear viscoelasticity solution can be obtained; and finally a graphical characterization of the nonlinearity of the sediment is derived.

Calculation of Shear Modulus from Vane Test Data - Elastic

Assumption. - First consider the sediment to be an infinite mass of homogeneous, isotropic linearly elastic clay. Consider an embedded vane rotated through an angle θ . Assuming that the vane is rotated fast enough to insure undrained conditions and migration of pore water is not important, the applied torque, T , may be characterized by:

$$T = f(a, L, G, \theta) \dots\dots\dots (6)$$

where a and L are the vane radius and length, respectively, and G is the elastic shear modulus. Eq. 6 can be alternately expressed as:

$$0 = f(T, a, L, G, \theta) \dots\dots\dots (7)$$

which, by dimensional analyses and the Buckingham Pi Theorem, can be expressed as:

$$0 = f\left(\frac{T}{Ga^2L}, \frac{a}{L}, \theta\right) \dots\dots\dots (8)$$

and can be solved for T :

$$T = Ga^2L \cdot f_1\left(\frac{a}{L}, \theta\right) \dots\dots\dots (9)$$

The linearity assumption implies that T is proportional to θ . Applying this to Eq. 9 and rearranging the geometry terms yields:

$$T = G\theta a^2L \cdot f_2\left(\frac{a}{L}\right) \dots\dots\dots (10)$$

The quantity $f_2\left(\frac{a}{L}\right)$ is a constant which depends at most on dimensionless ratios defining the vane geometry. It is noted that this

result was obtained using only the vane length and width as defining the vane geometry. If other geometry factors are used, however, the same result is obtained, i.e., f_2 is a dimensionless constant for any vane geometry, and depends on geometry ratios only. If f_2 is defined as the vane geometry factor, B , then Eq. 10 becomes:

$$T = Ba^2LG\theta \quad \dots \dots \dots (11)$$

Since B depends only on geometrical ratios it will be the same for all geometrically similar vanes, regardless of absolute size. (This fact will be used later to extend the laboratory study to the in situ case.)

Under the elastic assumption Eq. 11 can be used to compute the modulus G if torque versus rotation data were obtained. It is first necessary, however, to determine the numerical value of the vane geometry factor B . Methods of determining B are described at the end of this section. Attention will now be turned to the viscoelastic case.

Obtaining the Linear Viscoelasticity Solution from the Elastic Equation. - The above discussion has been limited to characterization of a linearly elastic material. Eq. 11 constitutes the elastic solution for a rotating vane in the clay mass. For many viscoelasticity problems and the present one in particular, the linear viscoelastic solution can be found from the Laplace Transform of the elastic equation, so long as the kind

of data (strain, strain rate, etc.) specified at any specific boundary point is the same at all times. This statement is known as the correspondence principle (30). The correspondence principle is valid as long as the material response can be described by constitutive equations of the convolution form which implies the material is nonaging and temperature dependency of the response is not important. Each of these conditions being satisfied in the case of the vane shearing of clay, the correspondence principle may be applied. First, taking the Laplace Transform, $\mathcal{L}\{f(t)\}$, of each of the variables in Eq. 11 yields:

$$\mathcal{L}\{T(t)\} = Ba^2 L G \mathcal{L}\{\theta(t)\} \quad (12)$$

Then, applying the correspondence principle the linear viscoelastic solution can be obtained by replacing G with $s \mathcal{L}\{G(t)\}$, where $G(t)$ is the relaxation modulus in shear, and s is the Laplace Transform parameter, and finding the inverse.

$$\mathcal{L}\{T\} = Ba^2 L s \mathcal{L}\{G\} \mathcal{L}\{\theta\} \quad (13)$$

Taking the inverse transform yields:

$$T = Ba^2 L \int_0^t G(t-\tau) \frac{d\theta}{d\tau} d\tau \quad (14)$$

where $G(t)$ is the viscoelastic relaxation modulus in shear, τ is a dummy time variable of integration and $(t-\tau)$ represents the time elapsed since rotation began. Eq. 14, then, is the viscoelastic equivalent of Eq. 11 and we see that the result amounts to the replacement of the product $G\theta$ with the so called convolution

integral, which forms the basis for linear viscoelasticity theory.

For constant rotation rates Eq. 14 can be simplified into a form analogous to Eq. 11 by first letting

$$\frac{d\theta}{dt} = C \quad \dots \dots \dots (15)$$

where C is a constant and thus, at any specified time t:

$$\frac{\theta}{t} = C \quad \dots \dots \dots (16)$$

Then $d\theta/dt$ can be removed from the integral to obtain:

$$T = Ba^2L \frac{\theta}{t} \int_0^t G(t-\tau) d\tau \quad \dots \dots \dots (17)$$

$$\text{for } \frac{d\theta}{dt} = C$$

Further, a change of variable in the integral:

$$t' = (t-\tau) \quad \text{at } \tau = 0, t' = t$$

$$dt' = -d\tau \quad \tau = t, t' = 0$$

yields:

$$T = Ba^2L \frac{\theta}{t} \int_0^t G(t') dt' \quad \dots \dots \dots (18)$$

or

$$T = Ba^2L \theta \left[\frac{1}{t} \int_0^t G(t') dt' \right] \quad \dots \dots \dots (19)$$

It is recognized that the term in brackets in Eq. 19 is the time averaged value of the shear modulus $G(t)$ and denoting this by \bar{G} ,

Eq. 20 is obtained:

$$T = Ba^2L \theta \bar{G} \quad \dots \dots \dots (20)$$

where

$$\bar{G} = \bar{G}(t) \equiv \frac{1}{t} \int_0^t G(t') dt' \dots \dots \dots (21)$$

Now the viscoelastic relaxation modulus of clays can often be characterized as a power law in time (25, 33). If such a relation is assumed for $G(t)$ we obtain:

$$G(t) = G_1 t^{-n} \dots \dots \dots (22)$$

where G_1 and n are constants. Using the definition of \bar{G} above (Eq. 21) we obtain

$$\bar{G} = \frac{1}{t} \int_0^t G_1 t'^{-n} dt' \dots \dots \dots (23)$$

or

$$\bar{G} = \frac{G_1}{1-n} t^{-n} \dots \dots \dots (24)$$

Evaluation of G_1 and n in Eq. 22 would constitute a solution to the linear viscoelasticity problem. Eqs. 20 and 24, together, provide the framework for determining these constants from constant rate vane shear data. The computational procedure is outlined below.

First, however, it is of interest to note that in applications where sediment response to cyclic or vibrational inputs is desired (such as the wave induced slope stability problem) then a frequency dependent complex shear modulus, G^* , is required, where:

$$G^* = G' + iG'' \dots \dots \dots (25)$$

G' and G'' are constants and $i = \sqrt{-1}$. G^* can easily be obtained, given the input frequency, ω , and the values of G_1 and n of Eq.

22. G' and G'' are computed from:

$$G' = [G_1 \Gamma(1-n) \cos \frac{n\pi}{2}] \omega^n \dots \dots \dots (26)$$

$$G'' = [G_1 \Gamma(1-n) \sin \frac{n\pi}{2}] \omega^n \dots \dots \dots (27)$$

where $\Gamma(1-n)$ is the Gamma function with argument $1-n$. Eqs. 26 and 27 are obtained from well known viscoelastic theory, given the power function, Eq. 22, and a sinusoidal input.

Computational Procedure and Characterization of Non-

linearity. - It is now shown how Eqs. 20 and 24 can be used to characterize the material from vane test data. Suppose a series of vane tests were run on the same material, each test at a different constant rotation rate, $\dot{\theta} \equiv \frac{d\theta}{dt}$. Continuous measurement of torque versus rotation angle would yield data such as shown in Fig. 8, where the ordinate variable is normalized torque, T_n :

$$T_n \equiv \frac{T}{Ba^2L} \dots \dots \dots (28)$$

By selecting an angle, say θ_a , \bar{G} can be computed for each rotation rate $\dot{\theta}_1, \dot{\theta}_2, \dot{\theta}_3$ etc. by Eq. 20, i.e.:

$$\bar{G} = \frac{T}{Ba^2L\dot{\theta}} = \frac{T_n}{\dot{\theta}} \dots \dots \dots (29)$$

By determining the corresponding time for each $\dot{\theta}$, the plot of $\log \bar{G}$ versus $\log t$ shown in Fig. 9 for θ_a can be obtained.

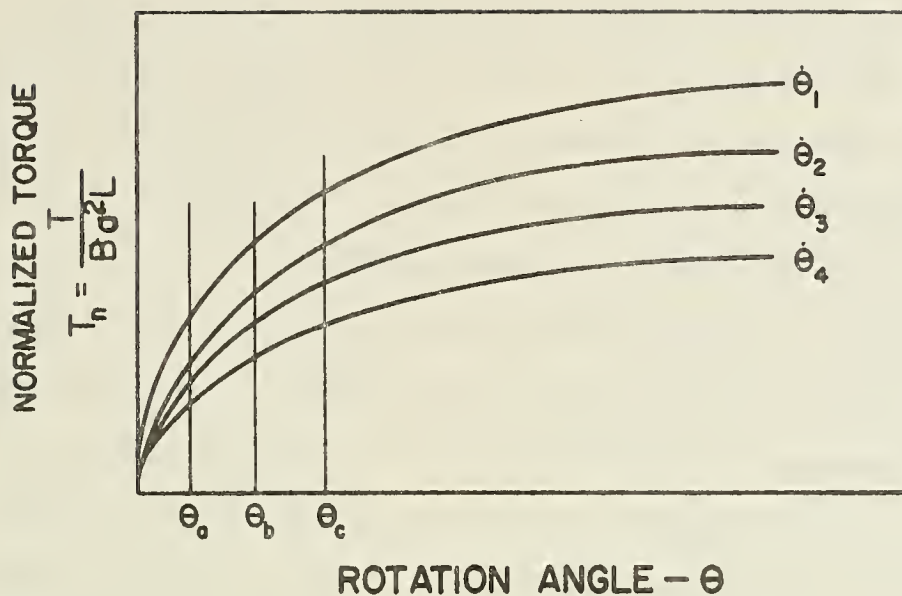


FIG. 8. - NORMALIZED TORQUE VERSUS ROTATION ANGLE AT VARIOUS ROTATION RATES

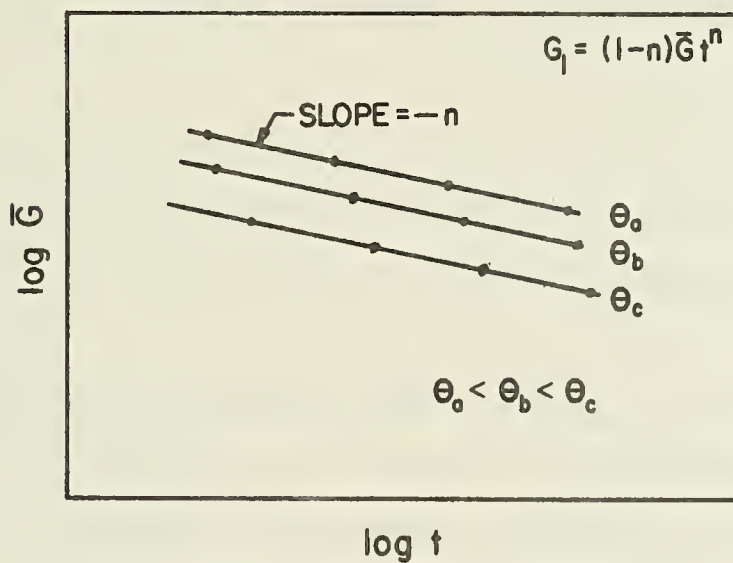


FIG. 9. - MODULUS VERSUS TIME FOR VARIOUS ANGLES OF ROTATION

Now, if the real behavior of the material can be represented by the power law (Eq. 22) then from Eq. 24 we see that the $\log \bar{G}$ versus $\log t$ plot at θ_a will be a straight line of slope $-n$. Also, if the material is linearly viscoelastic, by definition (see Eq. 21) \bar{G} is not dependent upon θ and the $\log \bar{G}$ versus $\log t$ plot for all angles will be the same straight line. Significant departure from the assumed power law can be noted if the data do not plot on a straight line, and nonlinearity (θ dependence) is revealed by separation of the plots for different angles θ_a , θ_b , θ_c etc. as shown in Fig. 9. Thus direct assessment of the nonlinearity is available from examination of the graph.

Once Fig. 9 is obtained n is found from the slope (slope = $-n$) and G_1 is obtained by selecting any time, finding the corresponding \bar{G} from the figure (at the desired θ) and computing G_1 from Eq. 24, i.e.:

$$G_1 = \bar{G} (1-n)t^n \dots \dots \dots (30)$$

With n and G_1 determined $G(t)$ can be determined for any t using Eq. 22, and the complex modulus, G^* , can be determined using Eqs. 25 through 27.

Determination of the Vane Geometry Factor, B. - In the discussion above the factor B was obtained as a dimensionless constant for any particular vane geometry, regardless of absolute size. In order to use vane shear data to find $G(t)$ it is

necessary to evaluate B for the vane shape being used. B can be determined in several ways:

1. By theoretical estimate.
2. By running vane tests on a material of known viscoelastic properties and computing B from Eq. 20.
3. By running vane tests on a thick fluid of known viscosity and computing B from the relation $T = Ba^2L\dot{\theta}\eta$ where η is the viscosity of the fluid.
4. By measuring G for the sediment by some other means and using it, with vane test data, in Eq. 20.

These methods will be explored further here.

It is first useful to derive the theoretical estimate. To accomplish this consider a homogeneous, isotropic, clay mass of infinite extent. Replace the vane by a long rigid cylinder of radius, a . The clay is considered linearly elastic and is assumed to adhere to the surface of the cylinder. As the cylinder is rotated the shear stress across the cylindrical surface is uniform. The shearing stresses and deformations in the clay surrounding the cylinder can now be derived in the manner presented by Cadling and Odenstad (4).

Fig. 10 depicts the shearing stresses acting on a volume element a distance, r , from the center of rotation. Due to the symmetry of rotation the element is subjected only to the net

shearing stresses τ_r and $\tau_r + d\tau$. The equation of equilibrium for a radial slice is:

$$\tau_r = \frac{a^2}{r^2} \tau_a \dots \dots \dots (31)$$

where τ_a is the shearing stress at the cylinder surface. Now introduce the relation:

$$\tau_r = G \gamma_r \dots \dots \dots (32)$$

where G , as usual, is the elastic shear modulus and γ_r is the shearing strain at r . Combining Eqs. 31 and 32 yields:

$$\gamma_r = \frac{a^2}{r^2} \gamma_a \dots \dots \dots (33)$$

where γ_a is the shearing strain at the cylinder surface. As depicted in Fig. 11, during rotation each clay particle moves a short distance on a circle of radius, r . The particles at any r move through an angle:

$$\theta = \theta(r) \dots \dots \dots (34)$$

If the particles at $r + dr$ were to move a distance $(r + dr) \theta$ on a circle, then no shearing would occur in the element at r . In reality, the particles at $r + dr$ move a distance $(r + dr)(\theta + d\theta)$. Hence, the strain at r is:

$$\gamma_r = \frac{(r + dr) \theta}{dr} - \frac{(r + dr)(\theta + d\theta)}{dr} \dots \dots \dots (35)$$

$$\gamma_r = -(r + dr) \frac{d\theta}{dr} \dots \dots \dots (36)$$

which, as the size of the element is allowed to vanish, yields:

$$\gamma_r = -r \frac{d\theta}{dr} \dots \dots \dots (37)$$

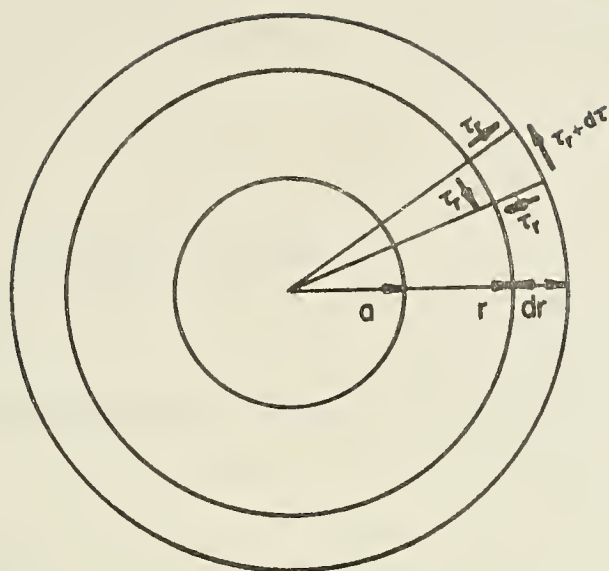


FIG. 10. - SHEARING STRESSES ACTING ON ELEMENT OF CLAY DUE TO ROTATING CYLINDER

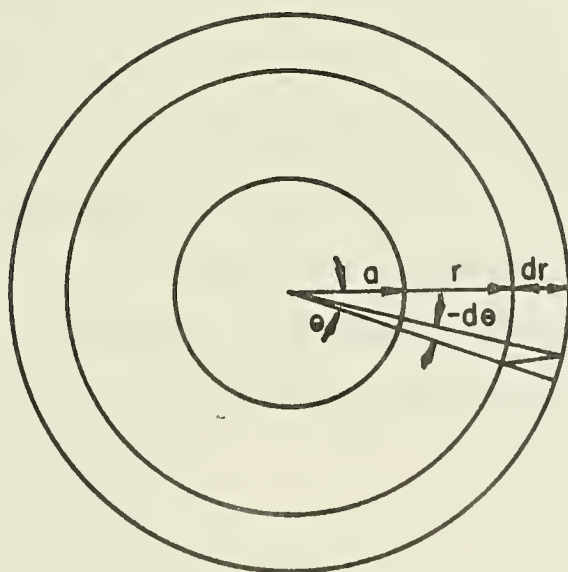


FIG. 11. - DEFORMATION OF CLAY SURROUNDING ROTATING CYLINDER

Now, combining this result with Eq. 33 and dropping the negative sign we obtain:

$$\frac{d\theta}{dr} = \frac{a^2}{r^3} \gamma_a \dots\dots\dots (38)$$

which can be integrated to yield:

$$\theta = \frac{1}{2} \frac{a^2}{r^2} \gamma_a + C \dots\dots\dots (39)$$

where C is determined when $\theta = 0$ at $r = \infty$ and is, $C = 0$. Therefore:

$$\theta = \frac{1}{2} \frac{a^2}{r^2} \gamma_a \dots\dots\dots (40)$$

from which we obtain, at the surface of the cylinder:

$$\theta_a = \frac{1}{2} \gamma_a \dots\dots\dots (41)$$

and substituting Eq. 32 at $r = a$:

$$\theta_a = \frac{1}{2} \frac{\tau_a}{G} \dots\dots\dots (42)$$

With this result in mind we now turn to the determination of the torque on a rectangular vane of length L, in terms of the shearing stress τ_a at the surface of the cylinder of revolution (the assumed failure surface). Neglecting end effects, the torque is the moment produced by the shearing stress τ_a on the surface of the cylinder, which is:

$$T = 2\pi a^2 L \tau_a \dots\dots\dots (43)$$

substituting τ_a from Eq. 42 yields:

$$T = 4\pi a^2 L \theta_a G \dots\dots\dots (44)$$

and since θ_a is just the angle through which the vane is turned we now drop the subscript and compare Eq. 44 with the Eq. 11 to obtain:

$$B = 4\pi \dots \dots \dots (45)$$

It is emphasized that this is merely an estimate. In practice B must be determined from one of the empirical procedures listed above, especially if the vane blades are not rectangular and the surface of revolution of the vane is not a cylinder.

Pursuing this development further, however, will yield an estimate of the effect of not having an infinitely wide mass of clay, i.e., the effect of container size. Assume that the vane is rotated about the longitudinal axis of a cylindrical sediment sample in a container of inside radius, b. The shearing displacement at the inside of the container will be zero. Making use of Eq. 39 but this time evaluating the constant, C, with $\theta = 0$ at $r = b$ yields:

$$C = -\frac{1}{2} \frac{a^2}{b^2} \gamma_a \dots \dots \dots (46)$$

$$\theta = \frac{1}{2} \gamma_a a^2 \left(\frac{1}{r^2} - \frac{1}{b^2} \right) \dots \dots \dots (47)$$

or, solving for γ_a :

$$\gamma_a = \frac{2\theta}{a^2 \left(\frac{1}{r^2} - \frac{1}{b^2} \right)} \dots \dots \dots (48)$$

Now, making use of Eqs. 43 and 32 at a we obtain:

$$\gamma_a = \frac{T}{2\pi a^2 LG} \dots \dots \dots (49)$$

Combining this with Eq. 48 at $r = a$, solving for T and rearranging, yields:

$$T = \frac{4\pi a^2 LG\theta}{(1 - \frac{a^2}{b^2})} \dots \dots \dots (50)$$

Comparing this with Eq. 11 yields:

$$B = \frac{4\pi}{(1 - \frac{a^2}{b^2})} \dots \dots \dots (51)$$

From this result we see that if a is less than about $.3b$ then the ratio a^2/b^2 will be small, $B \approx 4\pi$, and the effect of the container will be negligible for all practical purposes.

Attention is now turned to the empirical methods for determining B . The most convenient, from an experimental standpoint, are methods 2 and 3 (see page 33). However, method 2 is impractical because it is difficult to find linearly viscoelastic materials which can be used as standards. Method 3, based on the equation:

$$T = Ba^2L\eta\dot{\theta} \dots \dots \dots (52)$$

is more easily applicable, where η is the viscosity of a reference fluid. This equation is obtained in the same manner as was Eq. 11, where the linearly elastic material is replaced by a Newtonian fluid of viscosity η . For experimental purposes the fluid used should offer shearing resistances the same order of magnitude as those expected from the clay sediments at the rotation rates to

be used. The use of this technique is demonstrated in the following section on experimental procedure.

The last method available for determining B is to measure \bar{G} of the sediment by an independent experimental method and compute B using \bar{G} , vane test data and Eq. 20. One such independent method for finding \bar{G} is measurement of sediment response to a vibrational input. Briar and Bills (3) have demonstrated such measurements in solid rocket propellants. Their method employs a small piezoelectric disc which is inserted in the sample and electrically excited. The voltage and frequency response output, together with the response obtained in air can be used to compute the complex modulus, from which \bar{G} can be easily obtained (3). The technique has also been used by Cohen (6) and others, on submarine sediment samples. Cohen's device was a piezoelectric bar excited into torsional vibration.

EXPERIMENTAL PROGRAM

The laboratory phase of this research involved development of a precision laboratory vane shear device and test of submarine core samples at different rotation rates. As discussed below, the samples were obtained from three boreholes off the coast of Louisiana. The wire line vane shear device developed by McClelland Engineers was used to measure torque versus rotation, at several rotation rates, and at several locations in one of the boreholes. On the basis of the theoretical development above, the laboratory vane was constructed to be geometrically similar to the wire line vane, thus making possible a comparison of the laboratory and in situ rate tests.

The laboratory vane shear apparatus was designed to meet the following primary criteria.

1. Continuously record torque versus rotation data while rotating a vane at constant rotation rates in sediment core samples.
2. Operate at rotation rates ranging over several decades, with the rates available in the McClelland wire line vane included.
3. Incorporate a vane geometrically similar to that used in the McClelland wire line device to make possible comparison of results.

Description and Operation of Apparatus. - Fig. 12 shows the experimental apparatus for the vane tests, and Fig. 13 shows the details of the vane shear device. The device consists of a small variable speed D. C. motor which drives the vane shaft through a step function speed reducer with output to input speed ratios of 1:1 to 1:1000 in 10 steps. The total rotation speed range thus obtained is 5×10^{-5} radians/sec to 0.57 radians/sec. Torque on the vane due to sample shearing resistance is measured by a strain gaged torque transducer and is recorded on a Visicorder recording oscillograph as a plot of torque versus time. The torque sensitivity of the instrument is 0.001 in.-lb, with full scale settings from 0.2 in.-lb to 10 in.-lb available. With the vane and motor used, stiffness data on sediments ranging in stiffness from less than 10 psf to over 500 psf can be obtained. Rotation is measured by the change in resistance of a single turn linear, precision potentiometer connected to the vane shaft by anti-backlash gears. The gears provide a vane shaft to potentiometer shaft rotation ratio of 1:3.67. Rotation readout is a continuous plot of rotation angle versus time on a second channel of the Visicorder. Vane rotation changes of less than 0.005 radians are resolvable. Vane operation is controlled via a control module which houses the on-off-reverse switches for the vane motor and circuitry associated with the rotation transducer. The vane is shown in Fig. 14.

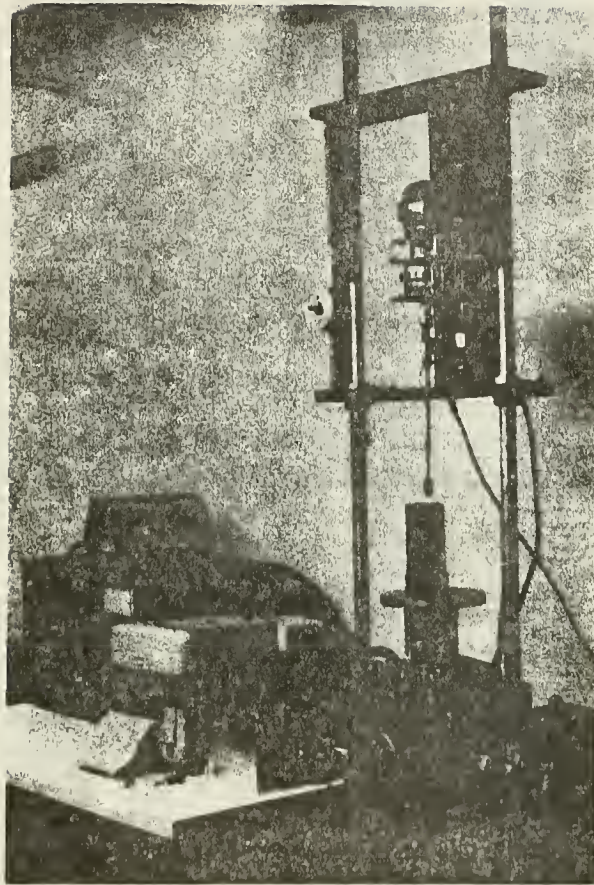


FIG. 12. - TEST APPARATUS FOR LABORATORY VANE
SHEAR RATE TESTS

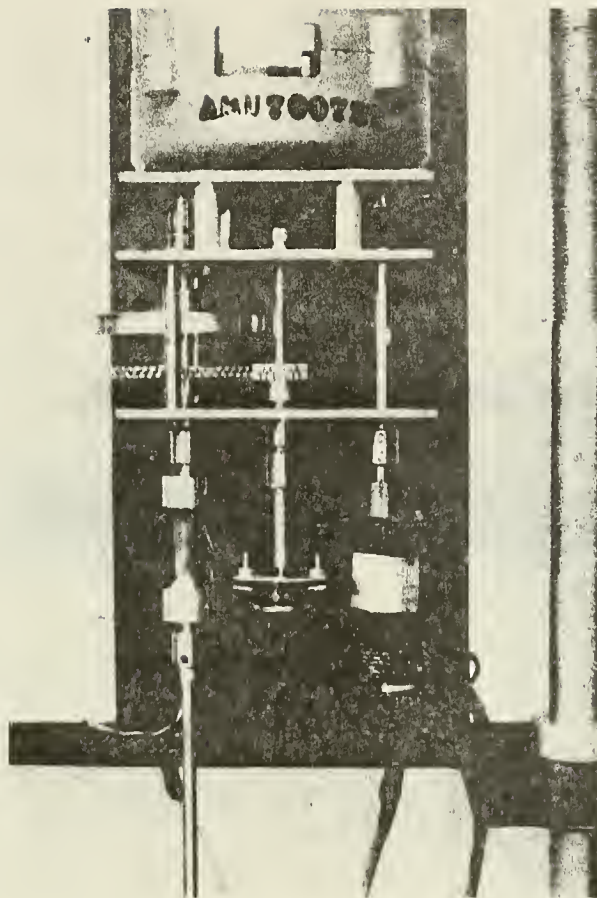


FIG. 13. - DETAILS OF VANE SHEAR DEVICE

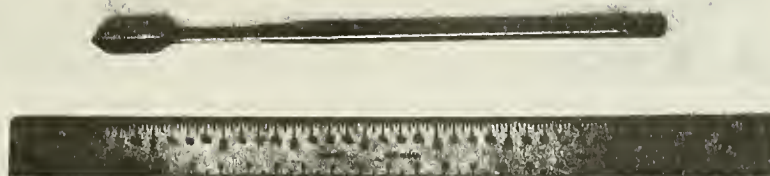


FIG. 14. - THE TEST VANE

The apparatus includes a pulley arrangement and torque transducer calibration jig which facilitates routine physical check calibrations of the torque transducer. By simply disconnecting a shaft coupling between the upper vane shaft and the step function speed reducer, and disengaging the gears to the rotation transducer, the upper end of the shaft is free to turn in a pair of precision ball bearings. By restraining the lower end of the transducer in the calibration jig and applying torque to the upper end via the pulleys by a string and weights, calibration is obtained. The calibration configuration is shown in Fig. 15.

The vane shear device is mounted on the uprights of a Wykeham Farrance Soil Test Machine. The machine's base pedestal serves as the sample pedestal and provides a means to very smoothly push the vane into the sample by slowly raising the pedestal. Detailed descriptions of the apparatus components and a description of initial calibration and check out procedures are found in Appendixes III and IV.

Sample Selection. - As shown in Fig. 12 (page 42) the test samples were 5 in. long, 2.125 in. diameter core tube samples. They were recovered from three boreholes (B-1, B-2, B-3) in the South Pass area of the Mississippi Delta off the Louisiana coast. The core samples were obtained by the down hole wire line core sampler and in situ vane shear rate tests were conducted at several locations. The in situ vane tests were accomplished by

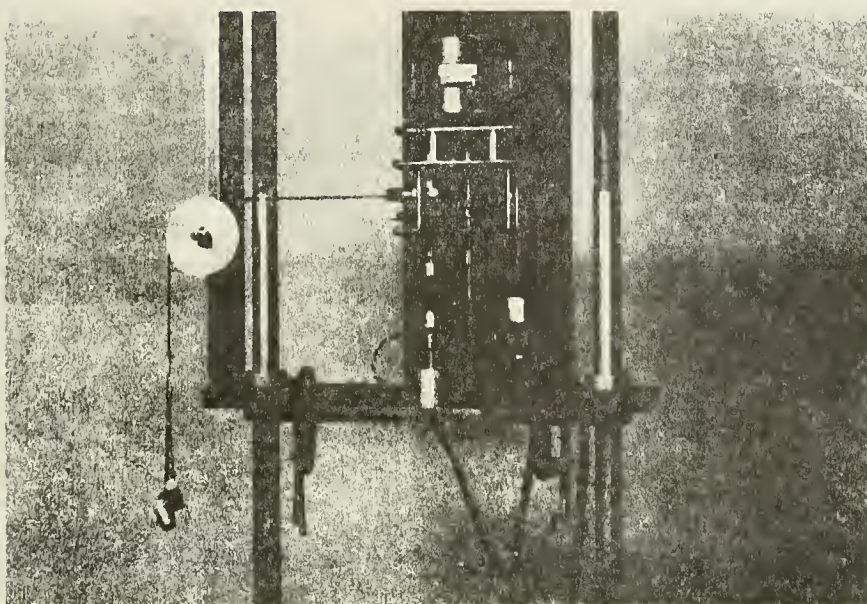


FIG. 15. - TORQUE TRANSDUCER CALIBRATION ARRANGEMENT

McClelland Engineers, Inc. using the wire line vane apparatus previously discussed (9). After recovery the samples were sealed and transported to the Texas A&M University campus, where they were stored in a controlled humidity cool room until used.

Samples from the sediment depths shown in Table 1 were selected for testing. These samples were selected to yield

TABLE 1. - SAMPLES TESTED

Borehole B-1	Borehole B-2	Borehole B-3
19 ft	22.5 ft	55 ft
46 ft	40.5 ft	
61 ft	72.5 ft	
85.5 ft	104.5 ft	
100 ft		

representative sediment profiles for boreholes B-1 and B-2 and to sample an area of extremely low strength in B-3. In situ rate test data were also available near each of the depths selected in borehole B-1.

An additional sample selection criterion was used. This was the degree of sampling disturbance as evidenced by X-rays. Fig. 16 is an X-ray photograph of an acceptable sample. Fig. 17 shows a sample that was rejected on the basis of excessive fracturing and nonhomogeneity, probably caused by gas expansion on recovery. Appendix V presents X-rays of all samples tested in this study.

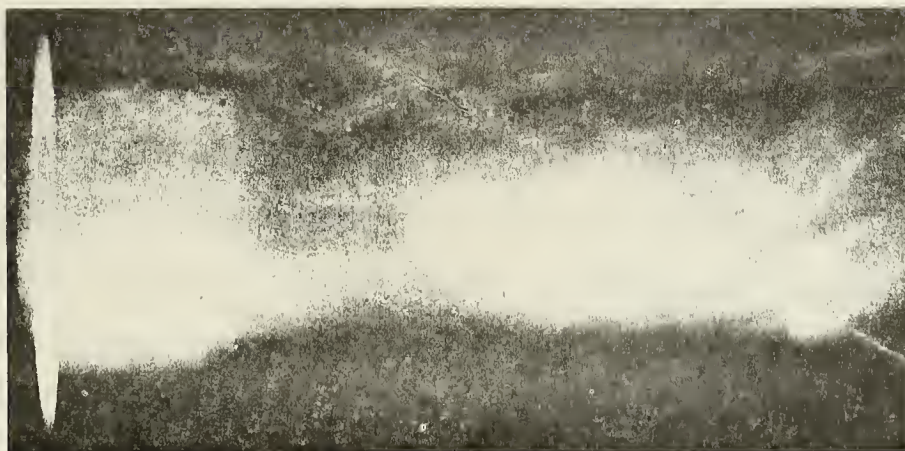


FIG. 16. - X-RAY PHOTOGRAPH OF ACCEPTABLE SAMPLE

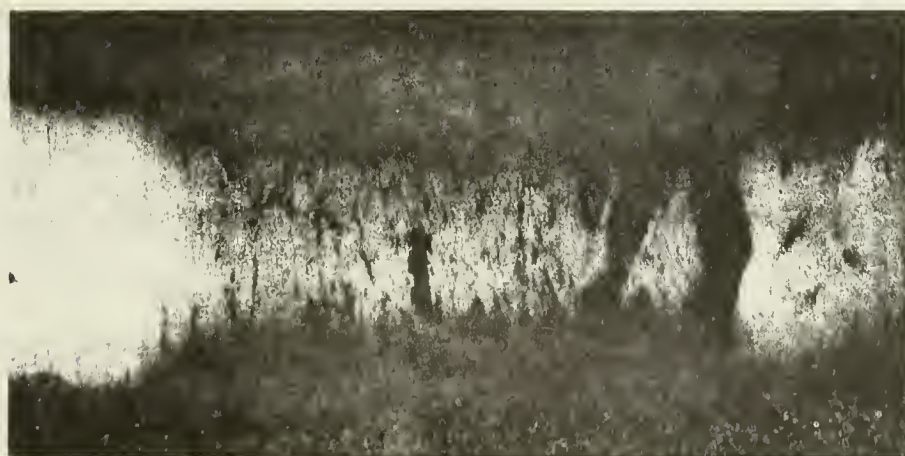


FIG. 17. - X-RAY PHOTOGRAPH OF UNACCEPTABLE
SAMPLE SHOWING FISSURES DUE TO GAS EXPANSION

Experimental Determination of Vane Geometry Factor - B. - The vane geometry factor for the test vane configuration was determined by rotating the vane in a reference viscosity fluid and computing B from Eq. 52. The fluid was Dimethylpolysiloxane silicon fluid sold under the trade name Dow Corning 200. Its rated viscosity at 25°C is 5000 poise. The fluid was calibrated at Texas A&M in a Weissenberg Model R-17 Rheogoniometer and found to be Newtonian over the required shear rate range with a viscosity of 5507 poise at 20°C. The vane tests were conducted at 20°C. Turning the vane in this fluid resulted in torques at high rotation rates roughly equivalent to those encountered in very soft submarine sediments.

The value of B determined by this method was 9.596. It is noted that this is somewhat below the theoretical value of $4\pi = 12.56$. This large difference is due to the fact that the vane does not have rectangular blades (see Fig. 14, page 44), as assumed when the theoretical value was determined. Thus the use of the overall vane length L, in Eq. 52, results in a smaller value of B.

Sample Test Procedure. - Sample testing was accomplished by running vane tests at several rotation rates at adjacent locations in each sample. The four rates were, nominally 0.26, 0.026, 0.013, and 0.0013 radians/sec. The two middle rates were selected to approximate the rates used in the in situ wire line device, and

the high and low rates provided the wide range deemed necessary to obtain sufficient data for use of the computational procedure discussed above. Continuous recordings of torque and rotation angle versus time were obtained for each rotation rate. During the testing sequence for each sample the samples were resealed and replaced in the cool, humid room whenever they were not actually being used. This eliminated moisture content changes. The test sequence on each sample was as follows.

1. Upon being opened each sample was visually inspected and a conventional vane test of ultimate strength was run using a motorized Wykeham Farrance miniature vane (Fig. 18). This test was run to obtain index lab strength values for the samples and to estimate the range of torques expected in the rate tests so the appropriate full scale torque range could be set on the recorder.
2. A physical calibration of the torque transducer was conducted over the range of expected torques.
3. Appropriate motor voltage and step function speed reducer settings were made to obtain the desired rotation rate, and the vane was rotated to obtain a zero rotation reading on the recorder.
4. A test run was then began by holding the sample on the pedestal, raising the pedestal, and forcing the vane

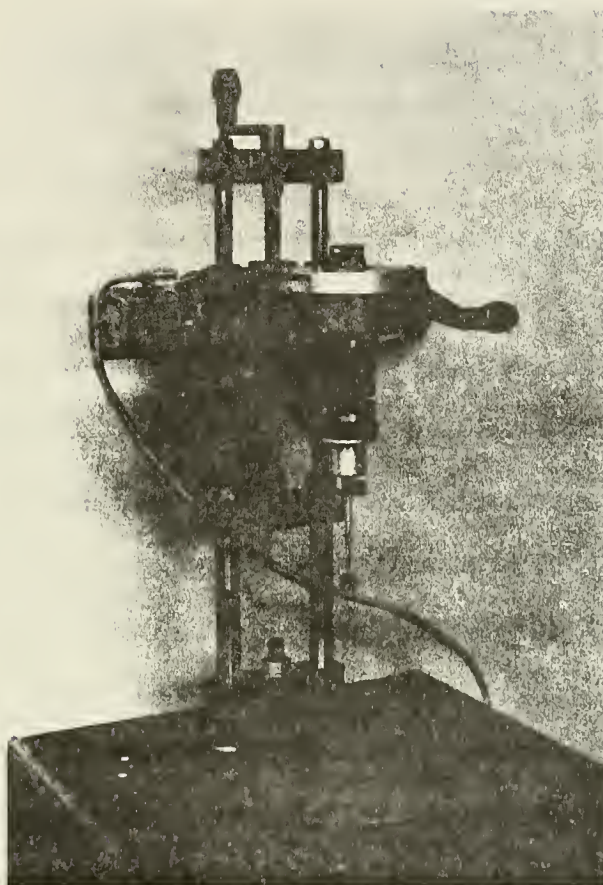


FIG. 18. - WYKEHAM FARRANCE MOTORIZED MINIATURE
LABORATORY VANE SHEAR DEVICE

into the sample at an undisturbed location. The recorder drive and vane motor were then actuated and the torque-rotation-time data were obtained at that rotation rate. Fig. 19 is an example of data so obtained.

5. Upon completion of each test, at one rate, the sample was removed and Steps 3 and 4 were repeated at the next rotation rate.
6. Immediately after the vane tests were complete moisture contents were obtained for each sample. In addition Atterberg limits were later obtained for each sample.

Data Reduction. - Each vane test on each sample resulted in data such as shown in Fig. 19. The data were reduced by selecting an angle, using the rotation calibration (see Appendix IV) and the known time scale on the chart to determine the corresponding time, and, using the torque transducer calibration data obtained for each set of runs, the corresponding torque was measured. Such torque-rotation-time data were obtained at 0.01 radian increments from 0 to 0.1 radians and at 0.15 and 0.20 radians for each run. Maximum torques (failure) normally occurred at or below 0.20 radians. The rotation rate for each test was not determined from instrument settings but was computed as the average rate to an angle of 0.10 radians computed from the angle-time data. Since the actual time associated with each angle, not the rotation rate, is used in the modulus calculations, this approximation of

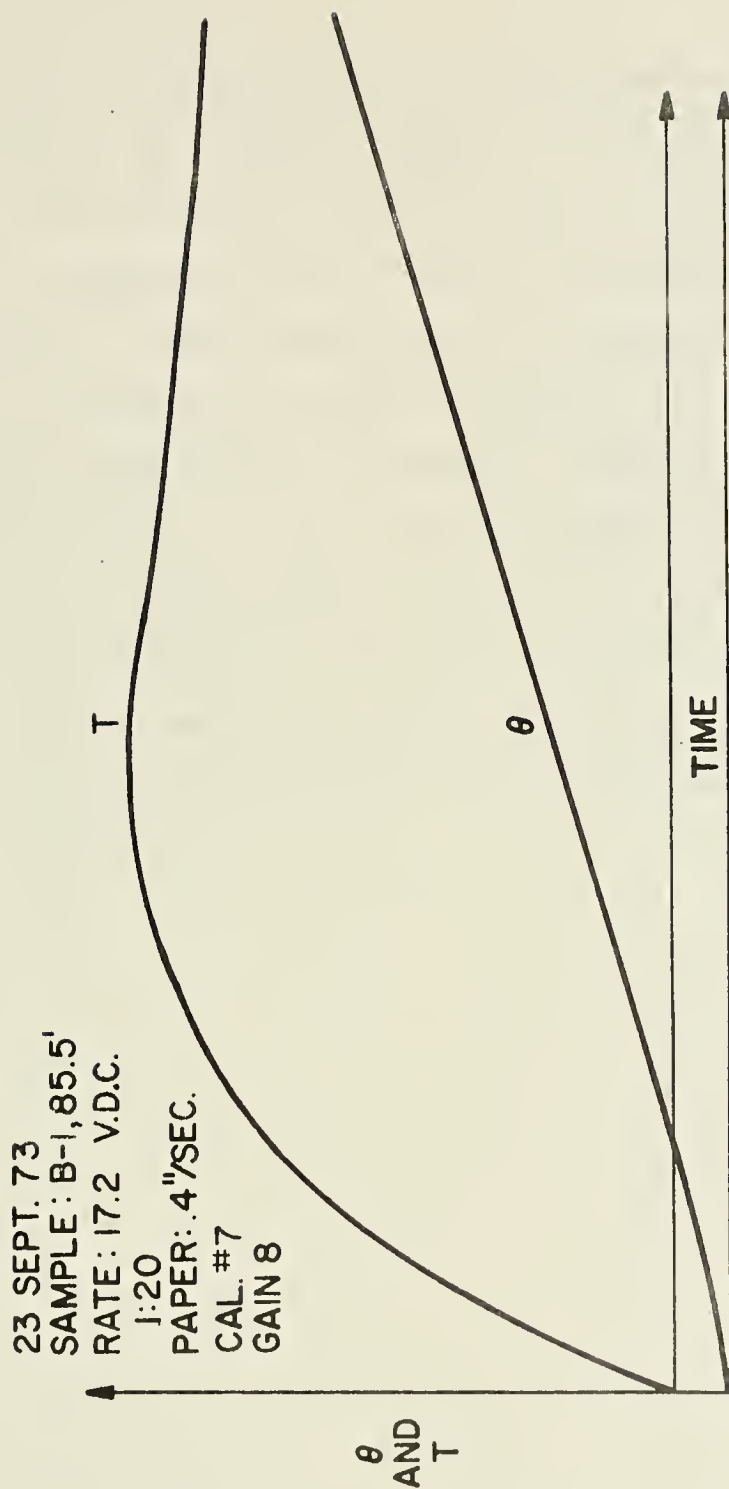


FIG. 19. - EXAMPLE OF TORQUE-ROTATION-TIME DATA
 (AXES ADDED)

rotation rate is of no consequence. The measured rotation angles were corrected for shaft twist between the vane and the rotation sensor using a correction factor calculated as the elastic shaft twist at the measured torque. The corrections were slight.

Torque, T , versus rotation angle, θ , plots were then made from the raw data for each sample, as shown in Fig. 20. Appendix VI contains these plots for all samples. From these plots the normalized torque, T_n , versus θ data were obtained, the values of the time averaged viscoelastic shear modulus, \bar{G} , were found, and G_1 and n of the power law (Eq. 22) were determined using the log-log plotting method shown in Fig. 9, page 31. Fig. 21 shows the log-log plot for Sample B-1 at 46 ft. Plots for all samples are in Appendix VI.

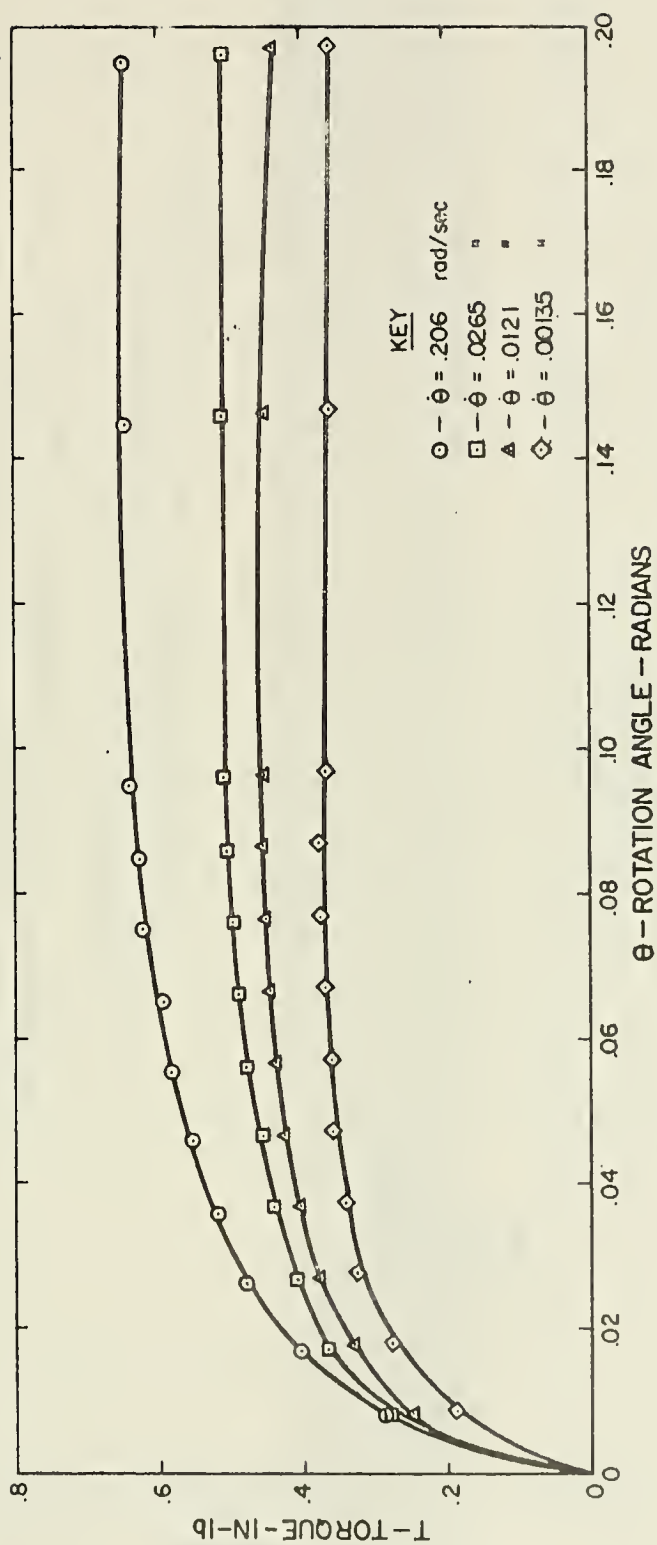


FIG. 20. - EXAMPLE OF TORQUE VERSUS ROTATION ANGLE PLOT
(B-1, 46 FT)



FIG. 21. - EXAMPLE OF LOG-LOG PLOT OF TIME AVERAGED MODULUS VERSUS TIME (B-1, 46 FT)

RESULTS AND DISCUSSION

Application of viscoelastic theory and the power law, Eq. 22, to vane shear data have yielded values of n and G_1 for each of the test samples. Examination of the log-log plots of Appendix VI indicates that n is very nearly independent of θ . However, due to the nonlinearity of the sediment,

$$G_1 = G_1(\theta) \dots \dots \dots (52)$$

and thus the log-log plots at different angles do not fall on the same line. Values of G_1 were computed at each of the several angles used for constructing the log-log plots. In addition, an estimate of an initial G_1 , G_1 at $\theta = 0$, was obtained by plotting G_1 versus θ for each sample on linear paper and extrapolating the graph to $\theta = 0$ using a straight line from the lowest θ data point. This procedure is common practice in viscoelastic theory to estimate the modulus at very short times from experimental data.

Experimental Results. - Table 2 presents the experimentally obtained values of n and G_1 for each sample.

The plots of G_1 versus θ , showing the angle dependency of G_1 , are presented in Figs. 22 through 31. Review of Table 2 and these figures indicate, as would be expected, a general decrease in n with depth and an increase in G_1 . This indicates decreasing time dependence of the modulus with depth and an accompanying increase

TABLE 2. - EXPERIMENTAL VALUES OF G_1 AND n

Sample	B-1, 19'		B-1, 46'		B-1, 61'		B-1, 85.5'		B-1, 100'	
n	.103		.080		.065		.041		.040	
G_1 (psi) at various θ (rad)	θ	G_1	θ	G_1	θ	G_1	θ	G_1	θ	G_1
	0	6.10	0	58.0	0	33.0	0	68.0	0	69.0
	.010	4.44	.0078	40.9	.0086	24.9	.0075	53.2	.0075	58.6
	.020	3.16	.0172	27.0	.0180	17.8	.0162	37.9	.0153	49.0
	.040	2.22	.0364	16.6	.0374	11.9	.0348	24.9	.0331	35.5
	.060	1.60	.0560	12.1	.0570	8.9	.0541	18.7	.0515	27.8

Sample	B-2, 22.5'		B-2, 40.5'		B-2, 72.5'		B-2, 104.5'		B-3, 55'	
n	.064		.044		.041		.029		.140	
G_1 (psi) at various θ (rad)	θ	G_1	θ	G_1	θ	G_1	θ	G_1	θ	G_1
	0	46.0	0	37.0	0	64.0	0	109.0	0	2.10
	.0081	36.7	.0086	27.7	.0075	52.7	.0064	94.2	.01	1.63
	.0171	27.1	.0179	19.1	.0159	43.6	.0135	81.6	.02	1.23
	.0362	17.9	.0373	12.4	.0343	28.4	.0298	58.7	.04	.83
	.0557	13.1	.0571	8.7	.0534	21.1	.0477	44.2	.06	.65

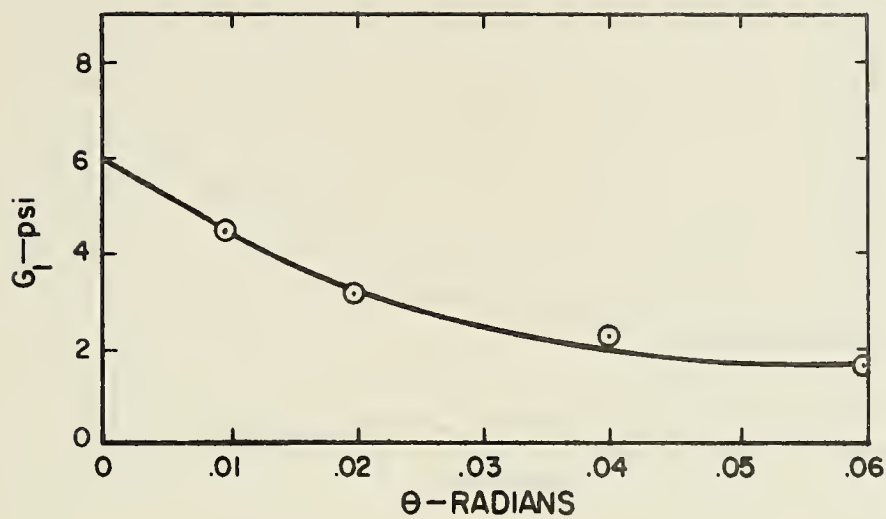


FIG. 22. - G_1 VERSUS θ , BOREHOLE B-1, 19 FEET

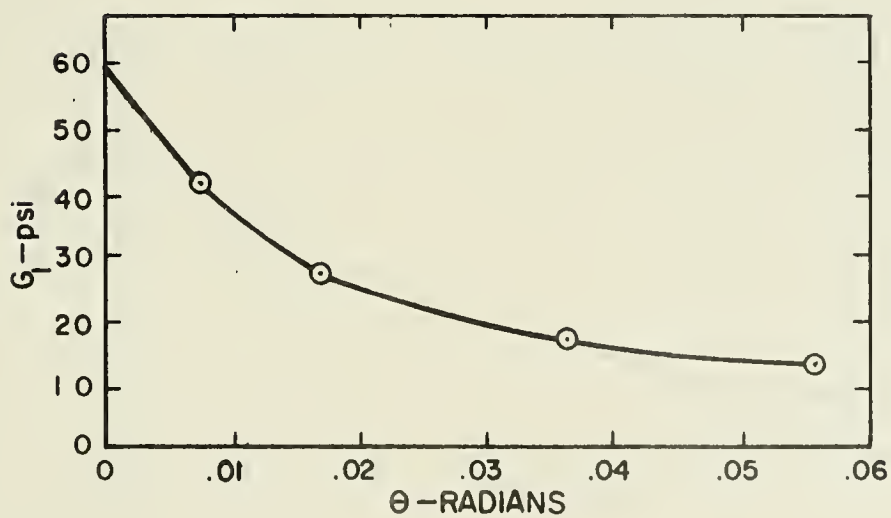


FIG. 23. - G_1 VERSUS θ , BOREHOLE B-1, 46 FEET

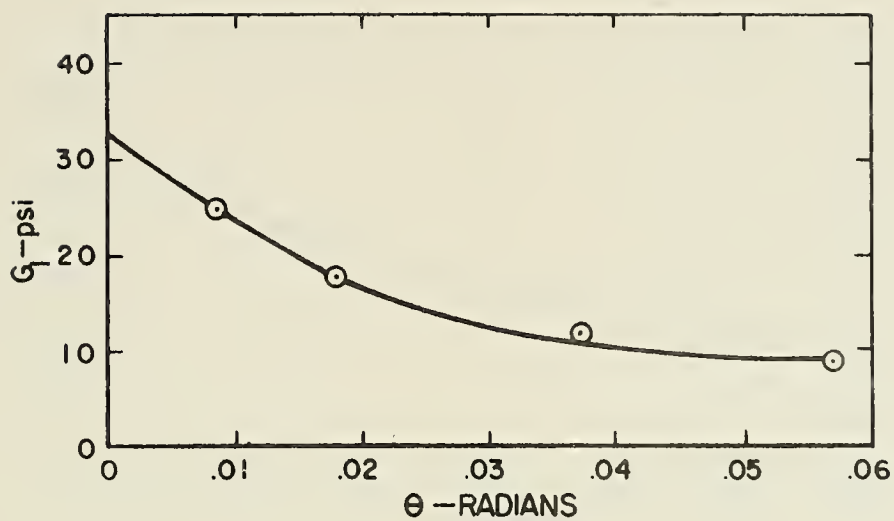


FIG. 24. - G_1 VERSUS θ , BOREHOLE B-1, 61 FEET

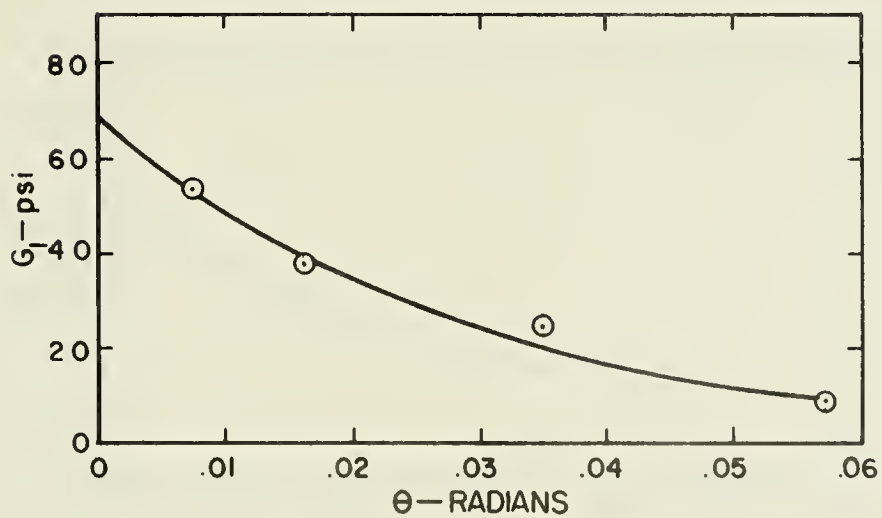


FIG. 25. - G_1 VERSUS θ , BOREHOLE B-1, 85.5 FEET

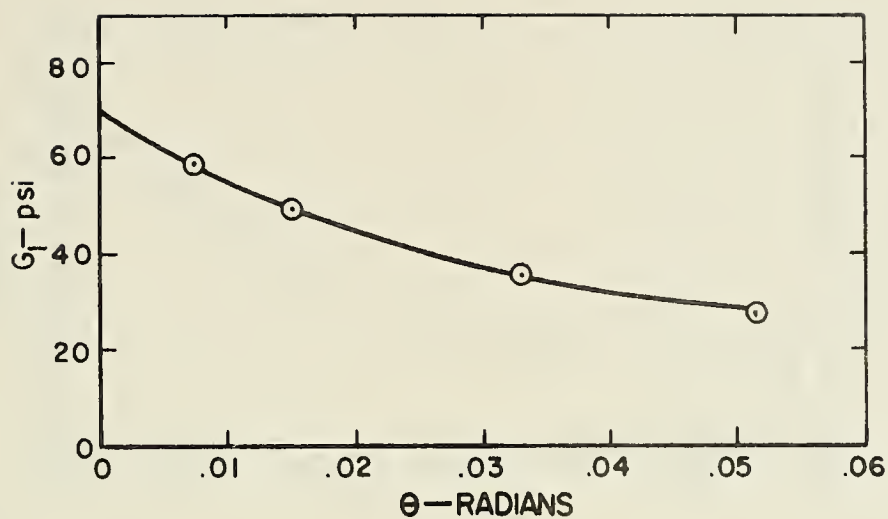


FIG. 26. - G_1 VERSUS θ , BOREHOLE B-1, 100 FEET

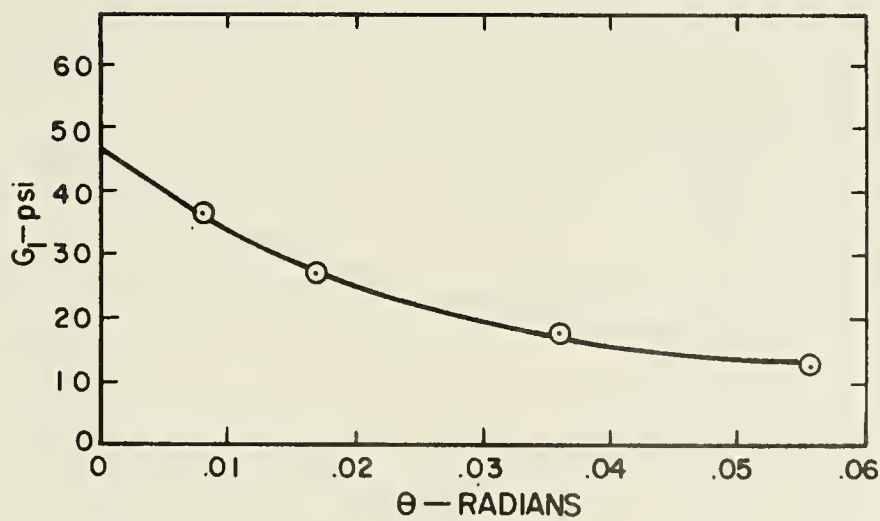


FIG. 27. - G_1 VERSUS θ , BOREHOLE B-2, 22.5 FEET

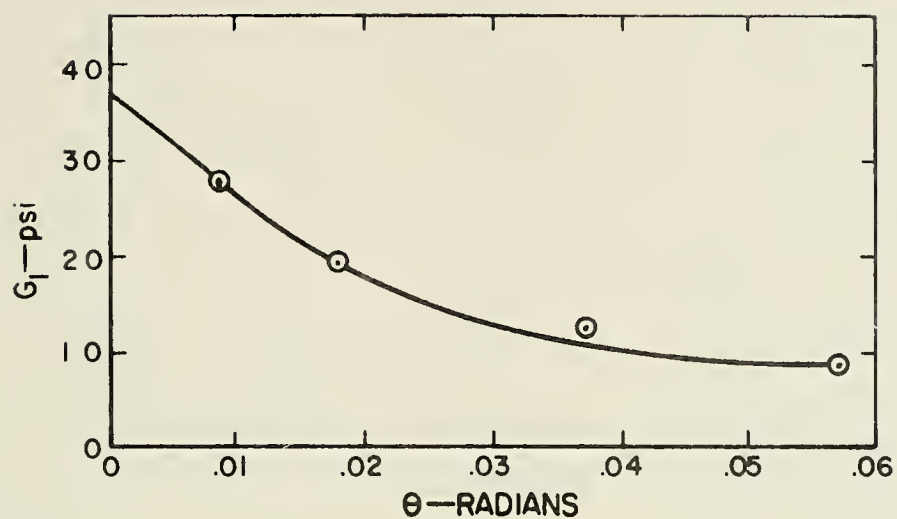


FIG. 28. - G_1 VERSUS θ , BOREHOLE B-2, 40.5 FEET

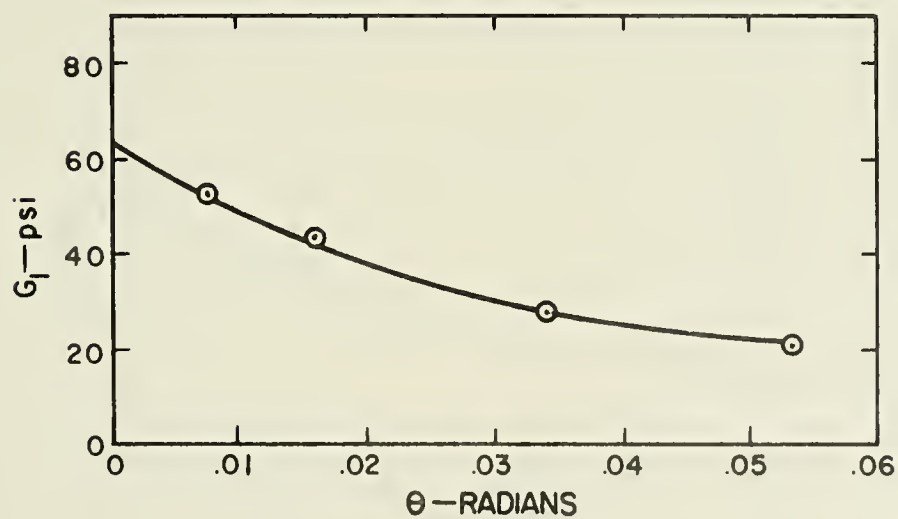


FIG. 29. - G_1 VERSUS θ , BOREHOLE B-2, 72.5 FEET

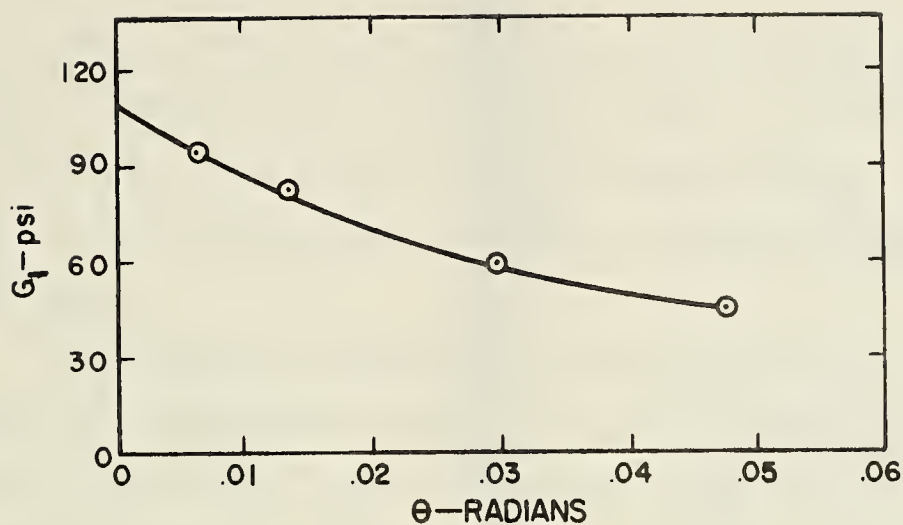


FIG. 30. - G_1 VERSUS θ , BOREHOLE B-2, 104.5 FEET

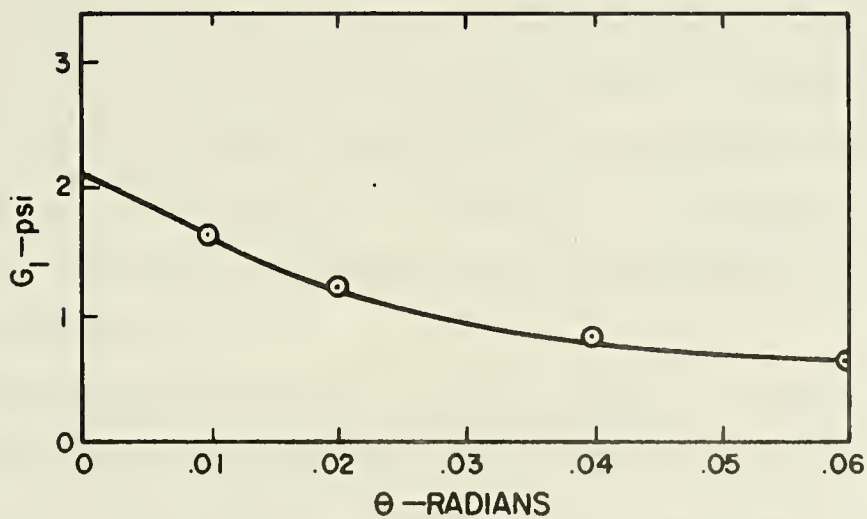


FIG. 31. - G_1 VERSUS θ , BOREHOLE B-3, 55 FEET

in stiffness. Fig. 32, a plot of n and G_1 at $\theta = 0$ versus depth, graphically depicts these variations with depth. It is noted that for sample B-3 at 55 ft the n and G_1 data appear anomalous. However, as was previously noted, this sample was from an extremely weak region.

The conventional laboratory soil mechanics tests on the samples are summarized in Table 3. It may prove useful to consider the possibility of using conventional parameters, such as liquidity index, L.I., and ultimate shear strength, C_u , as predictors of G_1 and n for use with power law modulus computations. Figs. 33 through 36 are plots of G_1 and n versus L.I. and C_u . The available data indicate strong relationships between L.I. and n , and between C_u and G_1 . This is consistent with the concept of viscoelasticity in clays, especially the correlation of n , the indicator of time dependence in the power law, and L.I., an indicator of the water content relative to the water content at which the clay tends to act as a fluid. At this time the available data are insufficient to attempt quantification of these relationships.

Comparison of Laboratory and In Situ Results. - Limited in situ torque versus rotation angle data, at several locations in Borehole B-1, were obtained during the original sampling. Data were obtained at three rotation rates. Three of these tests were selected for comparison with the laboratory results since they

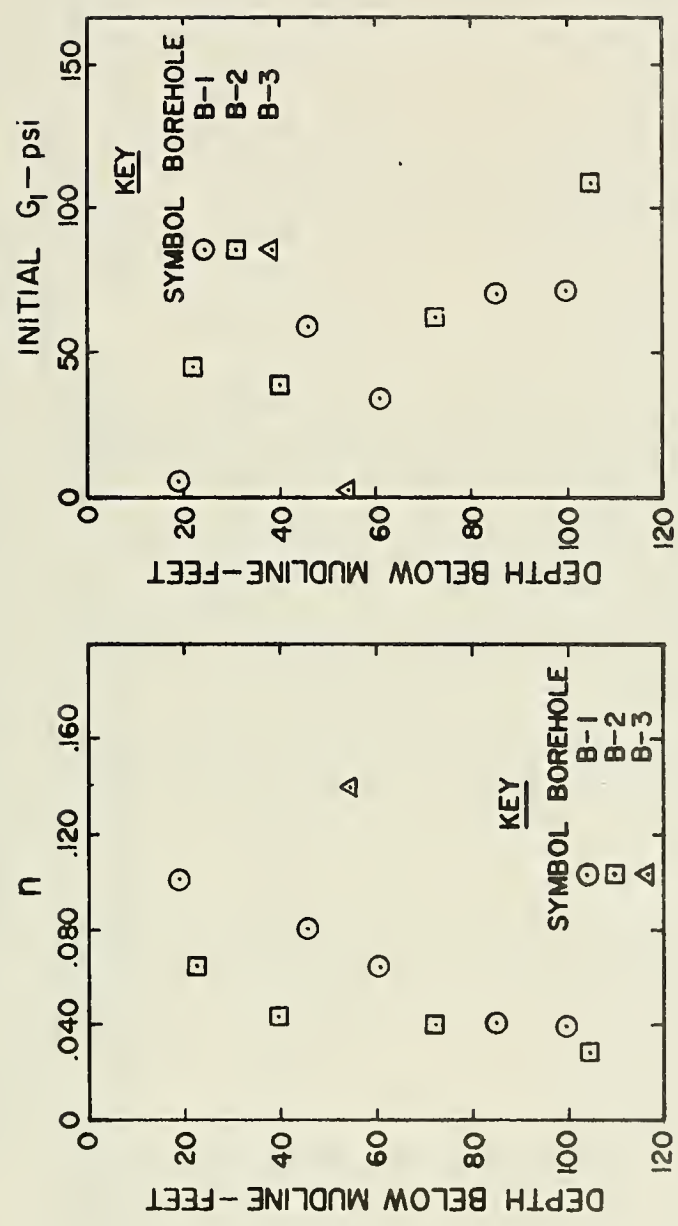


FIG. 32. - VARIATION IN n AND G_1 WITH DEPTH

TABLE 3. - MINIATURE LABORATORY VANE SHEAR STRENGTHS, NATURAL WATER CONTENTS AND ATTERBERG LIMITS AND INDICES FOR TEST SAMPLES

Borehole	Depth (ft.)	Natural Water Content w_n (%)	Liquid Limit w_l (%)	Plastic Limit w_p (%)	Plasticity Index P.I. (%)	Liquidity Index L.I.	Maximum Shear Strength C_u (psf)
B-1	19	76.6	74.5	29.4	45.1	1.05	35
B-1	46	57.3	74.6	30.1	44.5	.61	220
B-1	61	57.0	70.8	29.1	42.7	.65	150
B-1	85.5	77.3	97.0	36.6	64.4	.63	290
B-1	100	74.5	102.5	32.2	67.3	.63	428
B-2	22.5	65.8	84.7	30.0	54.7	.65	225
B-2	40.5	55.8	65.2	27.5	37.7	.75	132
B-2	72.5	72.2	86.5	34.0	52.5	.73	320
B-2	104.5	72.8	103.8	39.7	64.1	.52	645
B-3	55	78.6	65.3	24.6	40.7	1.33	25
$P.I. = w_l - w_p, \quad L.I. = \frac{w_n - w_p}{P.I.}$							

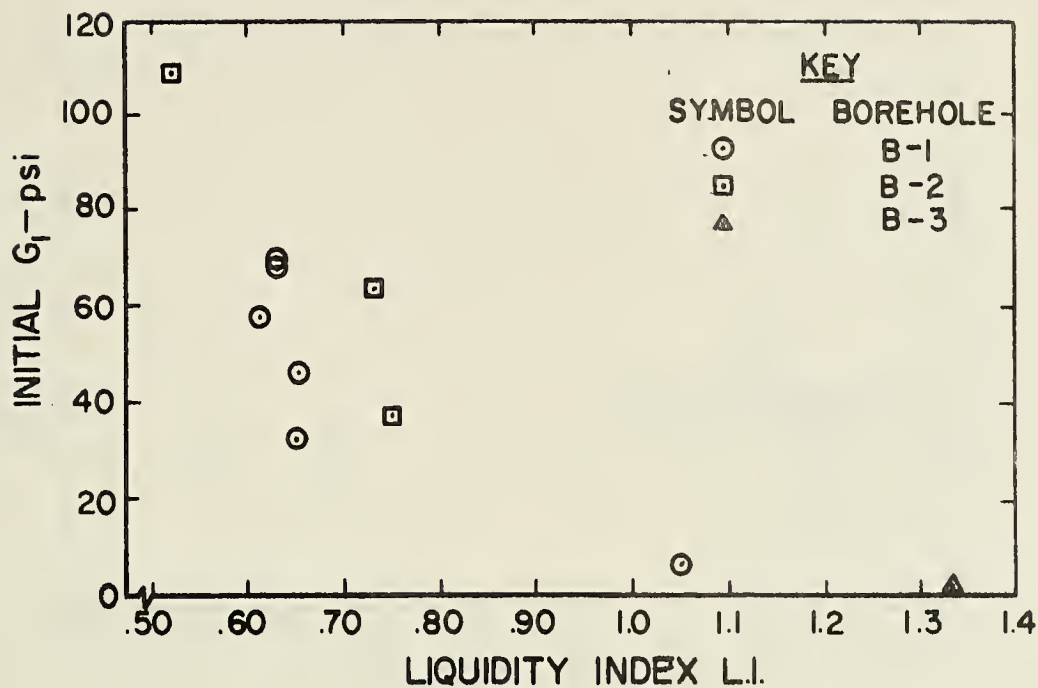


FIG. 33. - G_1 VERSUS LIQUIDITY INDEX

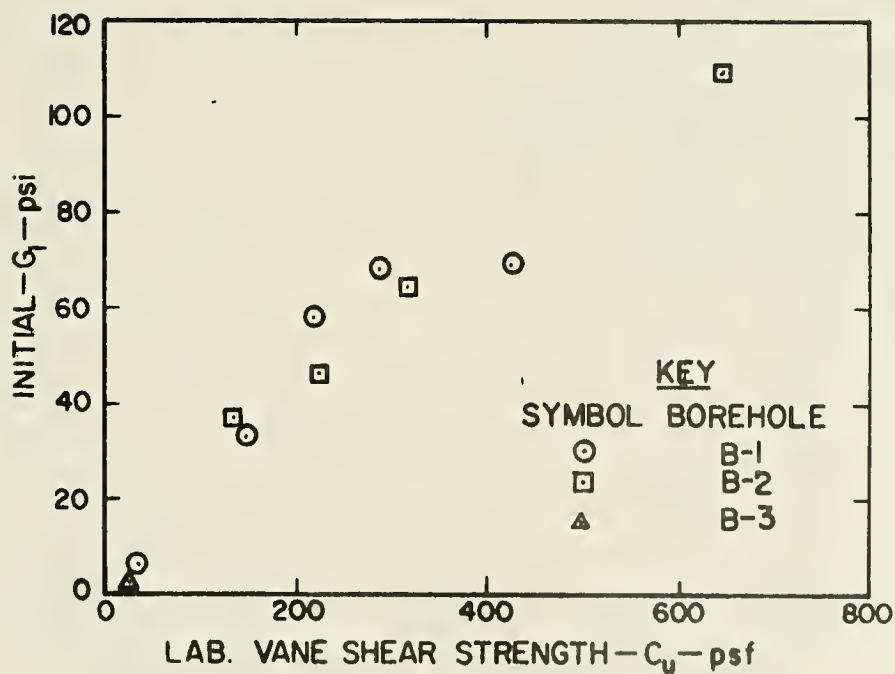
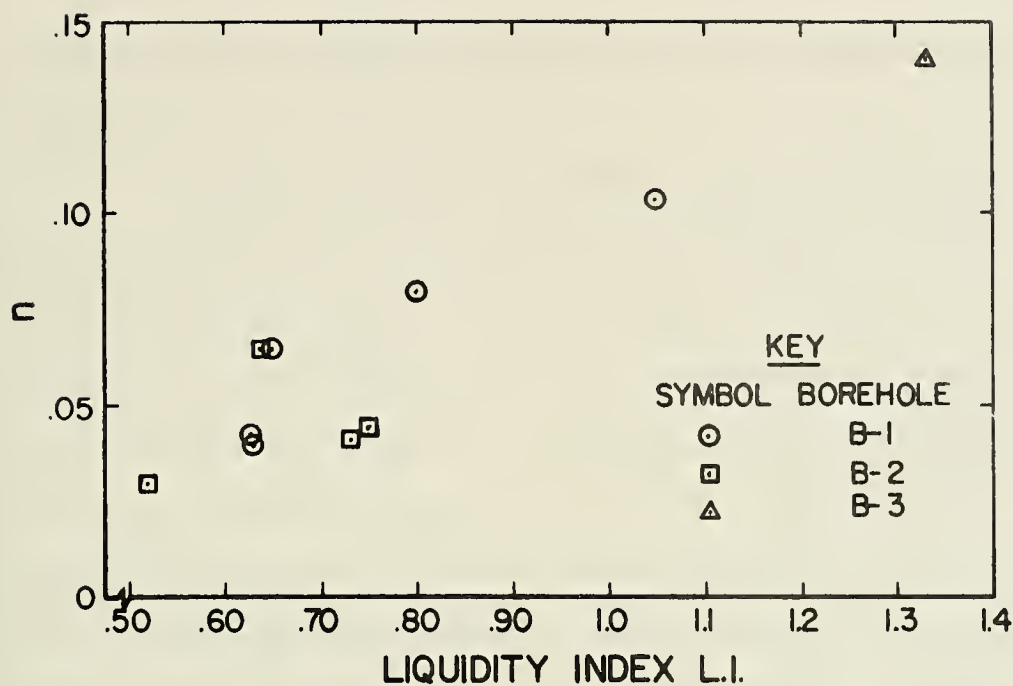
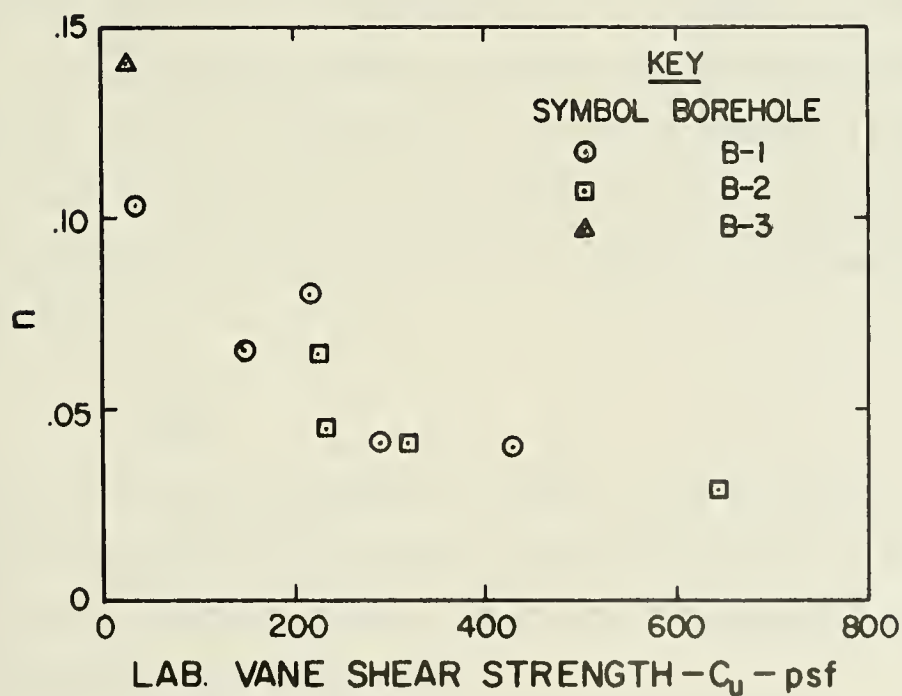


FIG. 34. - G_1 VERSUS ULTIMATE VANE SHEAR STRENGTH

FIG. 35. - n VERSUS LIQUIDITY INDEXFIG. 36. - n VERSUS ULTIMATE VANE SHEAR STRENGTH

were conducted at depths corresponding with laboratory sample depths (46 ft, 61 ft and 100 ft).

It is noted that the in situ tests were conducted at rotation rates between 0.0182 rad/sec and 0.0077 rad/sec. This narrow range (as opposed to a range of about 10^3 rad/sec for the laboratory tests) precludes the use of these data to compute values of G_1 and n as was done with the laboratory data. Time differences in the points obtained for the $\log \bar{G} - \log t$ plots are so small that the slope of the plot changes greatly for small changes in \bar{G} . Thus experimental error in torque, angle and time measurements would be amplified. For these reasons the in situ rate test data are not considered sufficiently reliable to attempt direct comparison of laboratory and in situ values of G_1 and n .

It is possible, however, to obtain a check on the validity of the power law representation of the shear modulus by using laboratory values of G_1 and n to predict the in situ torque versus rotation data. This can be done by considering the normalized torque:

$$T_n = \frac{T}{Ba^2L} \dots \dots \dots (28)$$

which can easily be computed for each in situ data point. Due to the vane similarity this can be directly compared to T_n predicted from the laboratory results. To do this substitute the power law for $G(t)$ into Eq. 14 to obtain:

$$T_n = \frac{T}{Ba^2L} = \int_0^t G_1 (t - \tau)^{-n} \frac{d\theta}{d\tau} d\tau \dots \dots \dots (53)$$

Now, it is noted that G_1 is dependent on θ but is not time dependent. If the rotation rate is constant then $\frac{d\theta}{d\tau} = C$. By using this and carrying out the integration:

$$T_n = \frac{G_1(\theta)}{1-n} Ct^{1-n} \dots \dots \dots (54)$$

Now since $\frac{d\theta}{d\tau} = C$ then at any time, t , $\theta = Ct$ and this can be substituted into Eq. 54 to yield:

$$T_n = \frac{G_1(\theta)}{1-n} \theta t^{-n} \dots \dots \dots (55)$$

Now, if it is desired to predict the in situ T_n at a particular $\theta - t$ pair (i.e. at angle, θ , with rotation rate $\frac{\theta}{t}$) Eq. 55 can be utilized by using n determined from a laboratory sample from the location where the prediction is desired and using the laboratory value of G_1 corresponding to the θ of interest.

These predictions have been calculated to angles of .06 radians for the Borehole B-1, 46 ft, 61 ft and 100 ft depths. Figs. 37, 38 and 39 show the comparisons. The predictions could have been carried out to larger angles if desired. In light of the fact that the in situ shearing resistances are expected to be slightly higher than those of samples (28), the comparisons are remarkably close. The large spread of some of the in situ data from the predicted curves is believed to be primarily due to non-homogeneity of the sediment and certain uncertainties associated

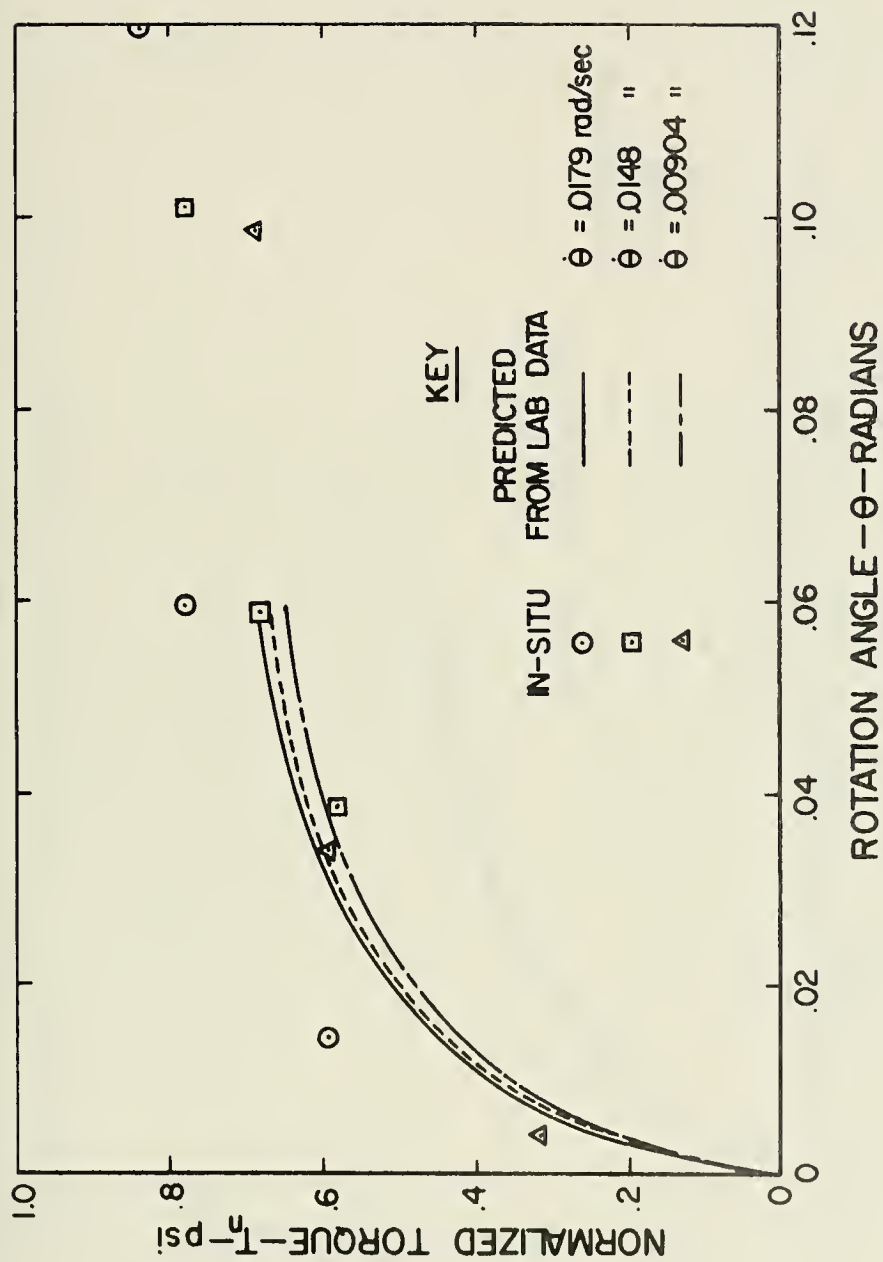


FIG. 37. - COMPARISON OF PREDICTED AND MEASURED IN SITU NORMALIZED TORQUE VERSUS ROTATION ANGLE - B-1, 46 FT

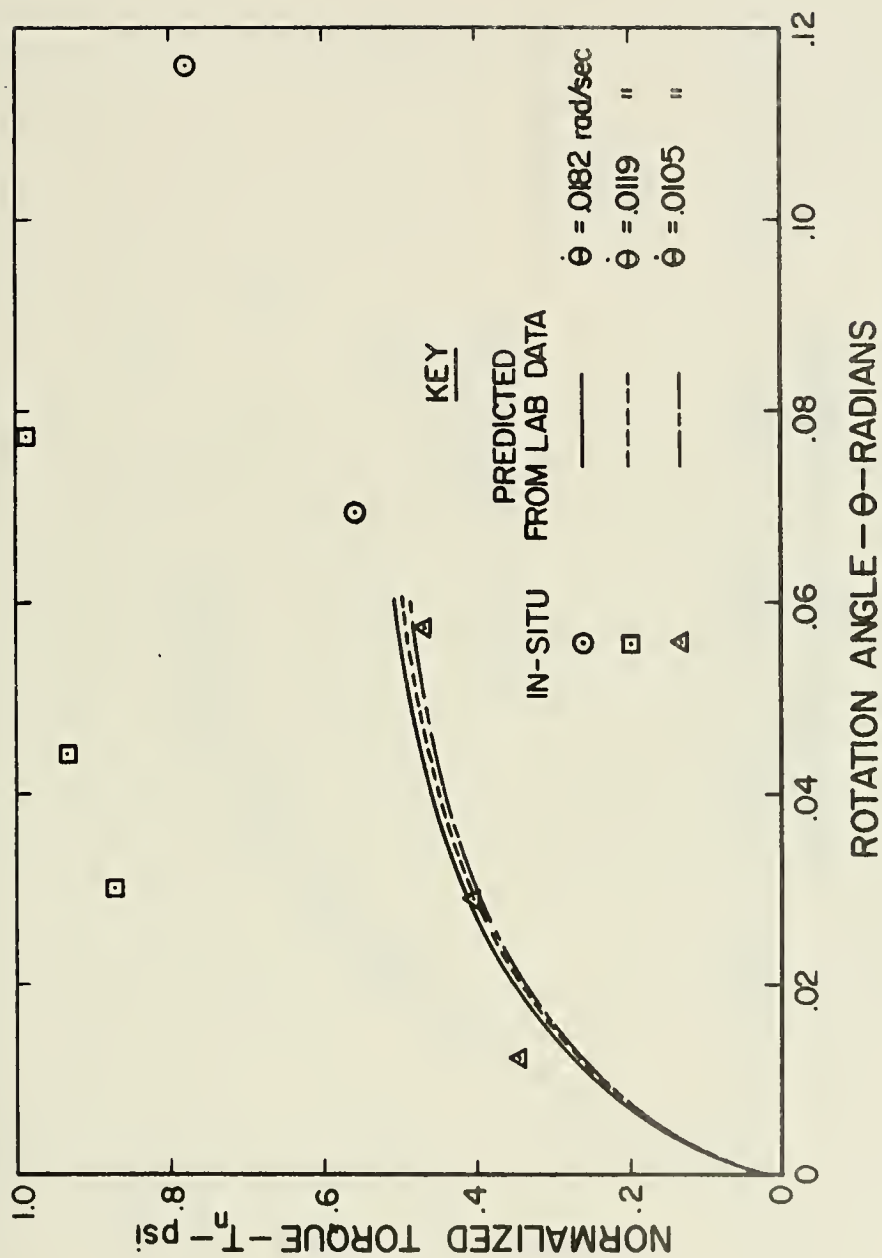


FIG. 38. - COMPARISON OF PREDICTED AND MEASURED IN SITU NORMALIZED TORQUE VERSUS ROTATION ANGLE - B-1, 61 FT

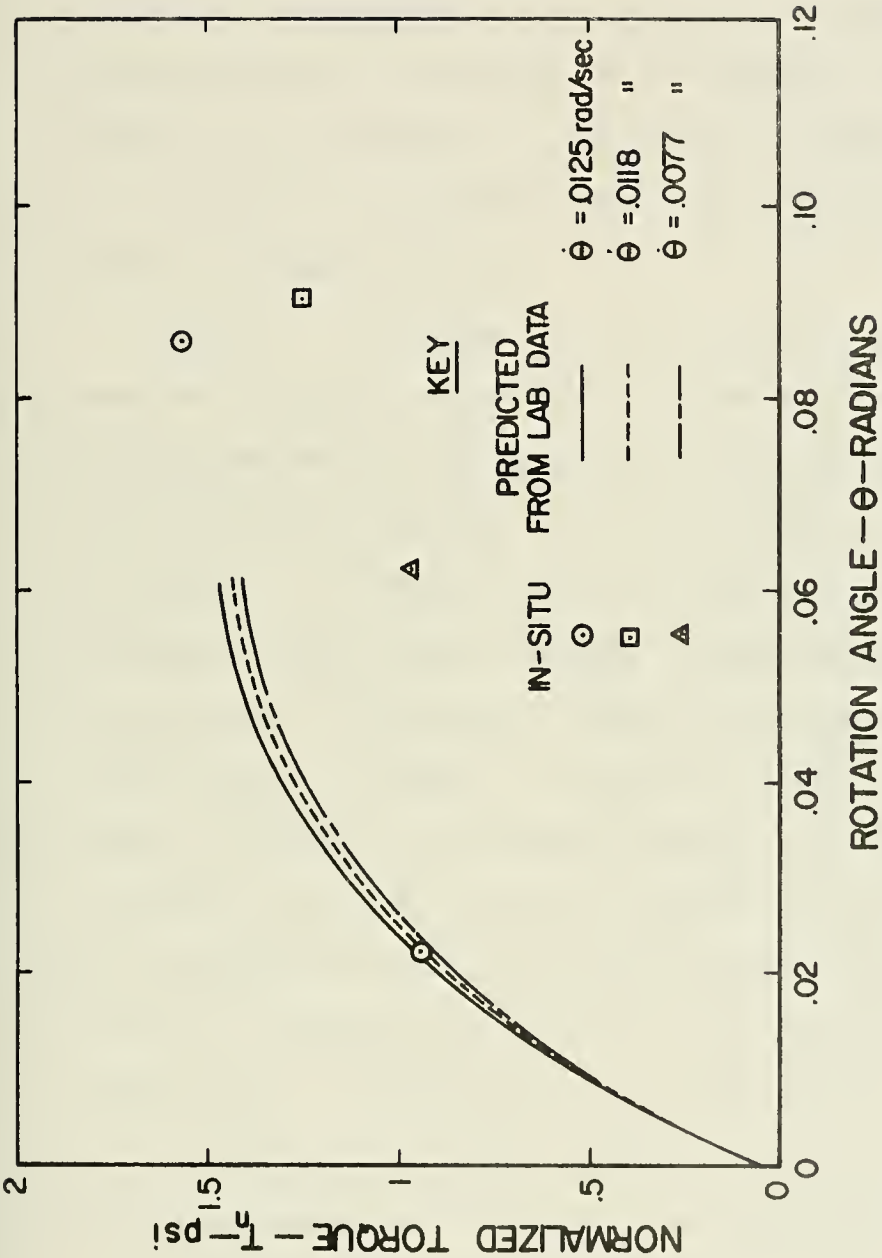


FIG. 39. - COMPARISON OF PREDICTED AND MEASURED IN SITU NORMALIZED TORQUE VERSUS ROTATION ANGLE - B-1, 100 FT

with the in situ tests. The comparisons tend to verify the procedure for determining the vane geometry factor and lend experimental evidence to the theoretical assertion that it is independent of absolute vane size, and that pore water migration is not important in this clay at the vane rate used. They also support practical use of the power law representation of the time dependent shear modulus of submarine sediments.

Comment. - The experimental results appear encouraging. The power law viscoelastic shear modulus and the vane test and analysis technique seem to lend themselves to practical determination of the modulus and prediction of in situ sediment stress-deformation behavior. The simple form of the equation makes it easily applicable in many types of problems including response to vibrational inputs. Available data indicate the procedure yields accurate results. However, to verify the validity, additional testing is necessary. The general procedure (i.e. application of the power law) might be verified by determining $G(t)$ by some other means and comparing with $G(t)$ predicted from the vane data and the power law. One other means might be the use of the vibrating disc technique (3). The equality of the vane factor B for the in situ and lab vanes might be further verified by running the two vanes in the same homogeneous clay material in the laboratory environment.

It is noted that no direct measurement of the in situ shear modulus was deemed possible in this study. This is only a result

of inadequate rotation rate range and uncertainties in the in situ angle-torque-time determinations. Development of an in situ vane device which can rotate at speeds about three decades apart and employ more accurate means to determine actual time versus rotation and torque, continuously, is required.

CONCLUSIONS

Submarine clays exhibit viscoelastic stress-deformation characteristics. This study has presented a practical method for determining a viscoelastic shear modulus for the sediments. On the basis of the theoretical and experimental considerations it is concluded that:

1. The time dependent shear modulus of submarine sediments can be reasonably represented by the power law equation, $G(t) = G_1 t^{-n}$, where G_1 is strain dependent.
2. The vane shear test, run at several rotation rates and measuring continuous torque-rotation-time data, provides a practical means of determining the shear modulus, both in the laboratory and in situ.
3. Laboratory vane shear data can be used to estimate the in situ stress-strain behavior, and, if sampling disturbance is neglected, to predict the in situ modulus.
4. The presently available wire line down hole vane shear device of McClelland Engineers does not have a sufficiently large range of rotation rates to utilize it for direct in situ modulus determinations. Also, refinement of the measurement methods for torque-rotation-time data is required for use of this instrument.

5. The experimental data indicate a relationship between liquidity index and the constant n in the power law.
6. The experimental data indicate a relationship between the maximum sediment shear strength and the initial ($\theta = 0$) value of G_1 .

APPENDIX I. - REFERENCES

1. Bea, R.G. and Arnold P., "Movements and Forces Developed by Wave-Induced Slides in Soft Clays", Preprints, Fifth Annual Offshore Technology Conference, Vol. II, May, 1973, pp. 731-742.
2. Bennett, G.B. and Mecham, J.G., "Use of the Vane Borer on Foundation Investigation of Fill", Proceedings, Highway Research Board, Vol. 32, 1953, pp. 486-499.
3. Briar, H.P. and Bills, K.W., Jr., "Development of an In Situ Transmitter for Solid Rocket Propellant Surveillance", Aerojet Solid Propulsion Company Final Report, Contract No. F04611-71-C-0044, Air Force Rocket Propulsion Lab, Edwards A.F.B., California, AFRPL-TR-72-93, December, 1972.
4. Cadling, L. and Odenstad, S., "The Vane Borer", Proceedings, Royal Swedish Geotechnical Institute, No. 2., Stockholm, 1950.
5. Carpenter, S.H., Thompson, L.J. and Bryant, W.R., "Viscoelastic Properties of Marine Sediments", Preprints, Fifth Annual Offshore Technology Conference, Vol. II, May, 1973, pp. 777-788.
6. Cohen, S.R., "Measurement of the Viscoelastic Properties of Water-Saturated Clay Sediments", Master of Science Thesis, U.S. Naval Post Graduate School, Monterey, California, 1968.
7. Demars, K.R. and Taylor, R.J., "Naval Seafloor Soil Sampling and In Place Test Equipment: A Performance Evaluation", Naval Civil Engineering Laboratory, Technical Report No. R730, Port Hueneme, Ca., June, 1971.
8. Doyle, E.H., "Soil-Wave Tank Studies of Marine Soil Instability", Preprints, Fifth Annual Offshore Technology Conference, Vol. II, May, 1973, pp. 753-766.
9. Doyle, E.H., McClelland B. and Ferguson, G.H., "Wire-Line Vane Probe for Deep Penetration Measurements of Ocean Sediments", Preprints, Third Annual Offshore Technology Conference, Vol. I, April, 1971, pp. 21-32.
10. Eden, W.J. and Hamilton, J.J., "The Use of a Field Vane Apparatus in Sensitive Clay", Symposium on Vane Shear Testing of Soils, American Society for Testing and Materials Special Technical Publication No. 193, 1957, pp. 41-53.

11. Fenske, C.W., "Deep Vane Tests in Gulf of Mexico", Symposium on Vane Shear Testing of Soils, American Society for Testing and Materials Special Technical Publication No. 193, 1957, pp. 16-25.
12. Ferry, J.D., Viscoelastic Properties of Polymers, John Wiley and Sons, New York, 1970
13. Fung, Y.C., "Foundations of Solid Mechanics", Prentice-Hall, Inc., Englewood Cliffs, New Jersey, 1965.
14. Gade, H.G., "Effects of a Nonrigid, Impermeable Bottom on Plane Surface Waves in Shallow Water", Journal of Marine Research, Vol. 16, No. 2, 1958, pp. 61-82.
15. Gibbs, H.J., "An Apparatus and Method of Vane Shear Testing of Soils", Symposium on Vane Shear Testing of Soils, American Society for Testing and Materials Special Technical Publication No. 193, 1957, pp. 9-15.
16. Grim, R.E., Clay Mineralogy. McGraw Hill, New York, 1953.
17. Gray, H., "Field Vane Shear Tests of Sensitive Cohesive Soils", Proceedings, American Society of Civil Engineers, Vol. 81, Paper No. 755, July, 1955.
18. Hall, E.B., "Shear Strength Determination of Soft Clayey Soil By Field and Laboratory Methods", Symposium on Soil Exploration, American Society for Testing and Materials Special Technical Publication No. 351, 1964, pp. 53-59.
19. Heck, J.R., "Engineering Properties of Sediments in the Vicinity of Guide Seamount", Master of Science Thesis, United States Naval Post Graduate School, Monterey, California, 1970.
20. Henkel, D.J., "The Role of Waves in Causing Submarine Landslides", Geotechnique, Vol. 20, No. 1, 1970, pp. 75-80.
21. Kinsman, B., Wind Waves, Prentice-Hall, Inc., Englewood Cliffs, N.J., 1965.
22. Lambe, T.W., "The Structure of Inorganic Soils", Proceedings, American Society of Civil Engineers, Vol. 79, No. 315, 1953.
23. Leonards, G.A. and Girault, P., "A Study of the One Dimensional Consolidation Test", Proceedings, Fifth International Conference of Soil Mechanics and Foundation Engineering, Vol. I, 1961.

24. Mitchell, J.K., "Fabric of Natural Clays and Its Relation to Engineering Properties", Proceedings, Highway Research Board, Vol. 35, 1956, p. 155
25. Mitchell, J.K., Campanella, R.G. and Singh A., "Soil Creep as a Rate Process", Journal of the Soil Mechanics and Foundations Division, American Society of Civil Engineers, Vol. 94, No. SM1, Proc. Paper 5751, January, 1968, pp. 231-253.
26. Mitchell, R.J., Tsui, K.K. and Sangrey, D.A., "Failure of Submarine Slopes under Wave Action", Proceedings of the Thirteenth International Conference on Coastal Engineering, American Society of Civil Engineers, July, 1972
27. Monney, N.T., "Analysis of Sediment Shear Strength at Varying Rates of Shear", Presented at ONR Seminar/Workshop: Geotechnical Properties of Deep-Sea Sediments, April, 1973.
28. Monney, N.T., "Measurements of the Engineering Properties of Marine Sediments", Journal of the Marine Technology Society, Vol. 5, No. 2, 1971, pp. 21-29
29. Murayama, S. and Shibata, T., "Flow and Stress Relaxation of Clays (Theoretical Studies on the Rheological Properties of Clay - Part I.)", Proceedings, Rheology and Soil Mechanics Symposium of the International Union of Rheoretical and Applied Mechanics, Grenoble, France, April, 1964.
30. Pipkin, A.C., Lectures on Viscoelastic Theory, Applied Mathematical Sciences, Vol. 7, Springer-Verlag, New York, 1972.
31. Richards, A.F., McDonald, V.J., Olson, R.D., and Keller, G.H., "In-Place Measurement of Deep Sea Soil Shear Strength", Symposium on Underwater Soil Sampling, Testing and Construction Control, American Society for Testing and Materials Special Technical Publication No. 501, 1971, pp. 55-68.
32. Schapery, R.A., "On the Characterization of Nonlinear Viscoelastic Materials", Polymer Engineering and Science, Vol. 9, No. 4, July, 1969, pp. 295-310.
33. Schapery, R.A., "On a Thermodynamic Constitutive Theory and Its Application to Various Nonlinear Materials", Proceedings of the IUTAM Symposium on Thermoelasticity, Springer-Verlag New York, 1969, pp. 259-285.

34. Schapery, R.A., Proposal, Wave-Sea Bottom Interaction Study, Submitted by Texas A&M Research Foundation to Chevron Oil Field Research Company, June, 1973.
35. Scott, R.F., Principles of Soil Mechanics, Addison-Wesley Pub. Co., Inc., Reading Mass., 1963.
36. Sherif, M.A., Bostrom, R.C., Stockman, R.H. and Burrows, C.M., "An Assessment of Existing Submarine Soil Strength Testing Techniques", Proceedings, International Symposium on the Engineering Properties of Sea-Floor Soils and Their Geophysical Identification, University of Washington, Seattle, 1971, pp. 49-74.
37. Singh, A. and Mitchell, J.K., "General Stress-Strain-Time Function For Soils", Journal of the Soil Mechanics and Foundation Division, American Society of Civil Engineers, Vol. 94, No. SM1, Proc. Paper 5728, January, 1968, pp. 21-46.
38. Sterling, G.H. and Strohbeck, E.E., "The Failure of the South Pass 70 "B" Platform in Hurricane Camile", Preprints, Fifth Annual Offshore Technology Conference, Vol. II, May, 1973, pp. 719-730.
39. Suklje, L. Rheological Aspects of Soil Mechanics, John Wiley and Sons, New York, 1969.
40. Wilson, O.B. and Andrews, R.S., "Measurement of the Dynamic Rigidity of Sediments", Proceedings, International Symposium on the Engineering Properties of Sea-Floor Soils and Their Geophysical Identification, University of Washington, Seattle, 1971, pp. 75-94.
41. Wilson, N.E., "Laboratory Vane Shear Tests and the Influence of Pore-Water Stresses", Laboratory Shear Testing of Soils, American Society for Testing and Materials Special Technical Publication No. 361, 1964, pp. 377-389.
42. Wright, S.G. and Dunham, R.S., "Bottom Stability Under Wave Induced Loading", Preprints, Fourth Annual Offshore Technology Conference, Vol. I, May, 1972, pp. 853-860.
43. Wu, T.H., Soil Mechanics, Allyn and Bacon, Inc., Boston, 1970.
44. Yong, R.N. and Warkentin, B.P., Introduction to Soil Behavior, Macmillan Co., New York, 1966.

APPENDIX II. - NOTATION

a = vane radius

B = vane geometry factor

C = a constant

C_u = maximum vane shear strength

d = vane diameter

η = viscosity

G = elastic shear modulus

$G(t)$ = viscoelastic relaxation modulus in shear

\bar{G} = average viscoelastic modulus in shear

G_1 = a constant in time

γ = shear strain

$\dot{\gamma}$ = shear strain rate

L = vane length

L.I. = liquidity index

$\mathcal{I}\{f(t)\}$ = Laplace transform of $f(t)$

n = a constant

ω = frequency

P.I. = plasticity index

r = radial distance from center of rotation

T = torque

T_n = normalized torque

t = time

τ = dummy time integration variable

τ = shear stress

$\dot{\tau}$ = rate of shear stress

θ = angle of vane rotation

w_l = liquid limit

w_n = natural water content

w_p = plastic limit

APPENDIX III. - DESCRIPTION OF EQUIPMENT

This Appendix is intended to provide a detailed description of the equipment. The test apparatus and a close up of the vane shear device are shown in Figs. 12 and 13 (pages 42 and 43).

The components and arrangement are listed and described in detail below.

List of Components

1. Vane Shear Device
 - (a) D.C. Motor
 - (b) Step Function Speed Reducer
 - (c) Bearing Plate and Gear Assembly
 - (d) Torque Transducer
 - (e) Vane Rotation Transducer
 - (f) Vane
 - (g) Mounting Assembly
 - (h) Calibration Assembly
2. Stand and Sample Pedestal
3. Motor Control and Transducer Circuitry Unit
4. Torque Transducer Signal Conditioner
5. Motor Power Supply
6. Strip Chart Recorder

Description of Components

1. Vane shear device (see Fig. 13, page 43).

(a) D.C. Motor - The vane rotation motor is an American Electronics Inc., No. 3255P reversible D.C. gear motor. It is operable between 5 and 35 VDC and, incorporating a gear reduction of 4126:1, produces output rotation rates of 0.5 to 5.5 rpm. Continuous duty torque is 10 in-oz. Motor dimensions are 1.375 in. diameter by 3.31 in. long. The motor is mounted to the back mounting plate with an aluminum bracket and vibration isolating rubber grommets. The output shaft is connected to the input shaft of the speed reducer with 0.25 in. stainless steel shafting and a vibration reducing semi-flexible coupling.

(b) Step function speed reducer - The speed reducer is an INSCO Model No. 00140 Step Function Speed Reducer which provides rotation output to input ratios of 1:1, 1:2, 1:5, 1:10, 1:20, 1:50, 1:100, 1:200, 1:500 and 1:1000. Changing the ratios is easily accomplished by turning a knob on top of the unit. The input and output shafts both come out of the bottom of the unit and are 0.25 in steel. The reducer is rated at 100 in-oz torque. The reducer is attached directly to the back mounting plate by machine screws.

(c) Bearing Plate and Gear Assembly - The bearing plate and gear assembly is mounted to a mounting plate on the bottom of the speed reducer by four machine screws with 0.9 in. sleeve stand offs. The Assembly consists of two 3/10 in. thick steel plates which are held together by four 2 in. spacer studs. The plates provide mountings for four precision, 0.25 in I.D., miniature ball bearings; two for the upper end of the vane shaft (between the torque transducer and the speed reducer) and two for the rotation transducer shaft. On the shafts, between the two bearing plates, are mounted the gears for the rotation measurement and the 1.5 in diameter torque transducer calibration pulley. The gears are anti-back lash stainless steel spur gears providing a rotation step up from vane shaft to rotation transducer shaft of 1:3.67. The bearing plates are slotted on the motor side to accomodate the motor to speed reducer shaft.

(d) Torque Transducer - The torque transducer is mounted as part of the vane shaft just below the bearing plate assembly. It is 2024-T3 aluminum 0.75 inch bar stock, 2.25 inches long with a 0.250 in. diameter centerdrilled hole running its length. The middle portion of the transducer is necked to provide 0.015 inch wall thickness and design stresses of 6000 psi in the outer fiber

at 150 in-oz torque. Torsional strain in the transducer is detected by a four arm balanced strain gage bridge. The strain gages are SR-4, 350 ohm. The bridge is connected directly to the signal conditioner.

(e) Vane Rotation Transducer - The vane rotation transducer is a Beckman Helipot Model 6103, 10,000 ohm ball bearing precision potentiometer. Full scale linearity is rated at $\pm 0.5\%$. The potentiometer is mounted to the back mounting plate with an aluminum bracket. The potentiometer shaft is driven by the vane shaft through the two anti back lash gears in the bearing plate and gear assembly. A 5 volt reference potential from the control unit is across the outside terminals of the potentiometer. Rotation is measured by measuring voltage changes at the rotor terminal as the potentiometer (and vane) rotates.

(f) Vane - The test vane is shown in Fig. 14, (page 44) and is composed of four stainless steel blades silver soldered onto a 7 in. length of 0.25 inch stainless shafting necked to 0.125 in. at the vane end. The vane blades are 0.0156 in. thick. The total length of the vane blades (tip to tip), L, is 1.15 in. and the total width is 0.50 in. (i.e. $-a = 0.25$ in.). Both ends of the blades are tapered at 45° angles. This vane is

geometrically similar to the vane used in the McClelland Engineers wire line vane shear device. The vane is connected to the bottom of the torque transducer by a shaft coupling.

(g) Mounting Assembly - The mounting assembly provides the structure for mounting the vane shear device to the uprights of the Wykeham Farrance Soil Test Machine. The assembly includes two horizontally mounted 0.5 in. steel top and bottom plates with holes in each end such that they slide over the uprights. (see Fig. 12, page 42). These plates are held in place on the uprights by collars. Between the top and bottom plates the .375 in. thick steel back plate is mounted vertically. The other components of the vane shear device are mounted to this plate.

(h) Calibration Assembly - The torque transducer calibration assembly is illustrated in Fig. 15, page 46). It is composed of the 1.5 in pulley mounted on the vane shaft, a second pulley mounted as shown in Figure 15, a piece of fishing line, calibration weights, and a three point clamping jig for immobilizing the bottom end of the torque transducer. The assembly is used by first removing the vane and disconnecting, and sliding up, the shaft coupling between the upper vane

shaft and the step function speed reducer. The fishing line is then connected to the vane shaft pulley and led over the other pulley, and the lower end of the torque transducer is retained from rotation by the clamping jig. The restraint is applied by a carefully tightened three set screw jig to avoid putting bending moments on the torque transducer. Mercury filled weights calibrated in even in-oz increments (computed on basis of 1.5 in. diameter pulley on vane shaft) are then hung from the line and the torque readout is obtained on the strip chart recorder.

2. Stand and Sample Pedestal - The uprights and pedestal of a Wykeham Farrance Soil Test Machine, Model T-56-B are used to support the vane shear device and provides a means to raise the sample, pushing it onto the vane. (see Fig. 12, page 42). The pedestal is operated by a hand crank.
3. Motor Control and Transducer Circuitry Unit - This unit was assembled to provide a convenient means to start, stop and reverse the vane motor and to provide a constant voltage source and calibration system for the rotation transducer. Fig. 40 shows the unit and Fig. 41 is a schematic. The motor control circuit consists of an on-off push button weitch and a motor voltage polarity reversing switch. The rotation transducer circuit is

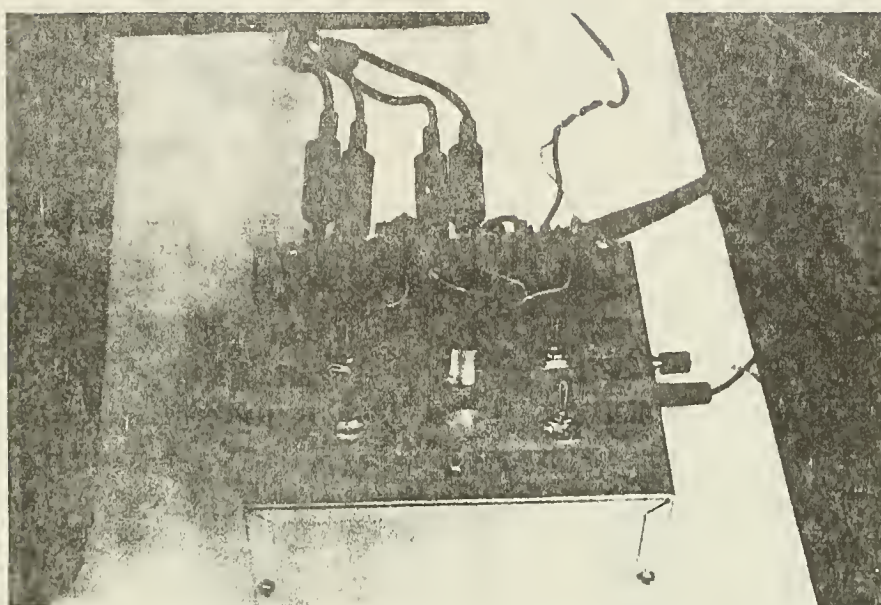


FIG. 40. - MOTOR CONTROL AND TRANSDUCER CIRCUITRY
UNIT

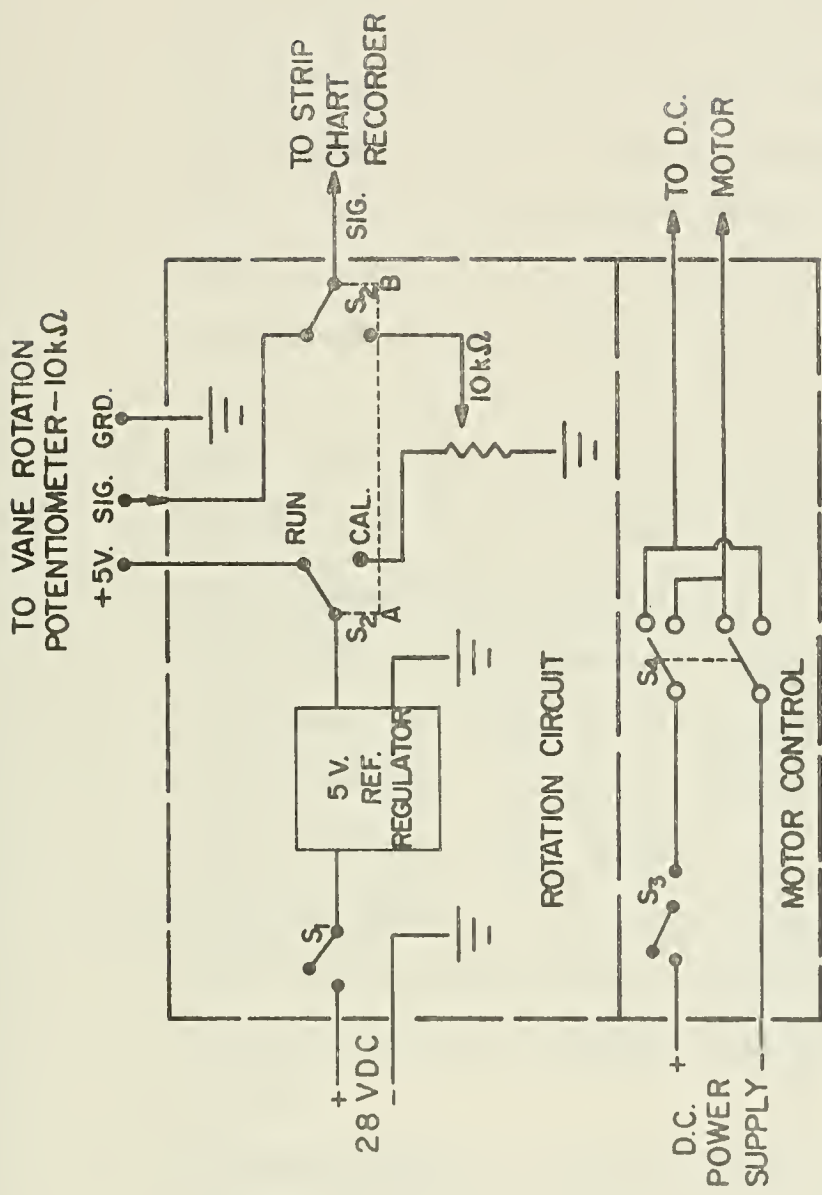


FIG. 41. - SCHEMATIC OF MOTOR CONTROL AND TRANSDUCER CIRCUITRY UNIT

driven by 28 VDC from an external battery. This is reduced to 5 volts by the reference voltage transformer. When the control switch is in the "run" position the 5 volts are applied across the rotation transducer (potentiometer) and the voltage at the potentiometer rotor is fed into the strip chart recorder. When the control switch is in the "cal" position a dummy potentiometer (5 turn, 10,000 ohm, high resolution) is switched into the circuit in place of the rotation transducer. This facilitates the setting of calibration reference steps on the strip chart printout.

4. Torque Transducer Signal Conditioner - The strain gage bridge of the torque transducer is connected to a Vishay Instruments, Inc., Model BA-4 Strain Gage Amplifier/Signal Conditioner. The output from the signal conditioner is fed to the strip chart recorder.
5. Motor Power Supply - The vane motor voltage is obtained from a Perkin Electronics Model TV R040-15 D.C. power supply which supplies a regulated voltage variable from 0-50 V.D.C.
6. Strip Chart Recorder - Continuous torque rotation-time recordings is accomplished by a Honeywell Model 906 C "Visicorder" recording oscillograph. This machine has six channels available, two of which are used. Chart

speeds of .4, 2.0, 10.0 and 40.0 inches per second are available and the chart speed is controlled such that it is an accurate time scale. The speed was checked using a time mark generator.

APPENDIX IV. - EQUIPMENT CALIBRATION AND CHECK OUT

A series of calibration and repeatability tests were conducted prior to core sample testing.

Torque Measurement. - Linearity and repeatability of the torque transducer system were ascertained using the torque calibration apparatus described in Appendix III. The torque system was found to provide sensitivity of 0.001 in-lb with a 0.2 in-lb full scale setting and has a range of 0 to 10 in-lb available through gain steps in the signal conditioner. No measurable nonlinearity was found.

Rotation Measurement. - The rotation measuring potentiometer was calibrated by mounting it on a large compass rose, with a pointer knob. 5 volts were put across the outside terminals and the voltage at the rotor terminal was measured as the knob was turned through 10^0 increments over the full throw of the potentiometer. The calibration factor was found to be 0.015 volts/degree or 0.859 volts/radian, and the potentiometer was within 0.5% linearity. When the calibration factor is divided by the 1:367 vane shaft to potentiometer shaft rotation ratio the resulting voltage per vane shaft rotation ratio is 3.151 volts/radian. This calibration factor was used to obtain unadjusted vane rotation angles from the strip chart read out. These angles were then adjusted by the

shaft twist at measured torque which was computed to be .0086 radians/in-lb.

Vane Motor Checks. - Motor speed versus input voltage was checked under loaded and no-load conditions. The loaded conditions were obtained by hanging weights from the calibration pulleys as in the calibration procedure. The motor speed was found load dependent at torques above its rated 10 in-oz. It was thus decided that only approximate (normal) rotation rates could be preset with the motor input voltage.

Time Scale Calibration. - It has been mentioned that the chart feed rate was used to obtain the times for the torque-rotation-time data. The accuracy of these rates for the recorder used was verified by connecting an electronic time work generator to a recorder channel.

Check Out Tests. - A series of tests were conducted on three carefully constructed remolded samples of submarine clays. Each sample was as nearly homogeneous as possible. The samples were at different water contents and their stiffness encompassed the expected range of stiffnesses of the hose hole samples. Each sample was tested at 3 rotation rates with at least one rotation rate repeated twice. Each test was at an undisturbed location. These tests confirmed the capability of the apparatus to produce the required torque rotation-time-data over the entire range of expected sediment shear strengths and at the wide range of speeds desired. In addition, the repeated runs (i.e. same sample-same

speed) yielded the same torque versus rotation curves and thus further confirmed repeatability of the apparatus.

APPENDIX V. - X-RAYS OF SAMPLES TESTED

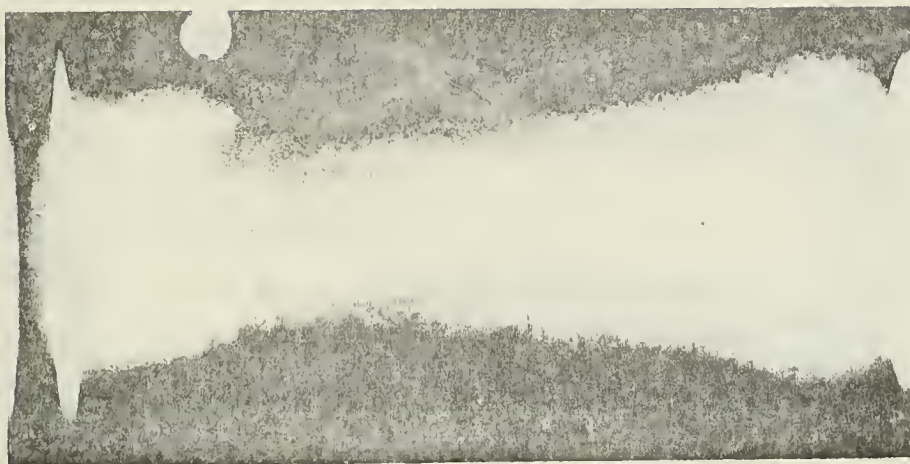


FIG. 42. - X-RAY PHOTOGRAPH, SAMPLE B-1, 19 FT

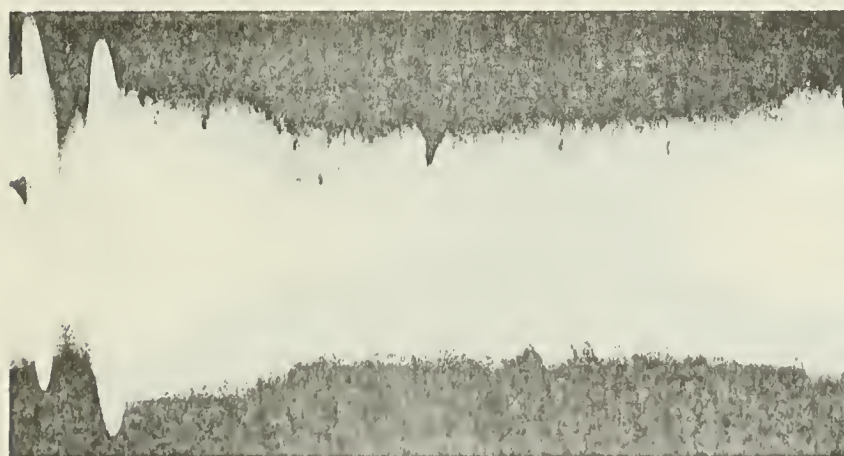


FIG. 43. - X-RAY PHOTOGRAPH, SAMPLE B-1, 46 FT

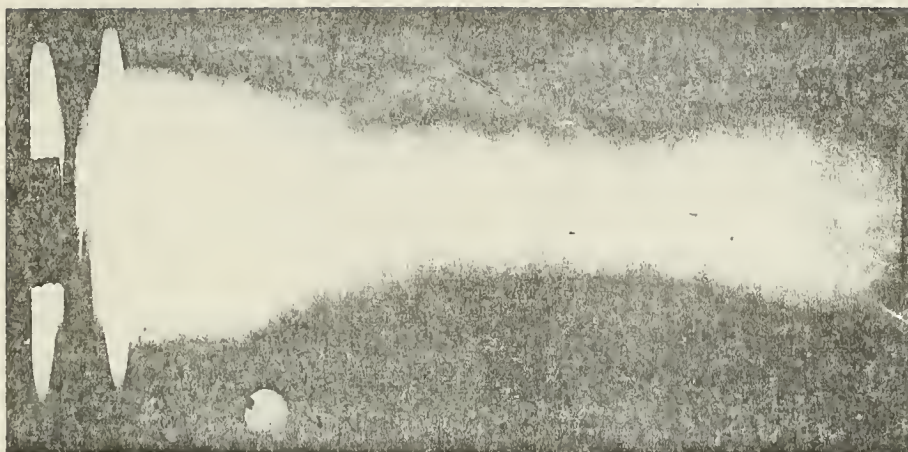


FIG. 44. - X-RAY PHOTOGRAPH, SAMPLE B-1, 61 FT



FIG. 45. - X-RAY PHOTOGRAPH, SAMPLE B-1, 85.5 FT

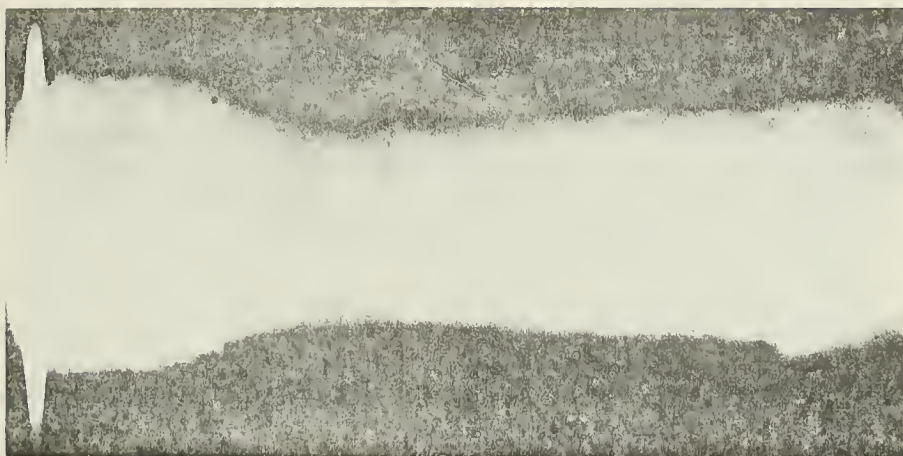


FIG. 46. - X-RAY PHOTOGRAPH, SAMPLE B-1, 100 FT

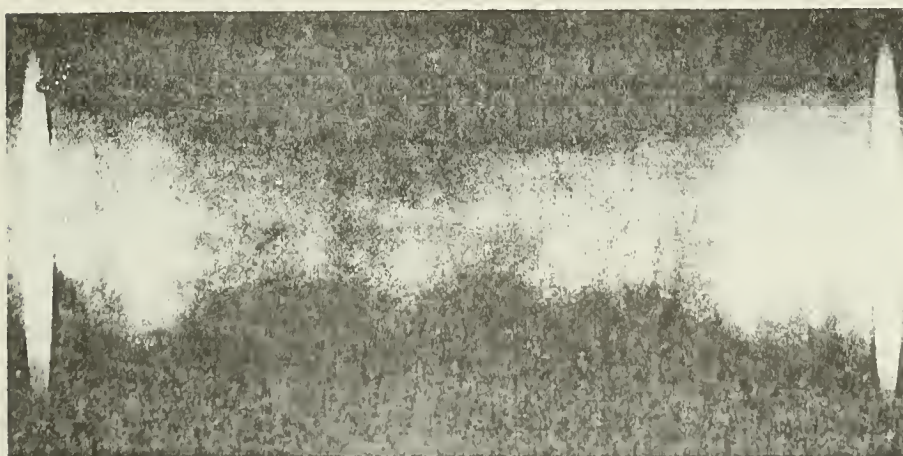


FIG. 47. - X-RAY PHOTOGRAPH, SAMPLE B-2, 22.5 FT

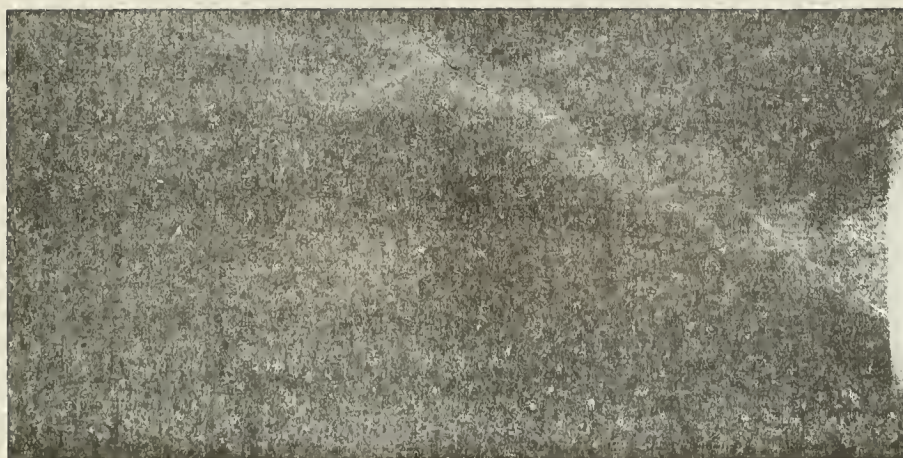


FIG. 48. - X-RAY PHOTOGRAPH, SAMPLE B-2, 40.5 FT

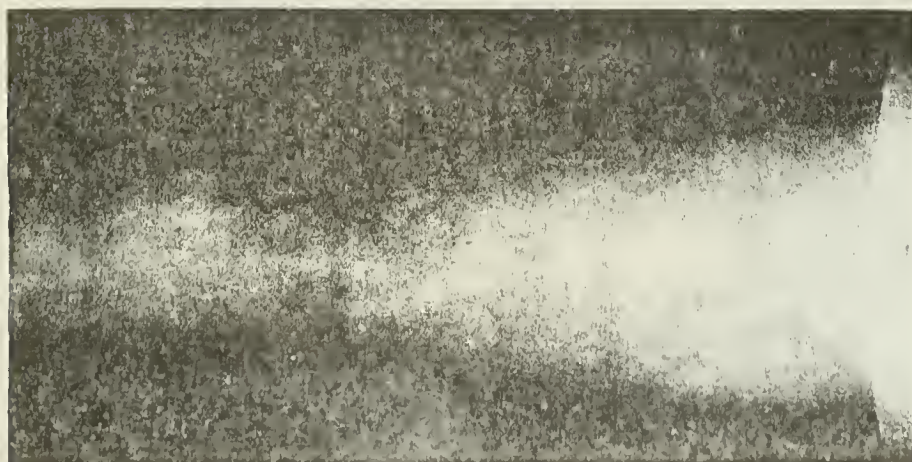


FIG. 49. - X-RAY PHOTOGRAPH, SAMPLE B-2, 72.5 FT

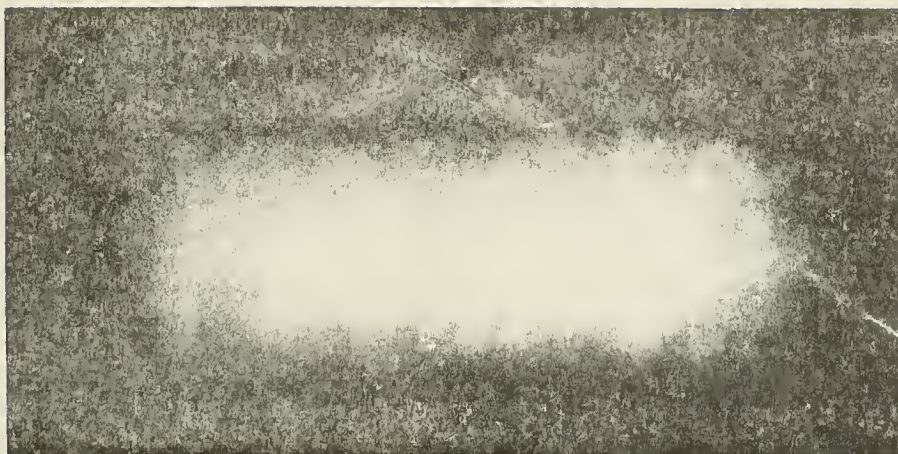


FIG. 50. - X-RAY PHOTOGRAPH, SAMPLE B-2, 104.5 FT



FIG. 51. - X-RAY PHOTOGRAPH, SAMPLE B-3, 55 FT

APPENDIX VI. - TORQUE VERSUS ROTATION
AND LOG-LOG PLOTS OF \bar{G} VERSUS TIME

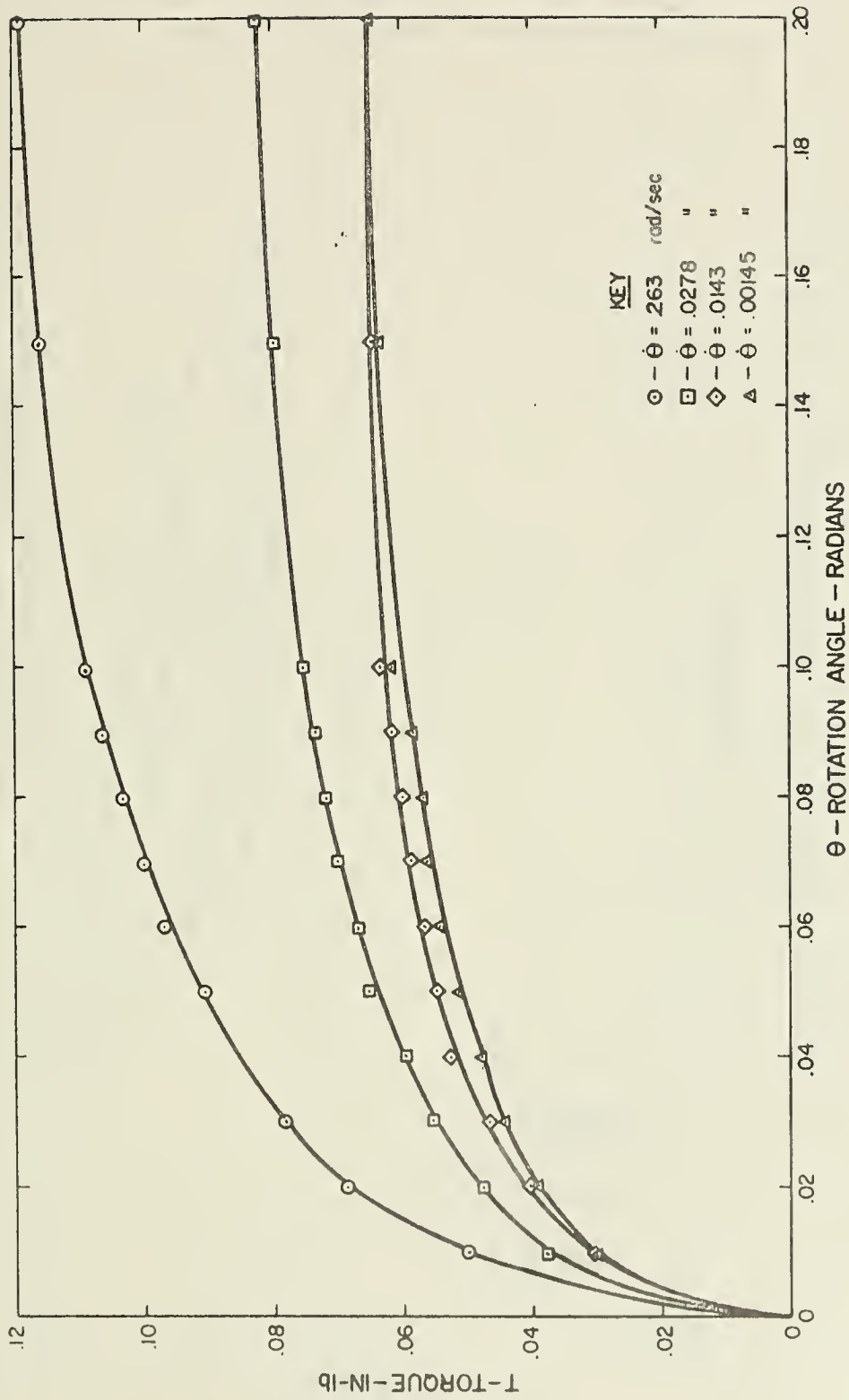
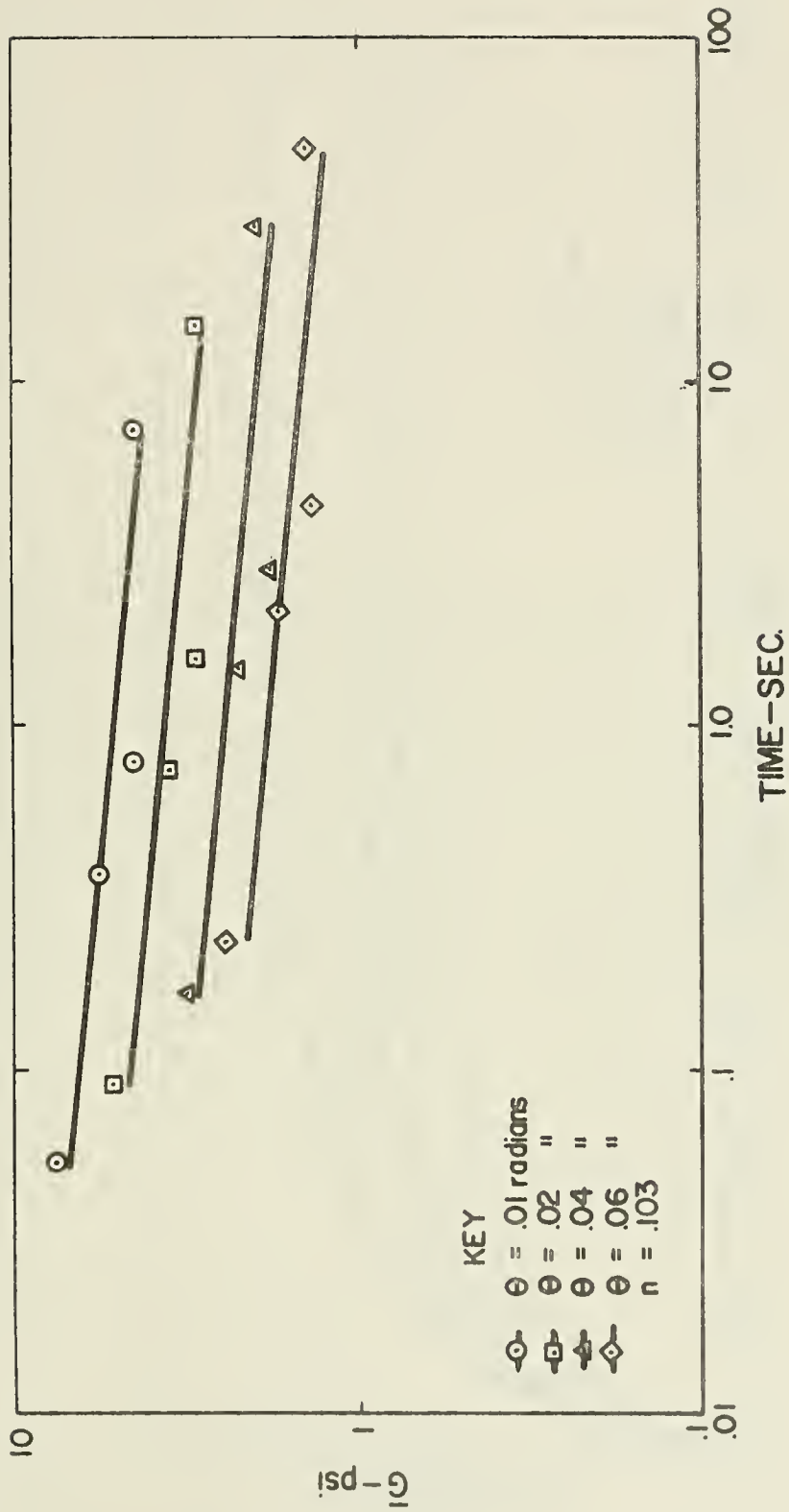


FIG. 52. - TORQUE VERSUS ROTATION, SAMPLE B-1, 19 FT

FIG. 53. - LOG-LOG PLOT OF \bar{G} VERSUS TIME, SAMPLE B-1, 19 FT

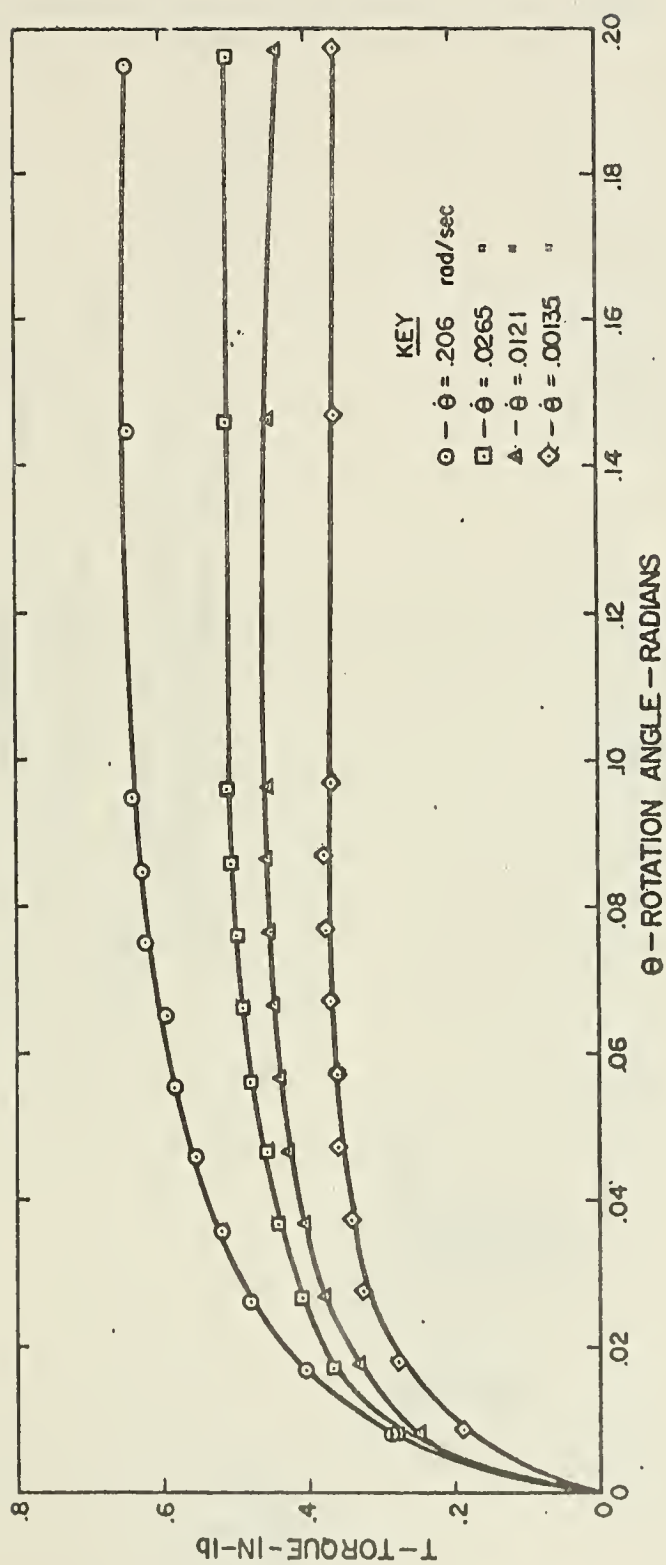


FIG. 54. - TORQUE VERSUS ROTATION, SAMPLE B-1, 46 FT

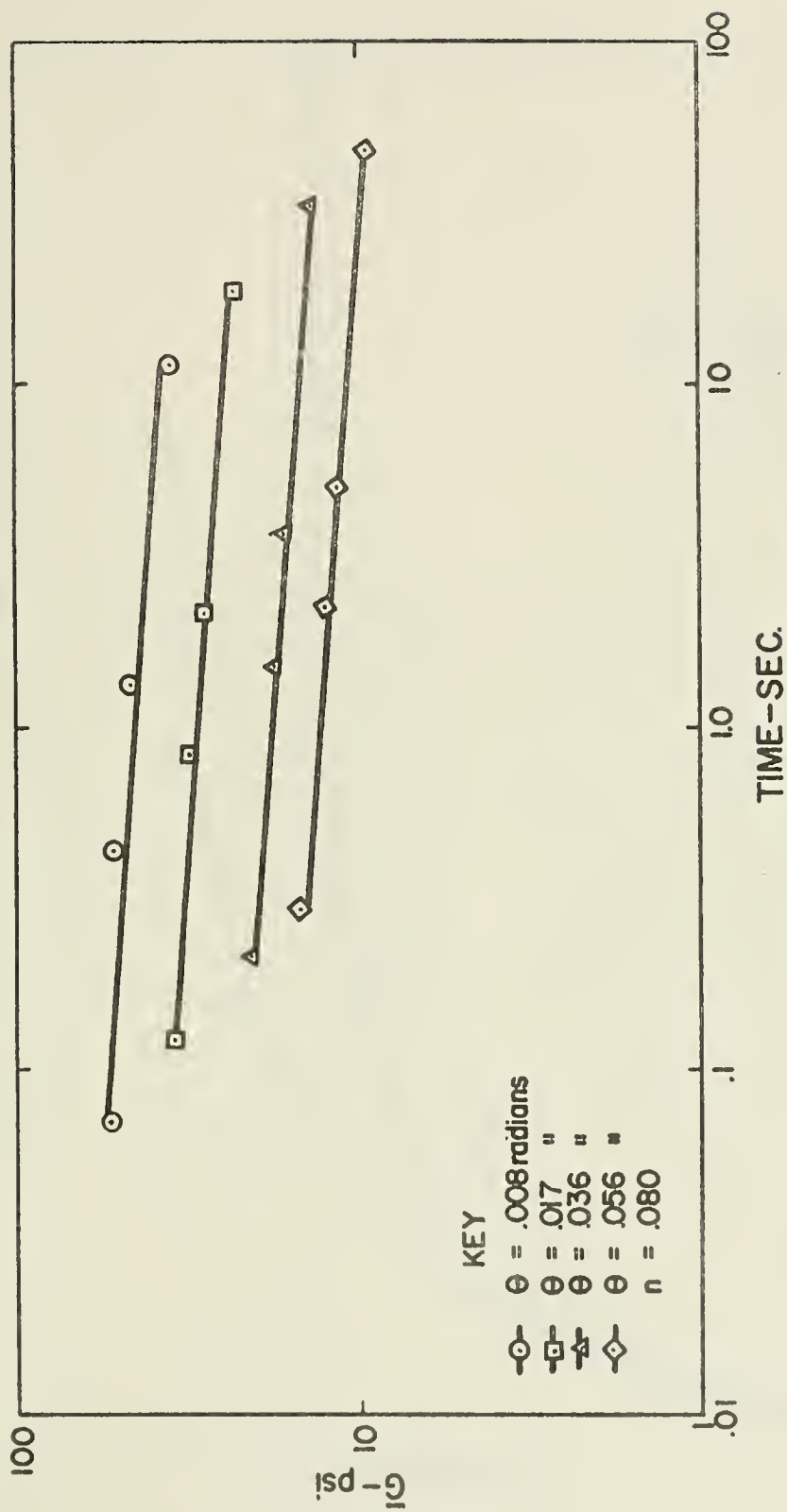


FIG. 55. - LOG-LOG PLOT OF \bar{G} VERSUS TIME, SAMPLE B-1, 46 FT

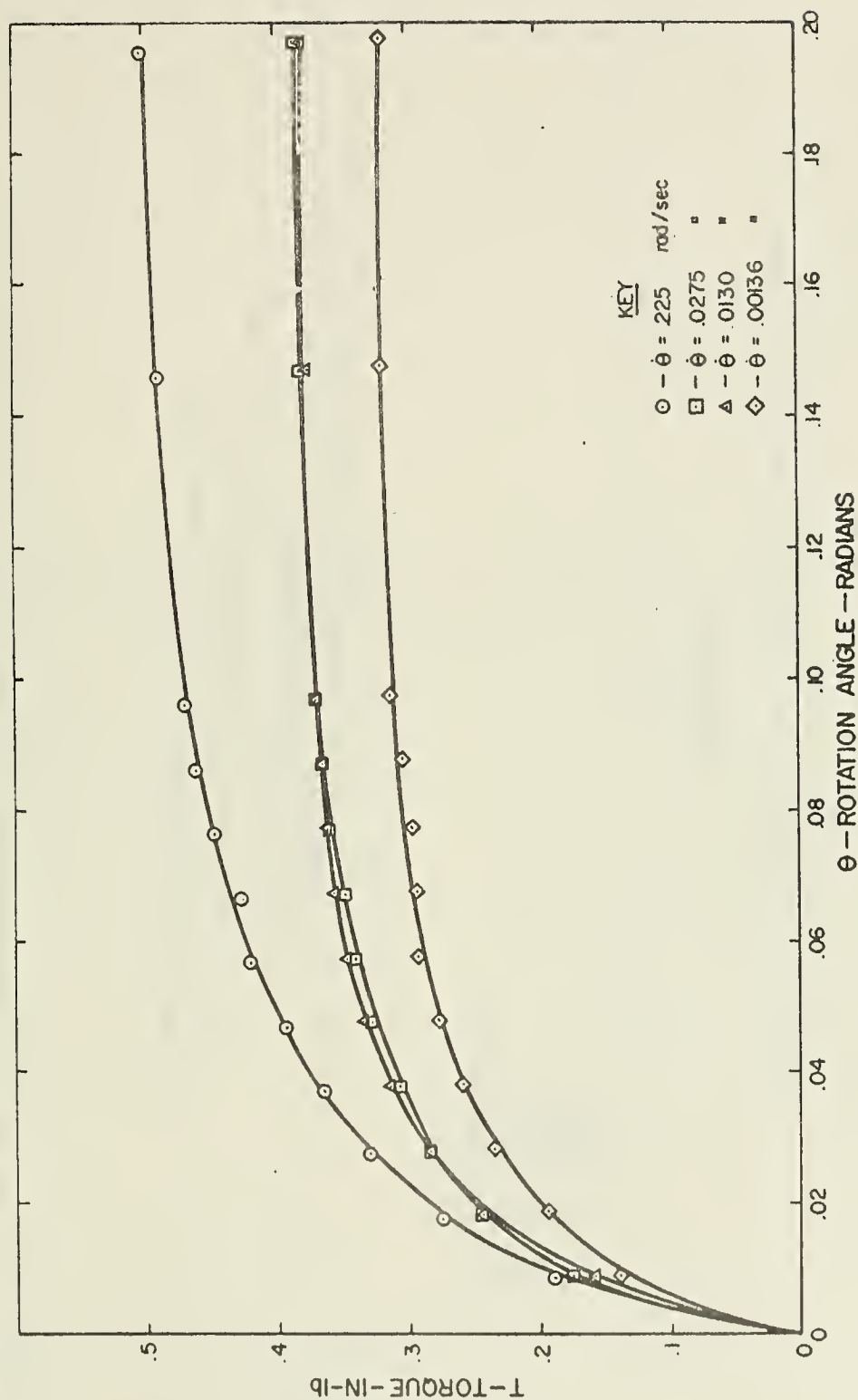


FIG. 56. - TORQUE VERSUS ROTATION, SAMPLE B-1, 61 FT

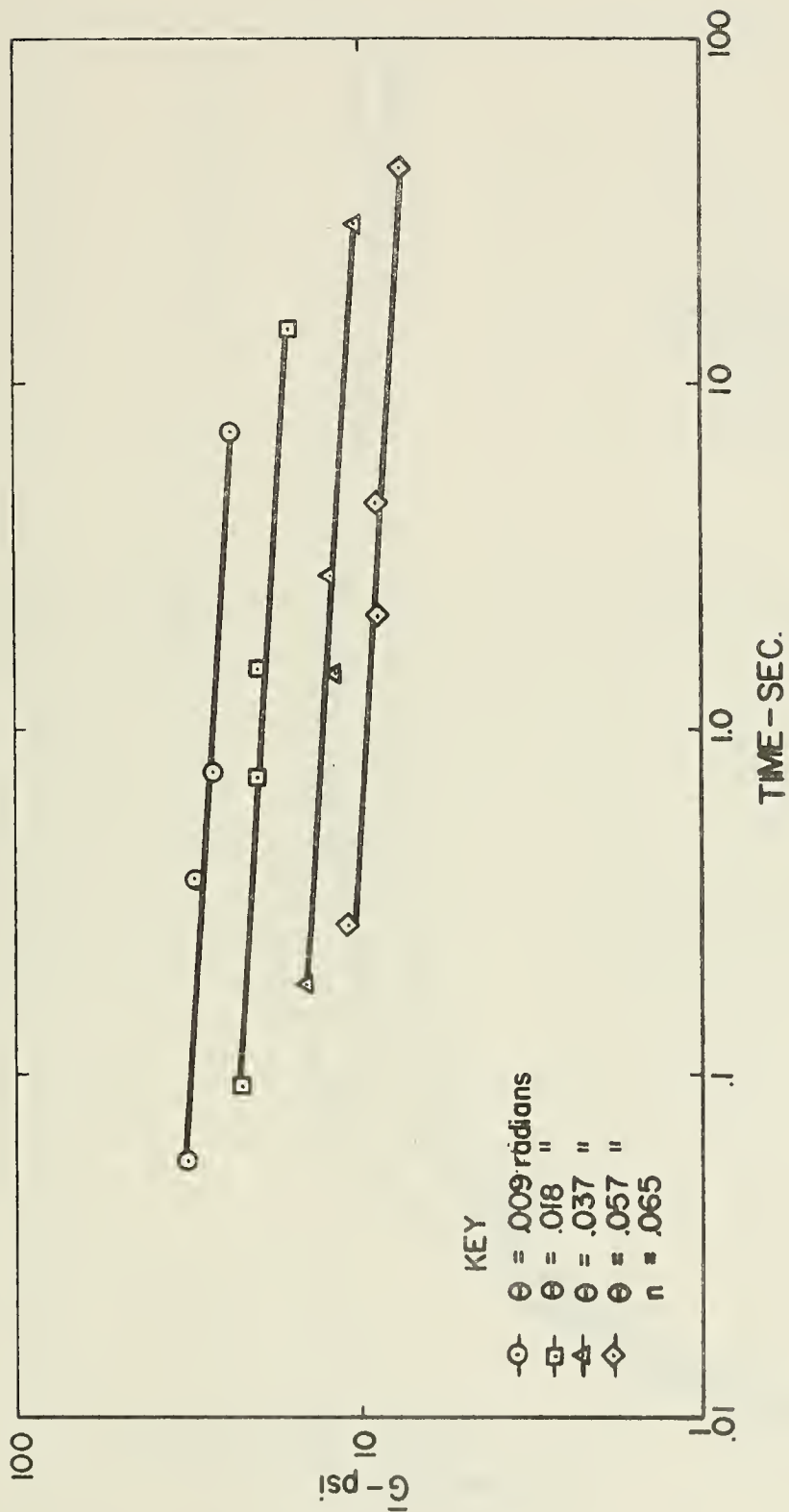


FIG. 57. - LOG-LOG PLOT OF \bar{G} VERSUS TIME, SAMPLE B-1, 61 FT

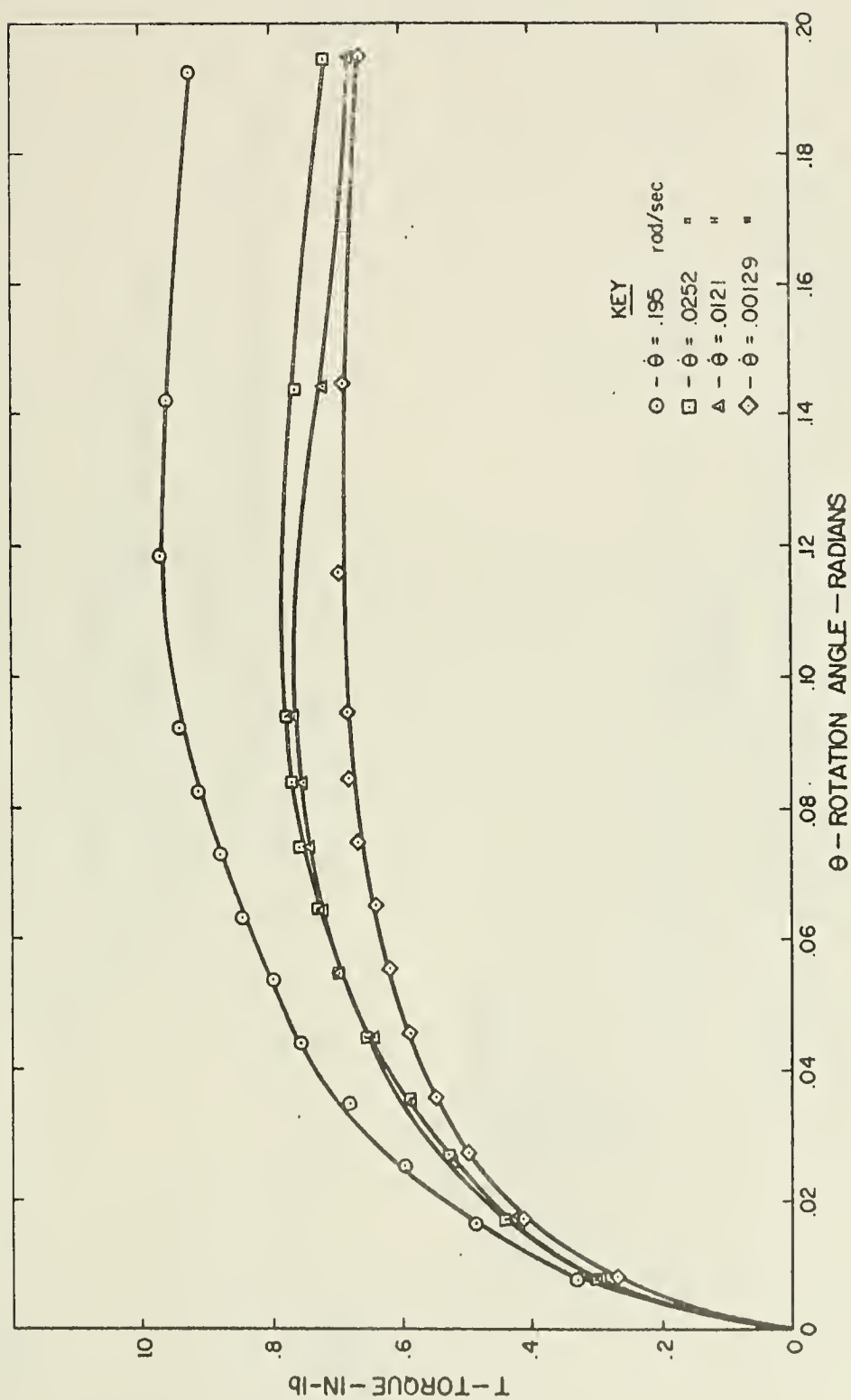


FIG. 58. - TORQUE VERSUS ROTATION, SAMPLE B-1, 85.5 FT

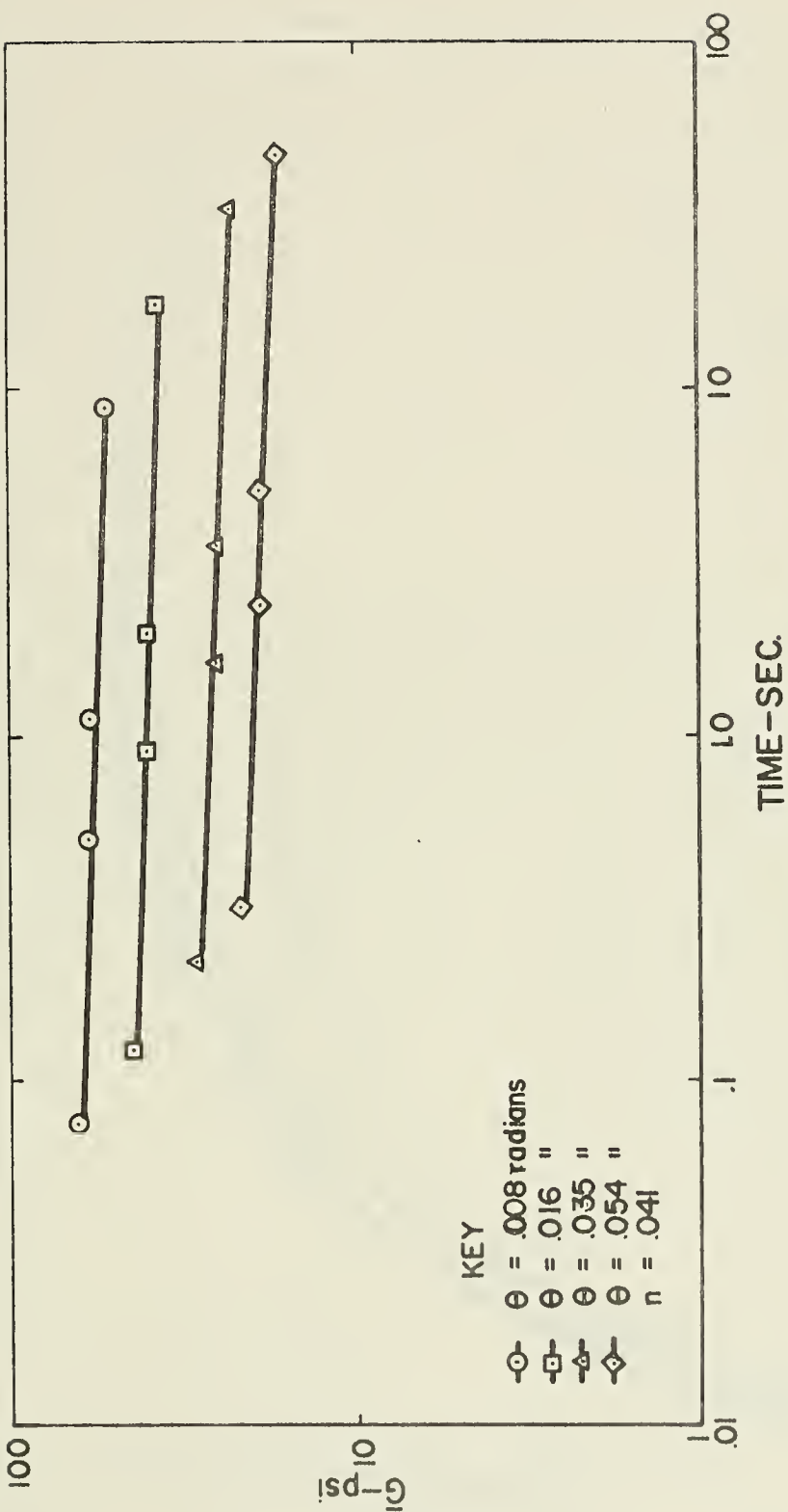


FIG. 59. - LOG-LOG PLOT OF \bar{G} VERSUS TIME, SAMPLE B-1, 85.5 FT

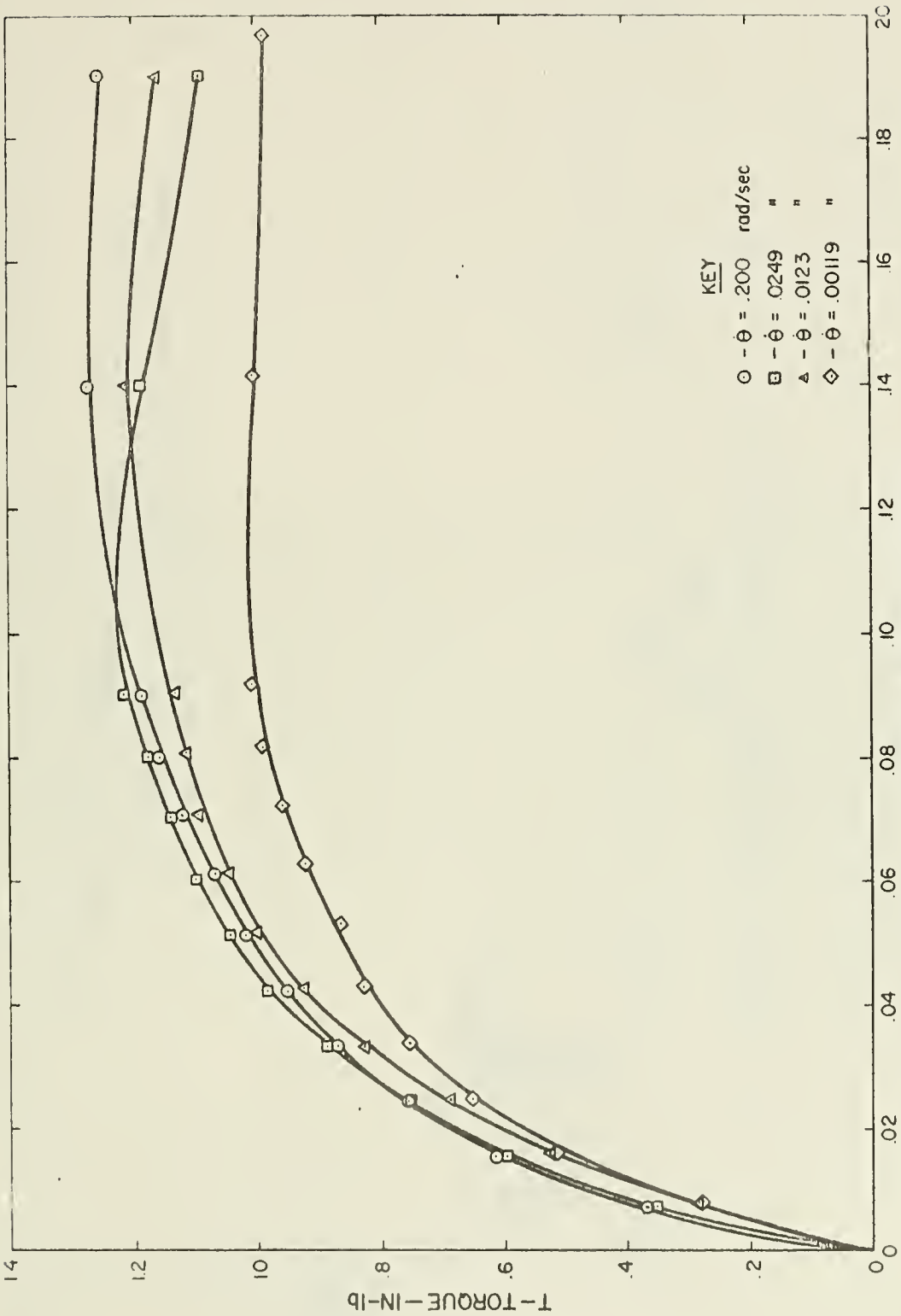
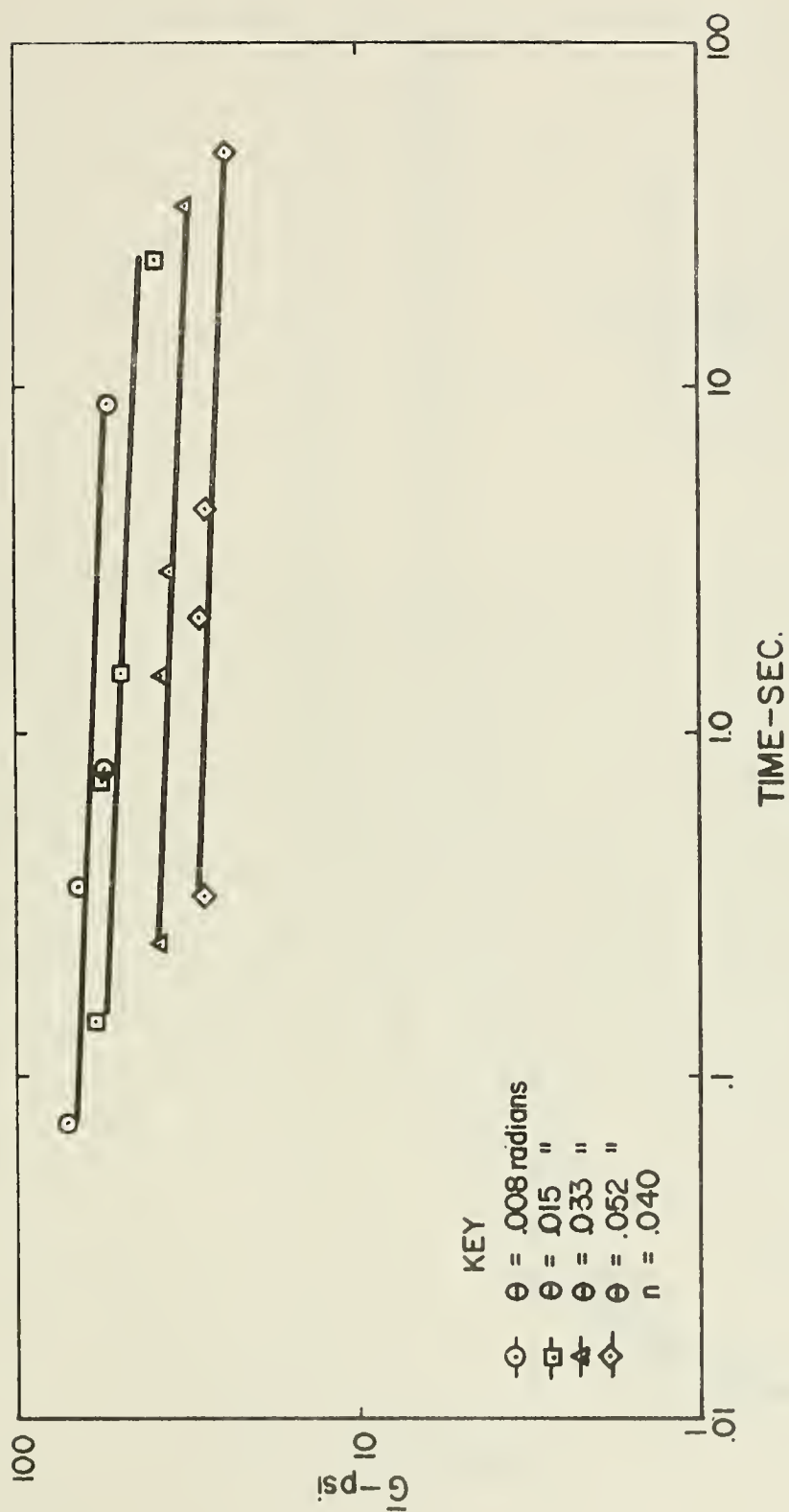


FIG. 60. - TORQUE VERSUS ROTATION, SAMPLE B-1, 100 FT

FIG. 61. - LOG-LOG PLOT OF \bar{G} VERSUS TIME, SAMPLE B-1, 100 FT

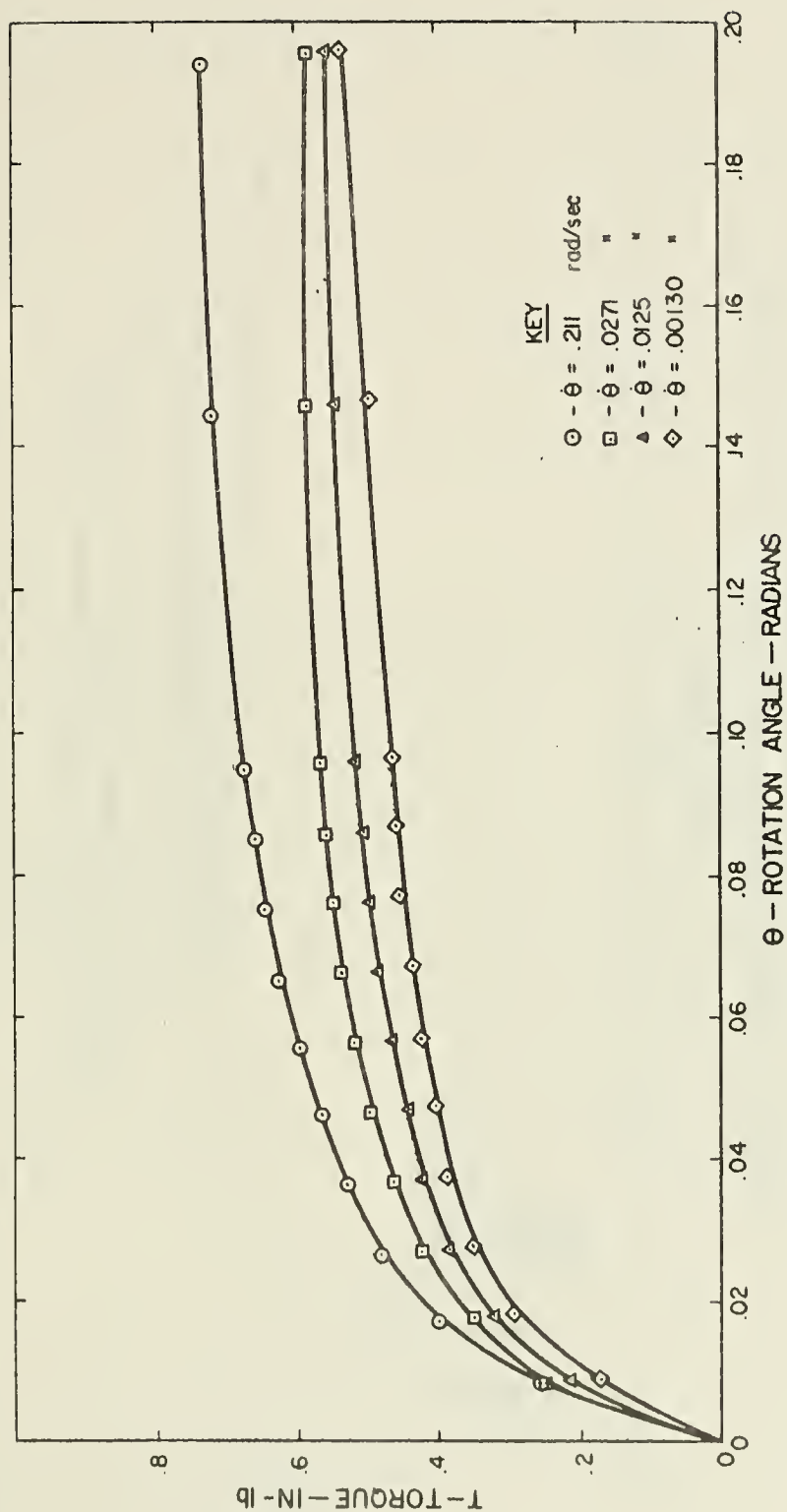


FIG. 62. - TORQUE VERSUS ROTATION, SAMPLE B-2, 22.5 FT

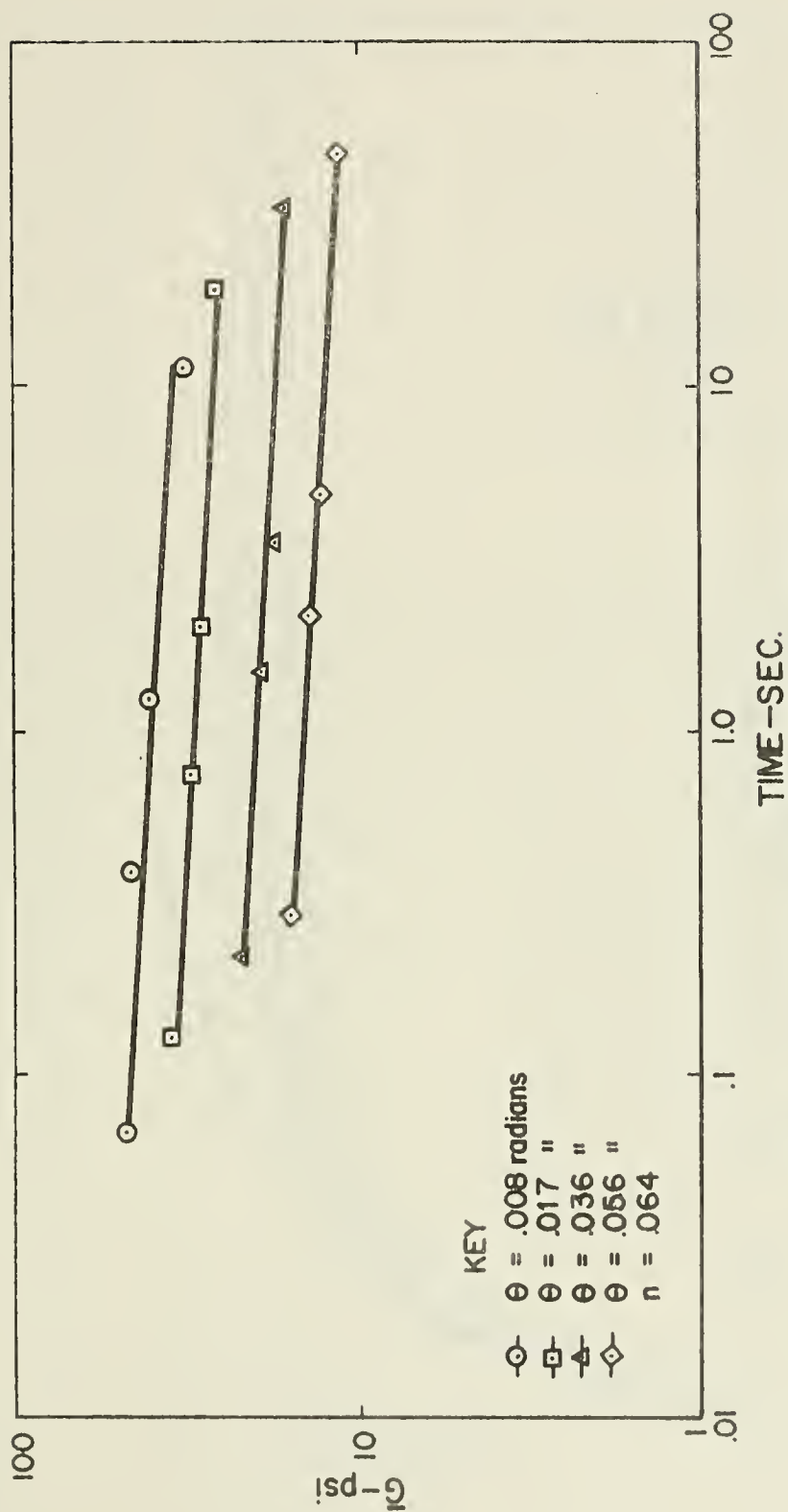


FIG. 63. - LOG-LOG PLOT OF \bar{G} VERSUS TIME, SAMPLE B-2, 22.5 FT

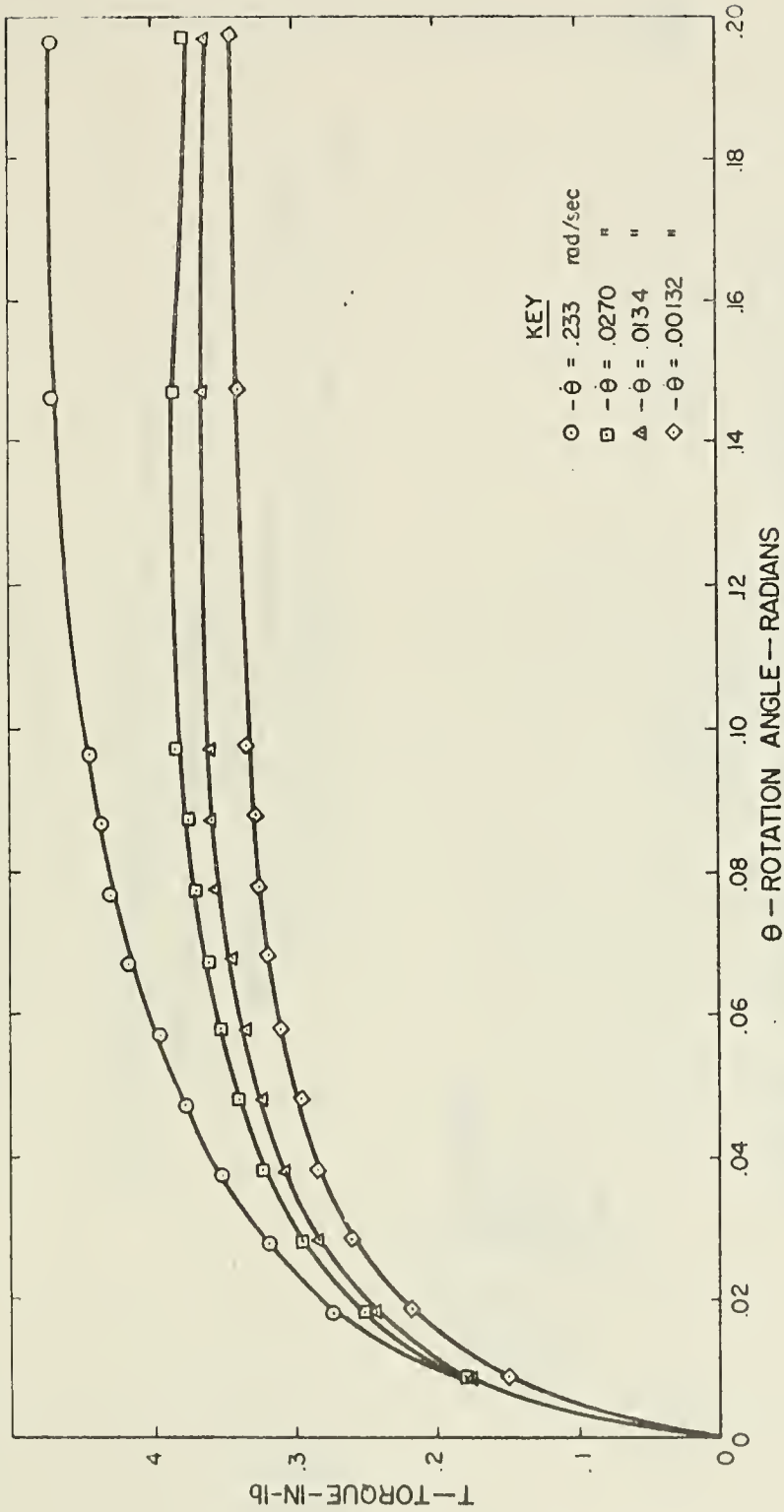


FIG. 64. - TORQUE VERSUS ROTATION, SAMPLE B-2, 40.5 FT

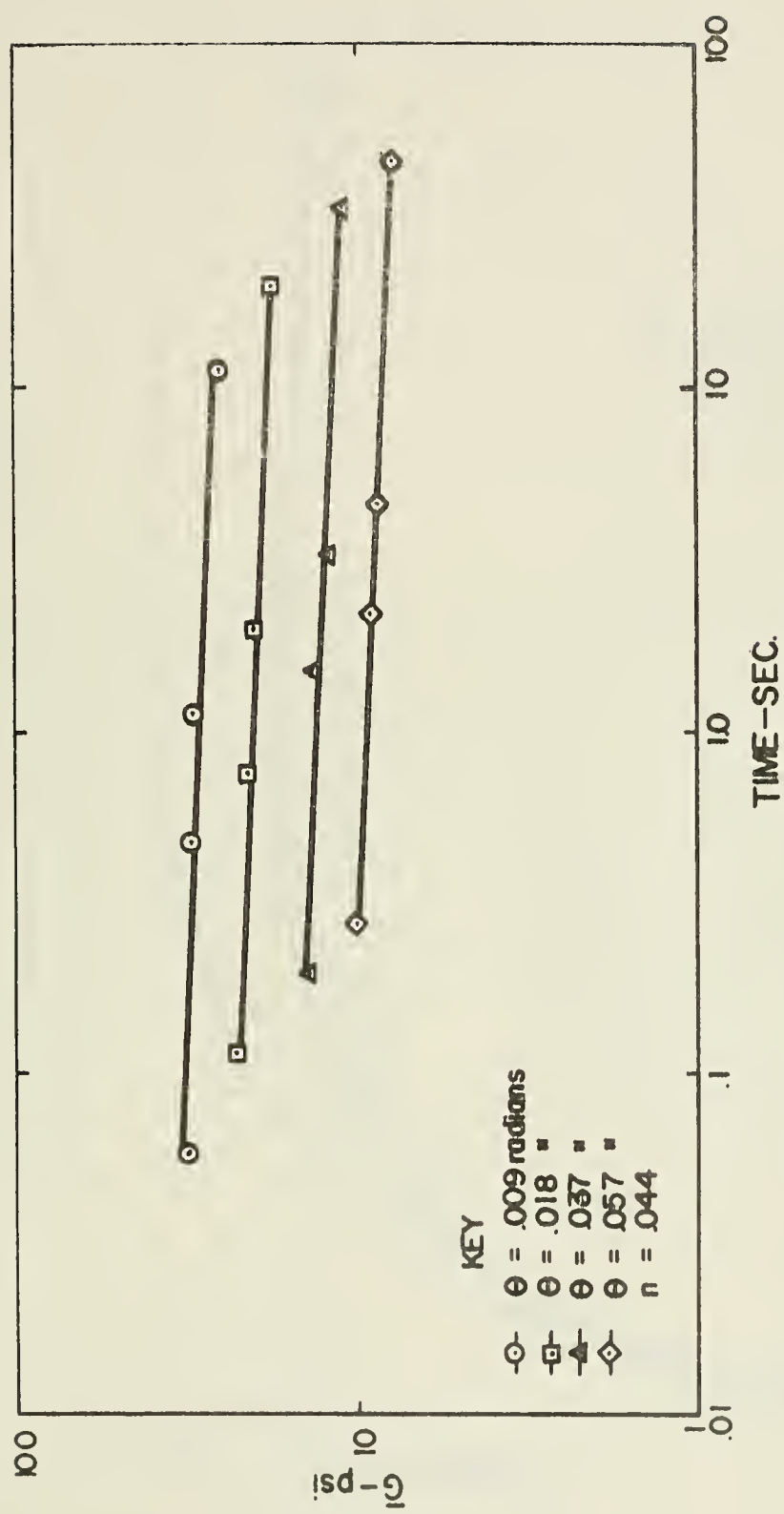


FIG. 65. - LOG-LOG PLOT OF \bar{G} VERSUS TIME, SAMPLE B-2, 40.5 F

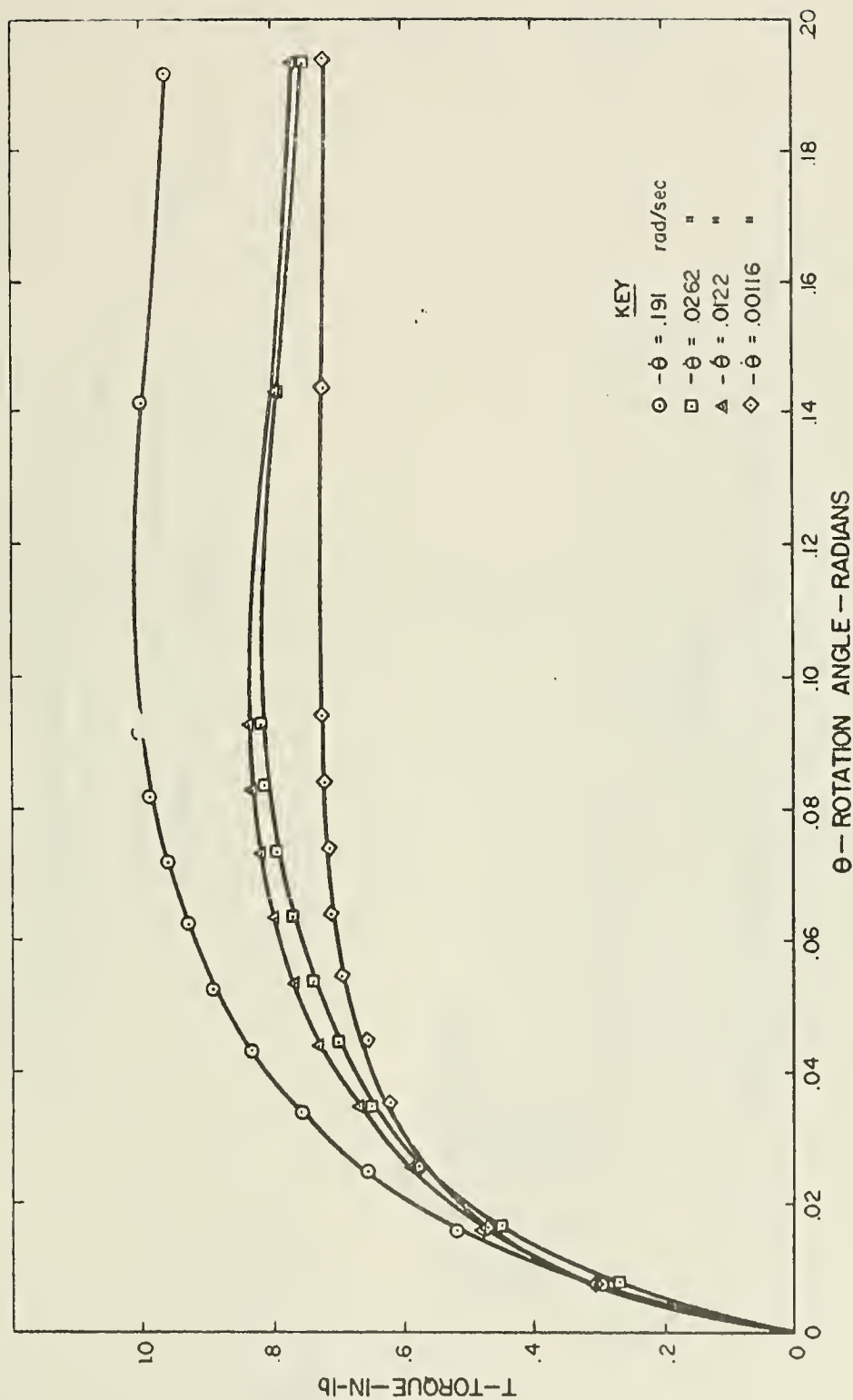
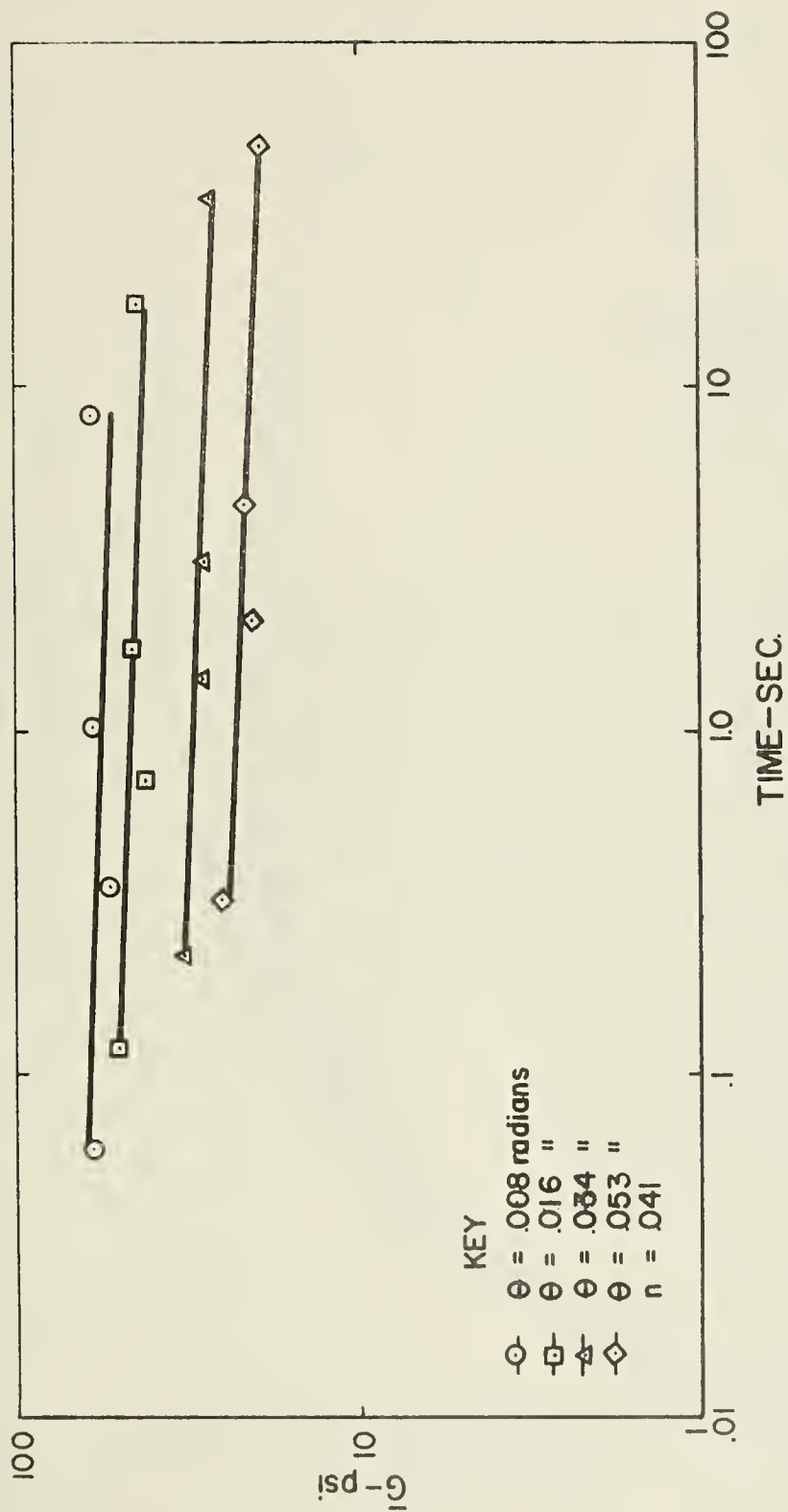


FIG. 66. - TORQUE VERSUS ROTATION, SAMPLE B-2, 72.5 FT

FIG. 67. - LOG-LOG PLOT OF \bar{G} VERSUS TIME, SAMPLE B-2, 72.5 FT

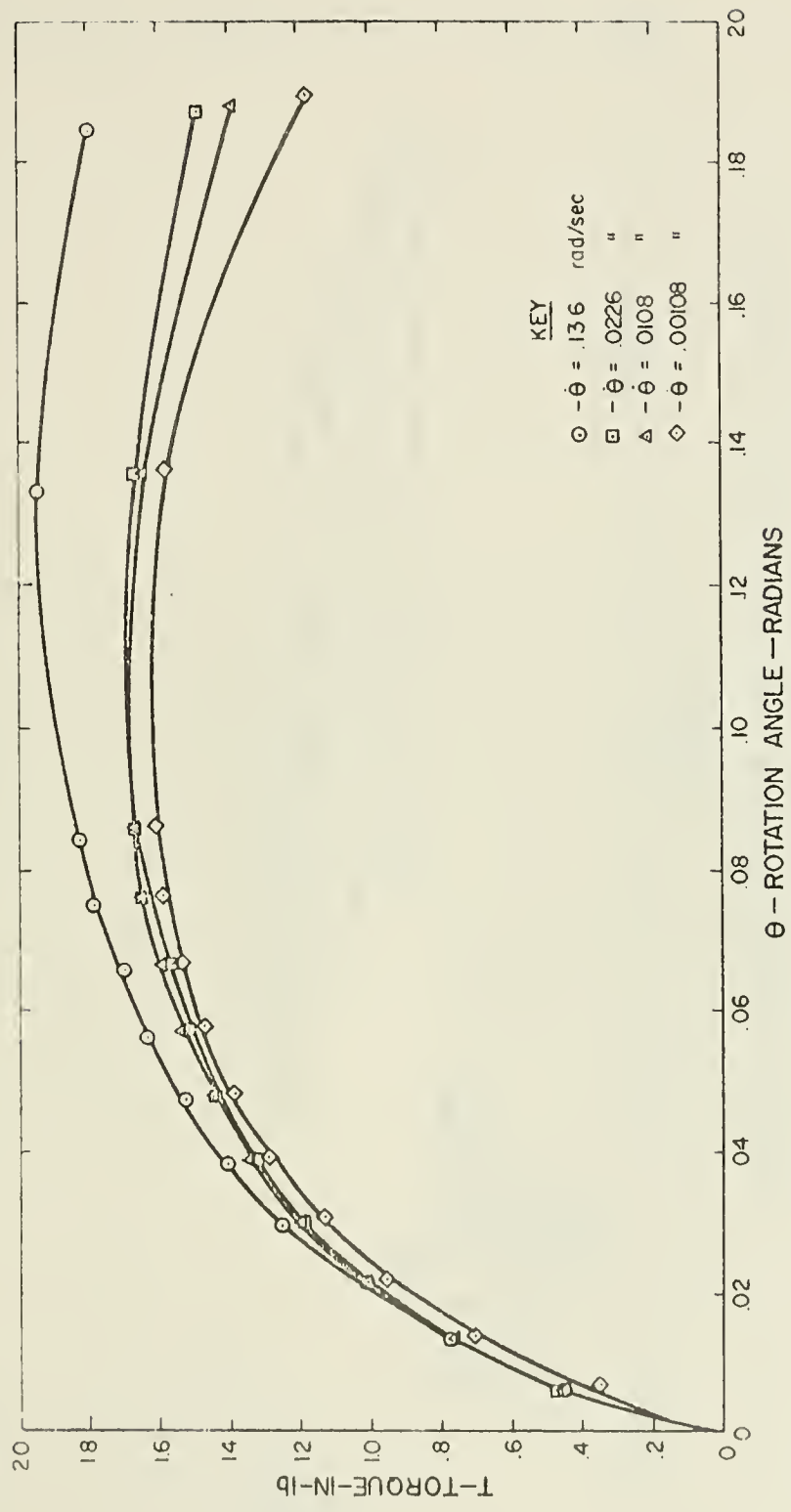
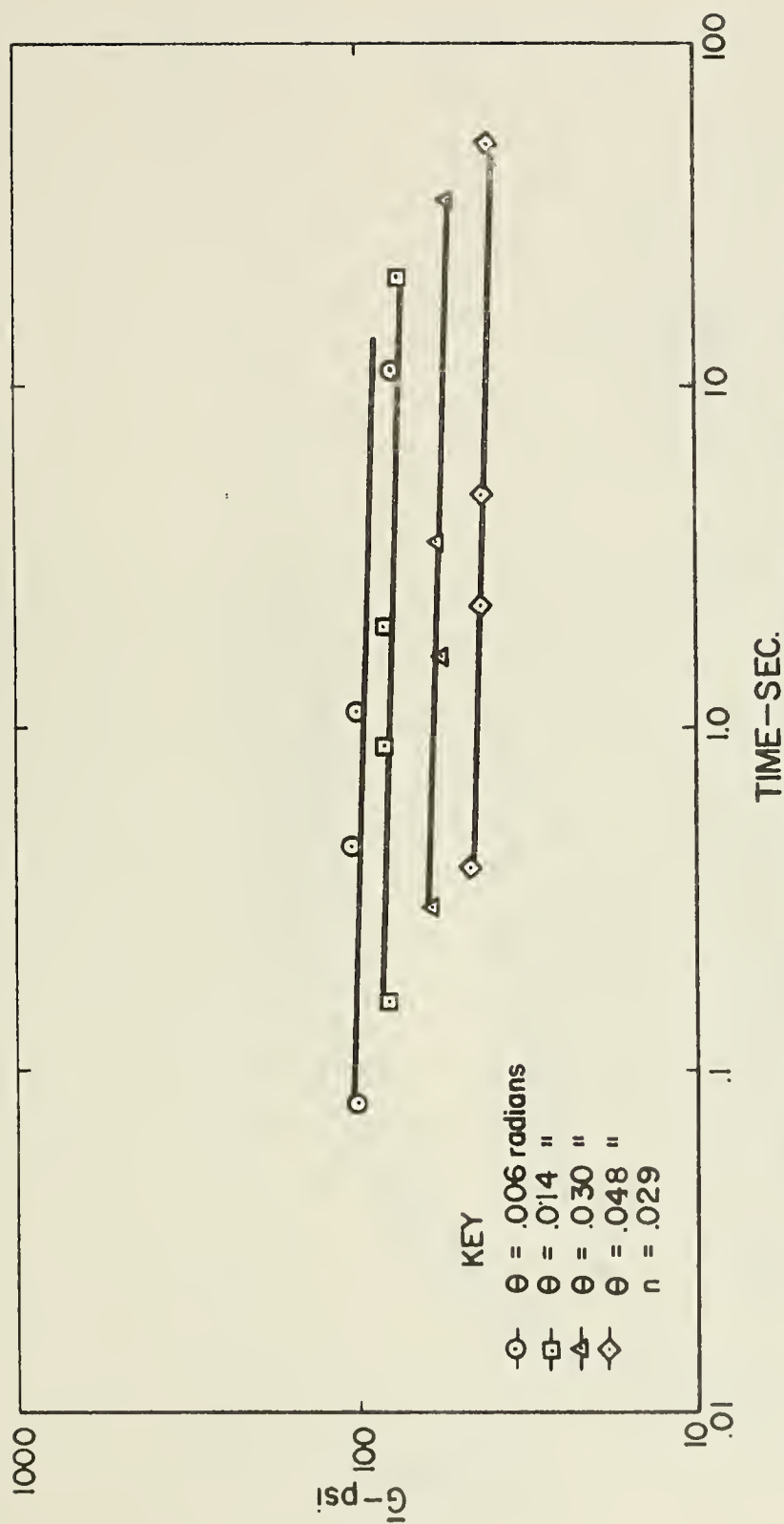


FIG. 63. - TORQUE VERSUS ROTATION, SAMPLE B-2, 104.5 FT

FIG. 59. - LOG-LOG PLOT OF \bar{G} VERSUS TIME, SAMPLE B-2, 104.5 FT

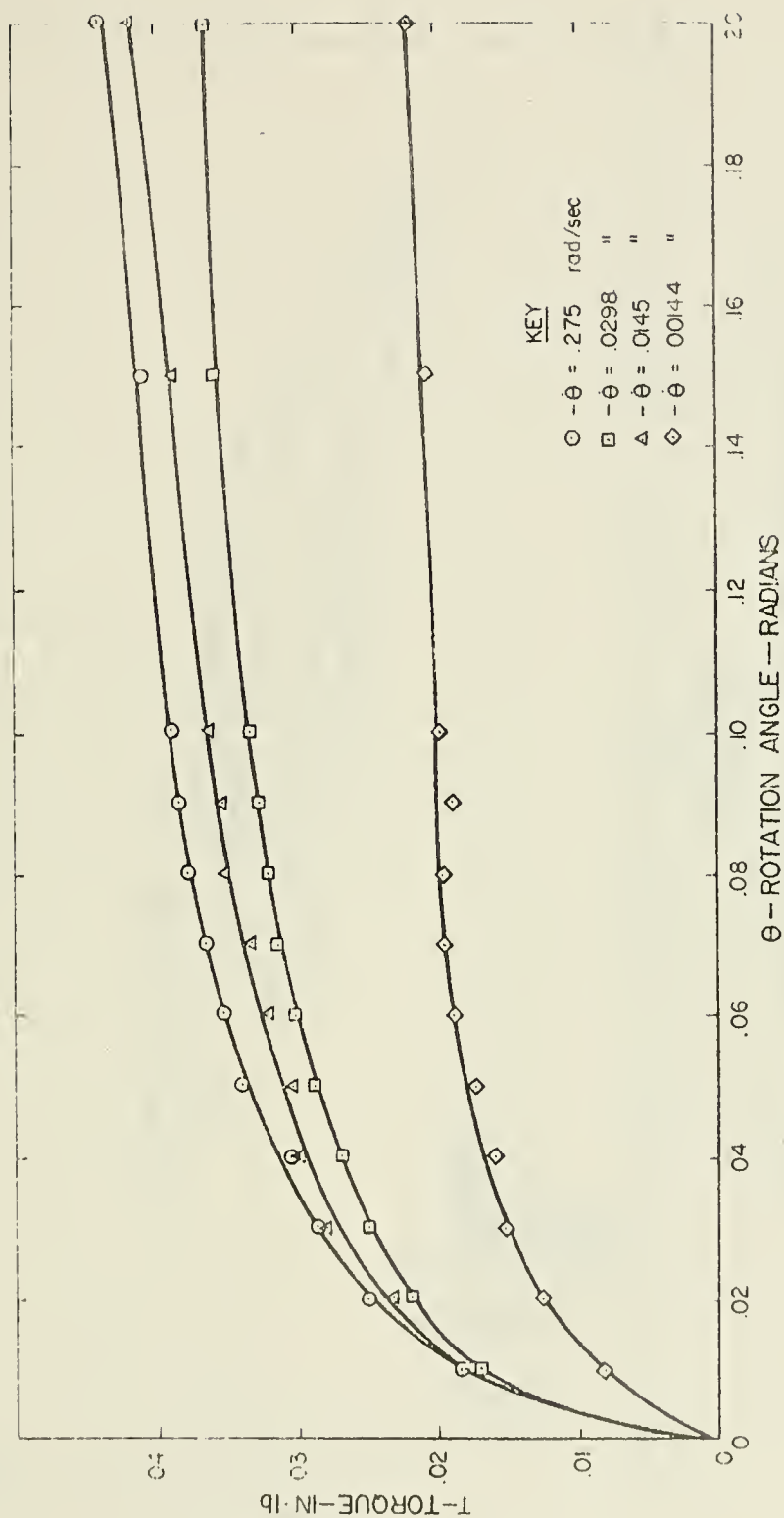
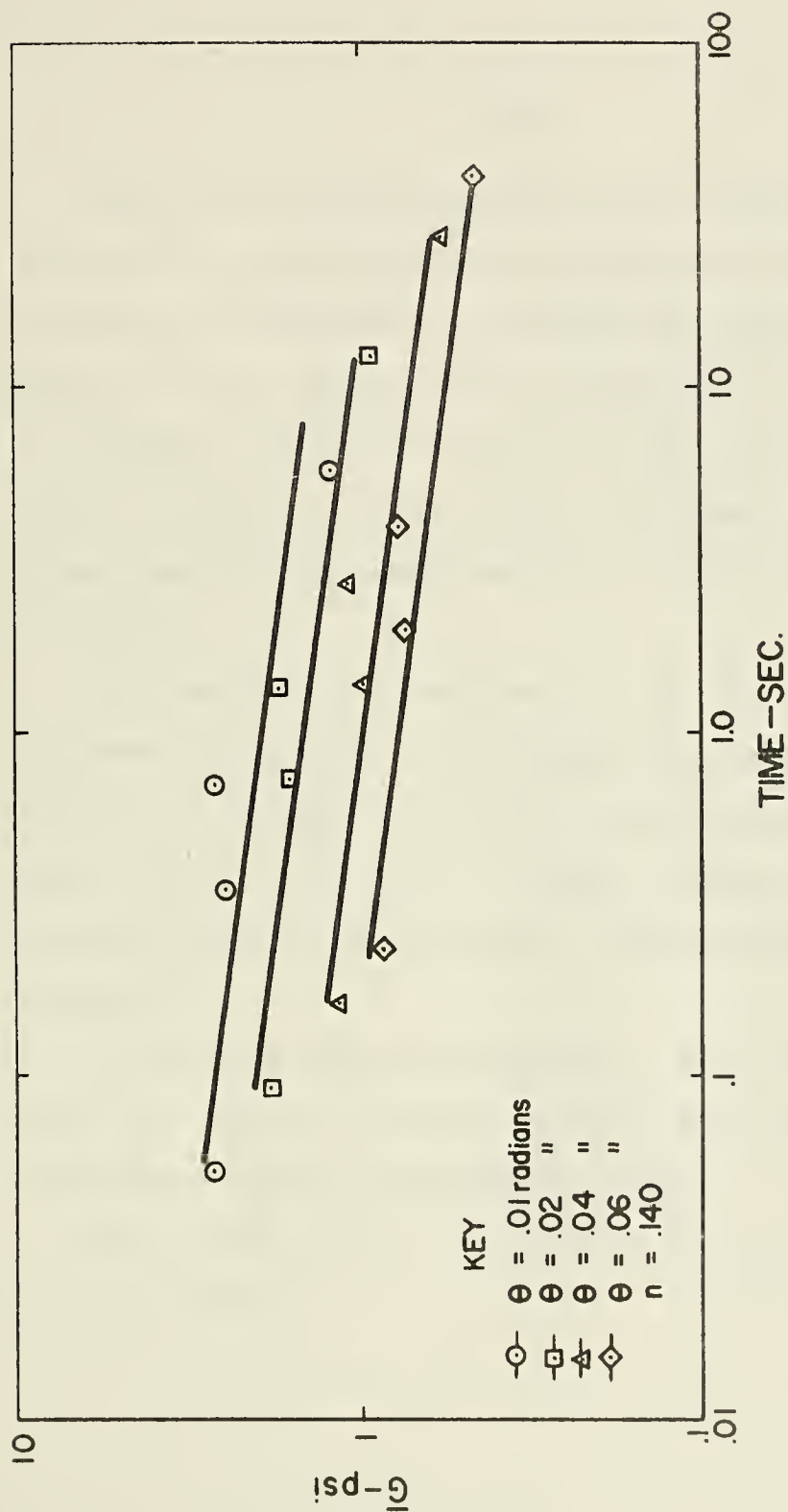


FIG. 70. - TORQUE VERSUS ROTATION, SAMPLE B-3, 55 FT

FIG. 71. - LOG-LOG PLOT OF \bar{G} VERSUS TIME, SAMPLE B-3, 55 FT

VITA

Herbert Scott Stevenson was born July 1, 1945 in Tucson, Arizona. He is the youngest of four boys born to John William and Nancy Louise Stevenson. He attended high school in Tucson. Having won a Naval Reserve Officer Training Corps scholarship, Mr. Stevenson attended the University of California, Los Angeles, earning a Bachelor of Science Degree in Engineering in March 1968. He was simultaneously commissioned Ensign, Civil Engineer Corps, U. S. Navy.

Since receiving his commission, Mr. Stevenson has served as a Research Officer, Naval Civil Engineering Laboratory, Port Hueneme California, and, just prior to his attendance at Texas A&M University, he was Officer in Charge, Underwater Construction Team ONE, Davisville, Rhode Island. He now holds the rank of Lieutenant.

Mr. Stevenson was married December 1, 1968. His wife's name is Connie. Mr. Stevenson's permanent mailing address is 311 Kearsarge Place, Lexington Park, Maryland.

The typists for this thesis were Mrs. Mary Ann Beeson and Mrs. Nancy Steele.

147516

Thesis

S71425 Stevenson

Vane shear determination of the viscoelastic shear modulus of submarine sediments.

DISPLAY

7 MAR 74

Thesis

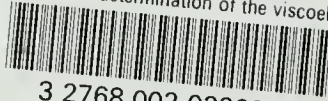
S71425 Stevenson

Vane shear determination of the viscoelastic shear modulus of submarine sediments.

147516

thes71425

Vane shear determination of the viscoela



3 2768 002 02290 7

DUDLEY KNOX LIBRARY